Linköping Studies in Science and Technology
Thesis No. 968

Active Engine Vibration Isolation using Feedback Control

Claes Olsson

REGLERTEKNIK
AUTOMATIC CONTROL
LINKÖPING

Division of Automatic Control
Department of Electrical Engineering
Linköpings universitet, SE–581 83 Linköping, Sweden
WWW: `http://www.control.isy.liu.se`
Email: `colsson5@volvocars.com`

Linköping 2002

Active Engine Vibration Isolation
using
Feedback Control

© 2002 Claes Olsson

Department of Electrical Engineering,
Linköpings universitet,
SE–581 83 Linköping,
Sweden.

ISBN 91-7373-398-9
ISSN 0280-7971
LiU-TEK-LIC-2002:41

Printed by UniTryck, Linköping, Sweden 2002

Abstract

Broad band active vibration isolation of automobile engine using linear and non-linear feedback control is considered. The objective is to reduce the forces transmitted to the chassis and body, and, thus, reducing vibrations and structure borne noise inside the vehicle compartment when the engine is subjected to different excitations. Moreover, the ability of the original passive suspension system to deal with high load transient excitation, e.g. due to a dropped clutch operation, has to be preserved. Engine excitations corresponding to idle and driving engine operating conditions as well as internal and external transient excitations have been investigated.

Solutions based on classical control and LQG (Linear Quadratic Gaussian) control methodologies have, to some extent, been treated. However, it turns out that the desired loop gain requires a control design method more suitable for shaping the loop gain and, at the same time, obtaining closed-loop stability. Using H_2 control theory and Gain Scheduling, a MIMO (multi-input multi-output) control algorithm dealing with the above mentioned excitations when taking system non-linearities into account, is developed.

The active engine suspension system design has been performed making use of a virtual simulation, analysis, and verification environment providing powerful opportunities to deal with time varying system characteristics.

Except for some restrictions originating from non-linearities, feedback loop shaping technique is found to be a suitable way to achieve desired closed-loop characteristics when dealing with such MIMO system. Where all engine excitations except those corresponding to high ramping speed or extremely high nominal engine torque, are successfully dealt with. However, to guarantee closed-loop stability, two kinds of non-linearities, reflecting the time varying system characteristics, have to be taken into account. Those are non-linear material characteristics of the engine mounts and large angular engine displacements. This requires the linear H_2 control theory to be extended using a non-linear Gain Scheduling control scheme.

The effects of input saturation have been investigated using describing function analysis for two different controller implementations, using computed and applied control force for state observation. It has, unexpectedly, been found that, avoiding closed-loop self-oscillations due to input saturation requires computed control force to be used for state observation.

Acknowledgments

This work has been carried out at Volvo Car Corporation in co-operation with the Division of Automatic Control, Department of Electrical Engineering, Linköping University. Besides VCC, the Swedish Strategic Foundation has also been financially supporting this project trough the national research school ENDREA.

I am most indebted to two persons in particular, my supervisors Dr. Ahmed El-Bahrawy, manager Research and Academic Collaboration at the Department of Chassis and Vehicle Dynamics at Volvo Car Corporation, Gothenburg, and Prof. Lennart Ljung, head of the Division of Automatic Control in Linköping. Having the opportunity of working with those very ambitious persons has made me realise the power of a creative and professional research atmosphere. The quality of this work has also been substantially improved thanks to Prof. Ljung´s excellent supervision and many valuable advices, especially concerning the control theory, and by splendid guidance, careful readings, many hints and directions, and high aiming by Dr. El-Bahrawy.

I would also like to acknowledge Prof. Svante Gunnarsson, Prof. Torkel Glad, and Adj. Prof. Anders Helmersson, for taking part in many fruitful discussion meetings and, especially, Svante and Anders and Jonas Jansson for reading the manuscript.

CONTENTS

1 INTRODUCTION 1

2 STATEMENT OF THE PROBLEM 5

3 MODELLING, SIMULATION, AND ANALYSIS ENVIRONMENT 13

4 REQUIREMENT SPECIFICATION AND CLASSICAL CONTROL APPROACH 19
- 4.1 The Concept of Active Engine Suspension 19
- 4.2 Principle of the Active Engine Mounts 20
- 4.3 Excitation and Control Object Dynamics 22
- 4.4 Closed-Loop System Requirements 27
- 4.5 Loop Gain Requirements 28
  - 4.5.1 Frequency Region I 30
  - 4.5.2 Frequency Region II 31
  - 4.5.3 Frequency Region III 32
- 4.6 Closed-loop Limitations 33
- 4.7 Classical Control 33

5 LQG CONTROL OF THE LINEARISED CONTROL OBJECT 37
- 5.1 General LQG Theory 37

5.2 Controller Design 40
5.3 Comments 45

6 H_2 CONTROL OF THE LINEARISED CONTROL OBJECT 47
6.1 General H_2 Theory 47
6.2 On the Choice of Weighting Functions 48
6.3 Broad Band Control 50
  6.3.1 Initial Design 50
  6.3.2 Final "Trade-Off" Design 51
  6.3.3 Simulations 54
6.4 Narrow Band Control 60
  6.4.1 Initial Design 60
  6.4.2 Final Design 62
  6.4.3 Simulations 64
6.5 Model Order Reduction 67
6.6 Robust Stability Analysis 74
6.7 Comments 75

7 LINEAR CONTROL OBJECT AND INPUT SATURATION 77
7.1 On Controller Implementation 77
7.2 The MIMO Case 78
7.3 A SISO Case Study 83
7.4 Describing Function Analysis 87
7.5 Comments 93

8 CONTROL OF THE NON-LINEAR CONTROL OBJECT 95
8.1 Stability Trade-off Design 96
8.2 Non-linear Material Effects 97
8.3 Large Angular Displacements Effects 99
8.4 Gain Scheduling and Non-linearities 104
8.5 Gain Scheduling and Input Saturation 106
8.6 Comments 110

9 GENERAL DISCUSSION 111
9.1 Engine Excitation Characteristics 111
9.2 Feedback Signal Choice 113
9.3 AES System Characteristics 113

10 CONCLUDING REMARKS 117

APPENDIX 119
A.1 Control Object Model Data 119
  A.1.1 Rigid Bodies 119
  A.1.2 Mounts and Bushings Damping 120
  A.1.3 Mounts and Bushings Stiffnesses 120
A.2 Modified Control Object Model Data 125

- A.2.1 Mounts and Bushings Stiffnesses 125
- A.3 Linearised Control Object Model Data 127
- A.4 LQG Design Parameters 130
  - A.4.1 Initial Design 130
  - A.4.2 Final Design 131
- A.5 Broad Band H_2 Design Parameters 131
  - A.5.1 Initial Design 131
  - A.5.2 Final “Trade-Off” Design 131
  - A.5.3 Initial Design 131
- A.6 Narrow Band H_2 Design Parameters 132
  - A.6.1 Initial Design 132
  - A.6.2 Final Design 133

Bibliography 135

Notation and Symbols

A^*	complex conjugate transpose of A
$\overline{\sigma}(A)$	largest singular value of A
$\underline{\sigma}(A)$	smallest singular value of A
s	Laplace variable

Abbreviations and Acronyms

D.C.	Direct Current
E	Engine rotational frequency in Hz (defined on page 6)
LHS	Left Hand Side
RHS	Right Hand Side
TR	Torque Rod
FR	Front
RR	Rear
M_x, M_y, M_z	Torque fluctuation in x-, y- and z-direction with respect to the engines local co-ordinate system
AES	Active Engine Suspension
PES	Passive Engine Suspension
LTI	Linear Time Invariant
LTV	Linear Time Varying
LMS	Least Mean Square
FIR	Finite Impulse Response
DFT	Discrete Fourier Transform
OLHP	Open Left Half Plane
LQG	Linear Quadratic Gaussian
SIL	Software In the Loop
rpm	Revolution per minute
SISO	Single-Input Single-Output
MIMO	Multi-Input Multi-Output

1

INTRODUCTION

Legal, computational, and marketing demands on car industry are to develop more and more comfortable, safer, as well as lighter vehicles with less fuel consumption and lower emission levels to constantly decreasing lead-time and costs, and improved or, at any rate, preserved quality. To fulfil all these challenges it is unavoidable to make use of non-conventional technologies where the conventional ones have already reached their limits. Achieving better NVH (Noise, Vibration, and Harshness) comfort necessitates the use and development of ANVC (Active Noise and Vibration Control) systems when product targets are beyond the scope of traditional passive insulators, absorbers and dampers.

The present project deals with the development of a design process, a virtual simulation environment, and integrated algorithms for direct and indirect ANVC (Active Noise and Vibration Control) for car industry, where, among others, the interaction between the design process and the development environment will be illuminated.

Two approaches exist when dealing with active reduction of noise and vibration for automobiles, the direct and indirect ANVC ones. ANC (Active Noise Control) systems using loudspeakers to counteract noise originating from the road and engine excitation process are an example of the direct approach, see for instance [11, 14, 28, 31, 35]. Whereas reducing structure borne noise and vibration induced by, for instance, engines, through reducing vibrations at the excitation source, is an indirect ANVC approach. This is also one of the main objectives of traditional passive engine suspension systems [22, 23, 24, 25, 27, 42] and when using active engine mounts, the corresponding systems are referred to as AES (Active Engine Suspension) systems. Many papers have been published on development of such systems where one of the earliest work has been presented by McDonald *et al.* [20]. They describe a multi-input multi-output (MIMO) active engine vibration isolation system for attenuation of transmitted forces using the *multiple error LMS (Least Mean Square) algorithm* [6, 7, 8, 9, 10, 12, 39, 41].

The LMS control approach is one of many adaptive feedforward algorithms used to adjust the coefficients of a set of filters for cancellation of an external excitation presumed to be sinusoidal. This algorithm and a similar one referred to as the *filtered-x LMS algorithm* [40] proposed by B. Widrow are by far the most common approaches when dealing with narrow band vibration isolation, especially when the dominating excitation is deterministic. More recent work on AES systems using the adaptive feedforward approach is presented in [26, 37].

However, it seems to be more difficult to find exhaustive literature on AES systems solutions comprising feedback control. A single-input single-output (SISO) feedback solution using Linear Quadratic (LQ) state feedback control based on a simple 2 kinematic DOFs (degrees of freedoms) engine model is presented by Kim and Singh in [17]. Although feedback control is unusual when dealing with AES systems, it has been applied to other applications for active vibration isolation. In [38], Watters *et al.* describe a SISO system for broad band active vibration isolation of a boat engine based on system identification [18] and classical control methodology [21]. Yet another successful broad band feedback vibration isolation system has been presented by Spanos *et al.* [33], where machine generated disturbances on board an experimental space vehicle setup were attenuated using SISO classical control loop shaping techniques. In both papers no consideration has been taken to non-linearities in the control object. Other examples on feedback active vibration isolation systems are given in [4, 36].

When attenuating transmitted forces over a broad band of frequencies, a feedforward approach has to utilise a multitude of narrow band filters which slows down the speed of convergence. Furthermore, these filters have to be continuously adapted when the spectral contents of the excitation is changing with time. Since, in contrast to feedback control, the performance of a feedforward controller is very sensitive to errors in the phase of the control filters, this could lead to poor performance [12].

Turning to broad band feedback control, the design relies very much on the quality of the model of the control object and the main concern is to achieve closed-loop stability [19]. The design of a feedback controller is more intricate than the design of a feedforward controller, anyhow, it gives design control over the loop gain [3], and consequently ability to design to performance specification and to provide reasonable closed-loop stability guarantees. It is also possible to estimate and consequently avoid excessive measurement noise amplification outside the desired bandwidth.

Several ways to obtain a suitable model of the control object for control design exist as well as numerous different simulation environments. Traditionally, a model for control synthesis is constructed using analytical formulations of the physical process equations or system identification where closed-loop simulations are carried out involving only one code, e.g. MATLAB$^{\text{TM}}$/Simulink. Those approaches show a number of drawbacks when dealing with control systems for large (with respect to number of DOFs) physically complex control objects, or development in early design stages where no physical system exists. Other ways to acquire a model for control design are the ones based on FE (Finite Element) modelling. One such method is described by Schönhoff *et al.* in [29, 30] where a reduced order FE-model is transferred to the control design and simulation environment for design and closed-loop validation. Another one is presented by Zehn and Enzmann in [43] where the FE-model is used to construct a model for controller design but the closed-loop simulations are carried out within the FE code. Moreover, when dealing with dynamics, a control object model for control synthesis could be extracted from a multi body system analysis and simulation environment, e.g. [1], to the control design one. The controller design could then be followed by validation using closed-loop co-simulation environment where data are interchanged between the two software set-ups (for physical modelling and control design) during simulation. This is the approach that has been used in this work which proves to be very powerful, especially when dealing with non-linear dynamics.

The objective of this thesis is to investigate the potential of MIMO feedback control for broad-band vibration isolation of a 12 kinematical DOF car engine suspended using rubber mounts with non-linear material characteristics, whereas adopting model based control design using the above mentioned virtual development environment.

The organisation of the contents is as follows. Chapter 2 outlines the statement of the problem and from this, a detailed requirements specification is obtained, see Chapter 4. In Section 4.7 and Chapter 5 the potential of classical control and LQG (Linear Quadratic Gaussian) control are, respectively, investigated. For this particular problem both those control design techniques show certain deficiencies and from this investigation H_2 control is identified as a suitable design approach. Chapter 6 shows a completely linear consideration and presents a H_2 controller design for a linearised model of the control object. The effects of input saturation are investigated in Chapter 7 and the final design steps are presented in Chapter 8 where the effects of non-linearity are considered. This includes an investigation of the potential of using Gain Scheduling [34] to deal with the non-linearity. This approach is commonly applied to aircraft control where the dynamics vary dramatically with airspeed, see [15], and is found to be useful also for this problem. Finally Chapter 9 presents a general discussion followed by some concluding remarks in Chapter 10.

2

STATEMENT OF THE PROBLEM

This thesis deals with active vibration isolation of an automobile engine. The engine is a three point suspended 5-cylinder combustion diesel engine that is attached to the vehicle body at the left and right hand sides via two rubber engine mounts. Furthermore, it is also connected to the subframe via a torque rod with rubber bushings at both ends, see Figure 2.1. The engine suspension system has to support the engine at static equilibrium state, prevent large movements due to transient and low frequency road excitations, and isolate engine dynamic vibration generated by engine and road excitations for different gearing ratios in the whole range of engine rotational speed. The physical system is non-linear due to material characteristics (rubber) and large displacements.

Figure 2.1 also shows the global complete vehicle co-ordinate system as well as the local one of the engine. The vehicle co-ordinate system has its origin outside the vehicle front, its x-axis pointing longitudinally from the vehicle front to its rear, and its z-axis pointing upwards. Whereas the local engine co-ordinate system located at centre of gravity of the engine with x-axis aligned with the centre line of the crankshaft pointing towards the gearbox and z-axis being parallel with the cylinder bores pointing upwards.

At and above idle frequency the engine is subjected to internal excitation, originating from rotating and translating masses and firing gas forces. It is also externally excited at all frequencies by the road roughness via the drive shafts, the body, and the subframe. Moreover, low frequency external transient excitation (called

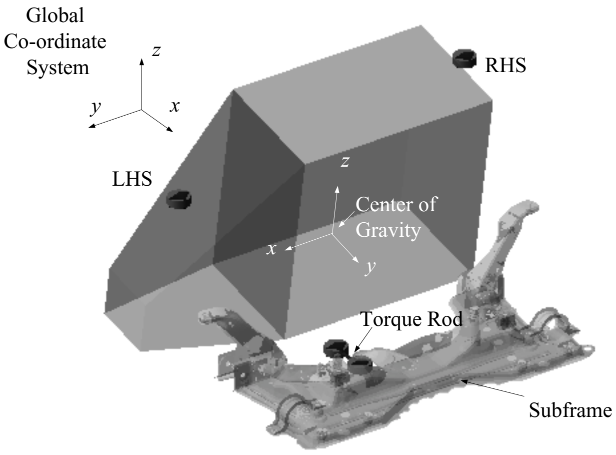

Figure 2.1 *Engine model with engine suspension layout, its connection to body and subframe, and its local co-ordinate system*

“Shunt and Shuffle”), that are generated through sudden breaking, dropped clutch, or when driving into obstacles, is also to be considered.

Internal excitation has been evaluated from measured cylinder pressure curves, specific engine loads (torque applied to breaks during gas pressure measurements), and inertial properties of engine parts (valves, pistons, balance axis, rods connecting crankshaft to the pistons, crankshaft, and piston pins) while neglecting flexibility. All internal forces are transformed to the engine centre of gravity, resulting in fluctuating moments and forces in all directions of the engine local co-ordinate system. The internal forces at the centre of gravity have been neglected since their contribution to the engine vibrations is very limited. Thus, internal engine excitation is for the most part described as fluctuating torque M_x, M_y, and M_z with respect to the engine co-ordinate system. Here M_x is the combustion fluctuating torque and M_y as well as M_z are the inertial fluctuating torque. The internal engine excitation is mainly order based. This means that for a specific engine speed, the spectral content of the excitation contains frequency components at frequencies equal to multiples of the rotational engine speed. For convenience the letter “E” is often used where: E = the rotational speed of the engine in Hz. A frequency component at 2.5 times the rotational speed is hence referred to as 2.5E.

Dealing with the internal engine excitation two load cases have been used when investigating the different control strategies. Those load cases give rise to principally different responses and are as follows:

- the idle operating condition of the specific engine at 700 rpm. Figures 2.2, 2.3

and 2.4 show the characteristics of the engine internal fluctuating torque excitation M_x, M_y, and M_z, respectively, applied to its centre of gravity relative its local co-ordinate system in frequency domain for idle operating condition, i.e. 700 rpm, and maximum idle load. As shown, for the five-cylinder engine, the spectral frequency components of high importance are related to a specific order or half of an order. The fundamental torque reaction occurs at 2.5E around x-direction (the 2.5E component of M_x torque). At idle, 2.5E corresponds to approximately 29 Hz since the ith order at N rpm fulfils the following relation:

$$f = N \cdot i/60 \tag{2.1}$$

where f is the frequency in Hz.

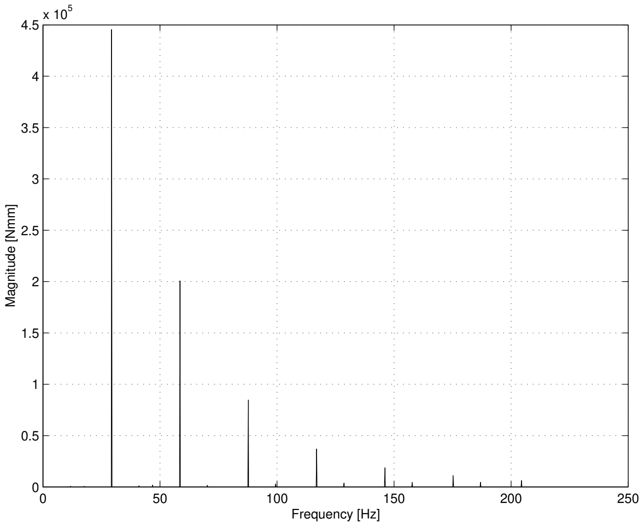

Figure 2.2 *Spectral frequency content of combustion fluctuating torque M_x at idle, i.e. 700 rpm. Frequency components from the left: 2.5E, 5E, 7.5E, etc.*

- the driving operating condition during a rotational speed 4-seconds sweep from 700 rpm, i.e. idling, to 5000 rpm. This corresponds to an acceleration of the car causing a torque applied to the engine block. This torque consists of a nominal torque depending on several parameters such as gear ratio and weight of the car and a fluctuating torque superimposed on the nominal one. Figure 2.8 shows a time history of the resulting torque, M_x, due to an acceleration of the car, including both the nominal and the fluctuating torque.

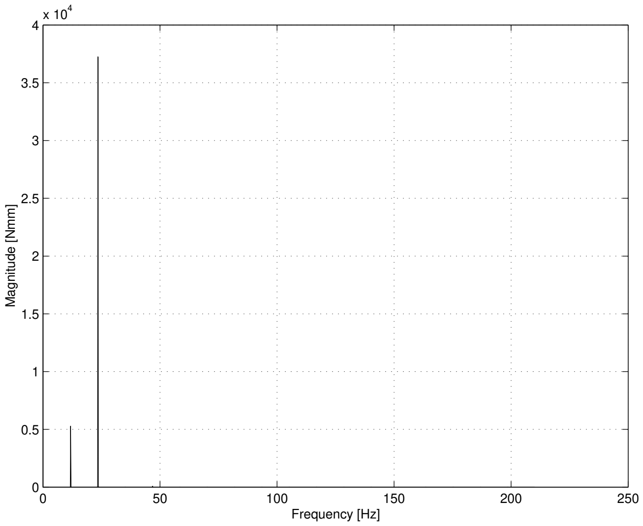

Figure 2.3 *As Figure 2.2 but for inertial fluctuating torque M_y. Frequency components from the left: 1E and 2E*

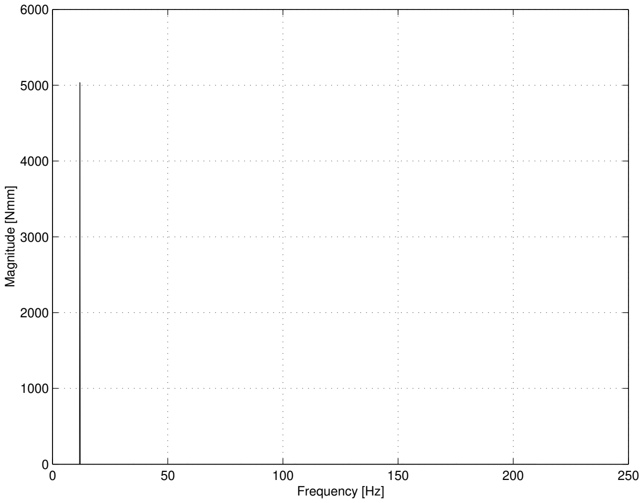

Figure 2.4 *As Figure 2.2 but for inertial fluctuating torque M_z. 1E frequency component is shown*

Figures 2.5, 2.6, and 2.7 show the frequency contents of the internal fluctuating torque M_x, M_y, and M_z, respectively, acting at the centre of gravity of the engine relative its local co-ordinate system for various rotational engine speeds. The magnitudes correspond to maximum cylinder pressure. From the figures the following observations can be made: The relative contribution of gas and mass forces to internal engine excitation, i.e. the combustion fluctuating torque M_x and the inertial fluctuating torque M_y and M_z, varies with rotational speed. M_x is to some extent relatively constant over the complete sweep range compared to M_y and M_z which increase with the square of speed dominating the excitation at high rotational speeds while M_x dominates it at low ones.

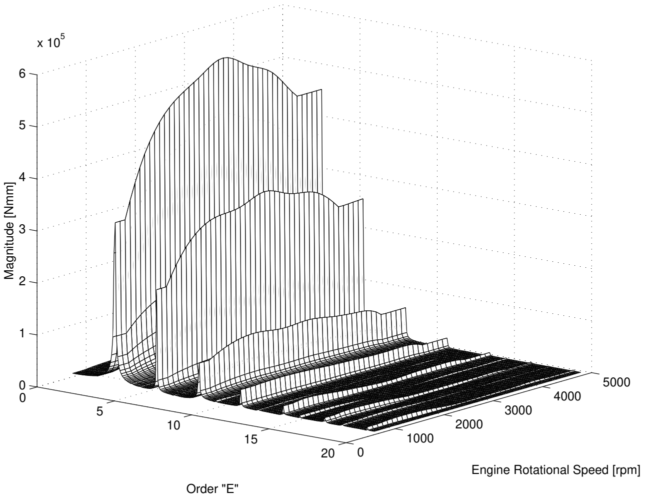

Figure 2.5 *Spectral frequency content of the combustion fluctuating torque M_x, for various rotational engine speeds and maximum load*

A typical transient “Shunt and Shuffle”-excitation has been obtained by measuring the resulting drive torque on the engine block (i.e. measured at one drive shaft) due to a dropped clutch operation. Figure 2.8 shows the time history of such a measurement.

Some prerequisites and restrictions on the problem formulation have to be taken into consideration. The specific engine suspension layout (called pendulum type layout for passive engine suspension) with its fixed connection points in the engine compartment, is the base for the investigated active suspension system. That is no redesign of the layout concept, to pay attention to others that could be more suitable for the fully active suspension, is hereby considered. Thus the active suspension elements have to be added to the existing passive ones.

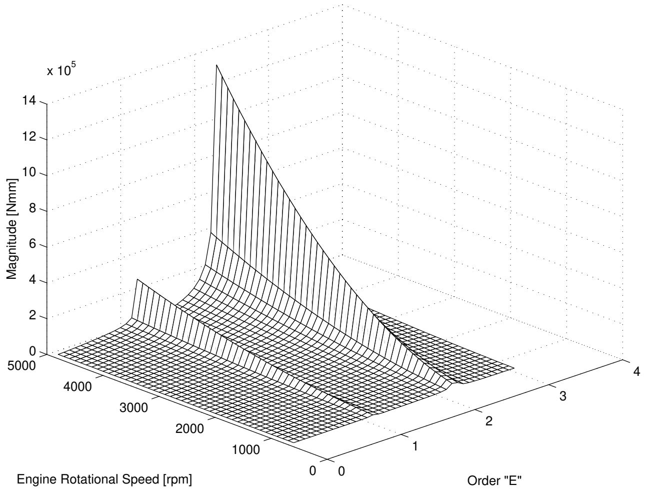

Figure 2.6 *As Figure 2.5 but for inertial fluctuating torque* M_y

Only fully active systems are considered, leaving, for instance, semi-active solutions and possible combinations of passive, semi-active, and active ones out off inquiry scope. Furthermore, the actuators are assumed ideal, e.g., no limitation on their performance, size, and energy consumption is accounted for.

The low frequency characteristics of the original passive suspension have to be preserved leaving the ability to deal with large amplitudes of vibration at low frequency, e.g. due to transient excitation.

Finally, the maximum rotational speed for the engine of interest is 5000. It is desirable that the controller could attenuate vibration levels up to the 5^{th} engine order corresponding to a frequency of 417 Hz. Hence, the bandwidth of application for the controller (here defined as the frequency range of operation with some or good attenuation) should be up to about 420 Hz. On the other hand, in all cases and to a great extent, the active system has to attenuate the dominating orders of M_x and M_y, i.e. the 2.5^{th} and the 2^{nd} order, respectively, corresponding to 208 Hz and 167 Hz at 5000 rpm.

For the above mentioned multi-input multi-output (MIMO) physical system, the problem definition is now to obtain analytically control strategy for attenuation of the total transmitted forces (in one suitably chosen direction at every suspension point) to the body and subframe. This will be done in order to handle all load cases stated above (constant engine speed, sweep in rotational engine speed, random excitation and various transient loads). The bandwidth of the controller (here defined as the frequency range of operation with some or good attenuation) should be about 450 Hz.

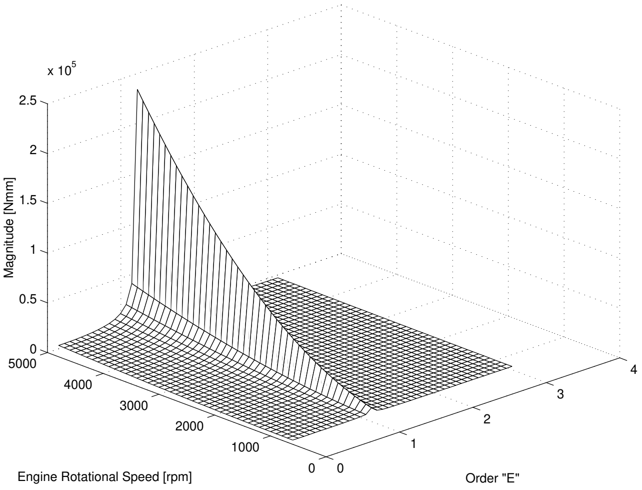

Figure 2.7 *As Figure 2.5 but for inertial fluctuating torque* M_z

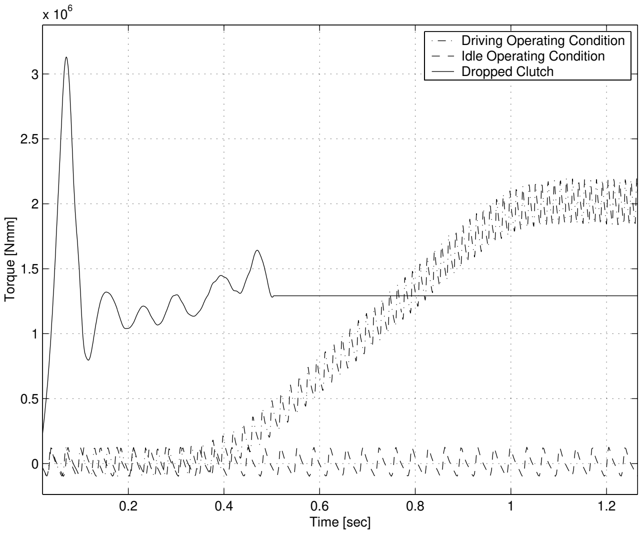

Figure 2.8 *Measured* 1^{st} *gear engine torque during a dropped clutch operation and the torque,* M_x*, corresponding to engine idle operating conditions and to an acceleration of the car, i.e. to driving operating conditions*

3

Modelling, simulation, and Analysis Environment

To deal with this problem in a proper way, it is essential to have an accurate model of the physical system (engine, engine suspension, receiver, and excitation) that comprises its frequency characteristics, its non-linearity, and its physical properties variation, and is available all the time for control strategy analysis, development, and verification in time domain. This will have a large impact on controller synthesis, performance, and stability verifications.

Two different software packages have been used for physical modelling of the engine and its suspension system (see Figure 3.1), control system modelling and design of controller, and virtual verification of outcomes, i.e. control algorithms. They are

- a multi body system analysis and simulation software for dynamics (ADAMS) [1]
- a real-time analysis and simulation software for control synthesis (MATLAB™/ Simulink)

The physical system has been modelled in ADAMS making use of masses, springs, and dampers with clamped free ends (see Appendix A.1). Rigid bodies, with centers of gravity, masses, and moments of inertia, have been used for modelling of the engine and the torque rod, giving an analysis model with 12 kinematical degrees of freedom (DOFs). The engine mount at left and right hand side

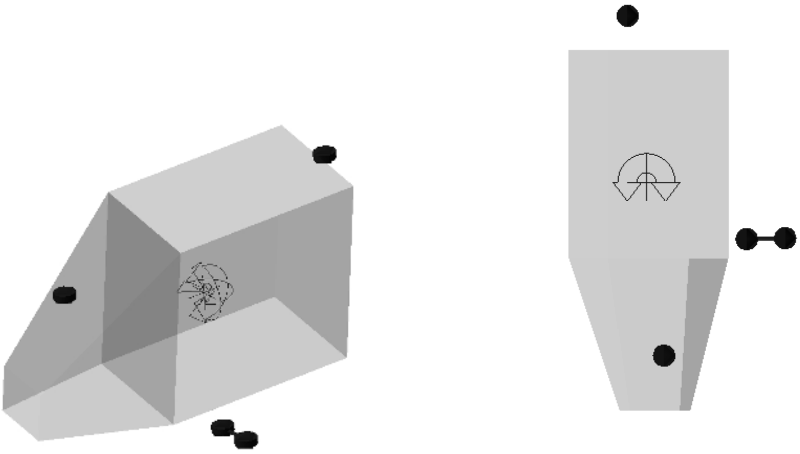

Figure 3.1 *Rear isometric view (left) and top view (right)*

of the engine, as well as the bushings connecting the torque rod to the engine and the subframe are modelled using 6DOFs (three translational and three rotational) spring and damper elements with non-linear stiffness and linear damping characteristics in all directions and clamped free ends. Thus, the body and subframe attachment points are regarded as rigid in all directions. However, the dynamic stiffness of the connecting subsystems are, in practice, limited, and considering this matter could be an extension to the work done.

Having created a model of the system of interest, ADAMS could be used for time domain analysis. This is done using time integration of the equations of motion automatically created by ADAMS. Non-linear systems as the one studied here is represented in ADAMS by non-linear first order differential equations generally written

$$\begin{aligned} \dot{x} &= f(x,u,m) \\ z &= h(x,u,m) \end{aligned} \tag{3.1}$$

The control object, i.e. the engine, is defined as a physical dynamical system with well-defined inputs (excitations) and outputs (responses). The inputs to the control object are the internal excitation (m in (3.1)) as well as the outputs of the controller (u in (3.1) are the forces from the active force actuators) whereas the inputs to the controller are the responses of the control object (z in (3.1) are the total transmitted forces in the three clamped suspension points in the direction of the actuators). A more thorough description of the control object inputs and outputs is given in Section 4.1. After definition of inputs and outputs, the chosen analysis

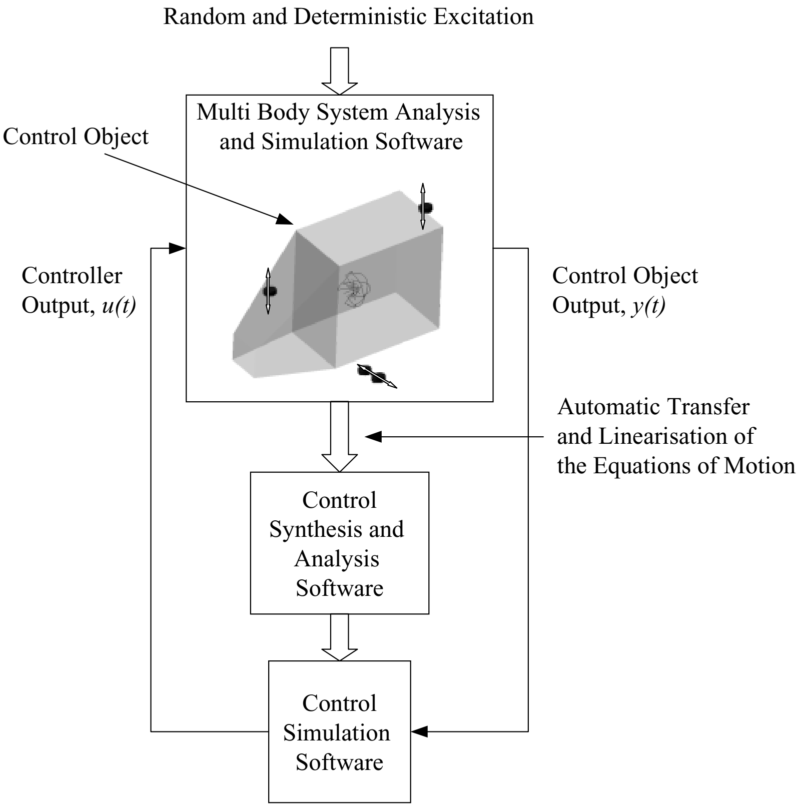
Random and Deterministic Excitation
Multi Body System Analysis and Simulation Software
Control Object
Controller Output, u(t)
Control Object Output, y(t)
Automatic Transfer and Linearisation of the Equations of Motion
Control Synthesis and Analysis Software
Control Simulation Software

Figure 3.2 *Analysis, closed-loop simulation, and verification environment*

and verification environment offers a possibility to linearise the equations of motion for the control object around any given working-point automatically [32]. A linearised model of the control object obtained using this approach is a minimal realisation in state space representation according to (3.2). Such representation could then be imported into MATLAB™ and used for control synthesis. However, the linearisation is only guaranteed to be valid for small amplitudes variations around a specific operating point chosen for linearisation. Figure 3.3 demonstrates differences in responses between non-linear and linearised control object when subjected to the "Shunt and Shuffle" excitation with large signal amplitudes.

$$\begin{aligned} \dot{x} &= Ax + Bu + Nm \\ z &= Cx + Du \end{aligned} \tag{3.2}$$

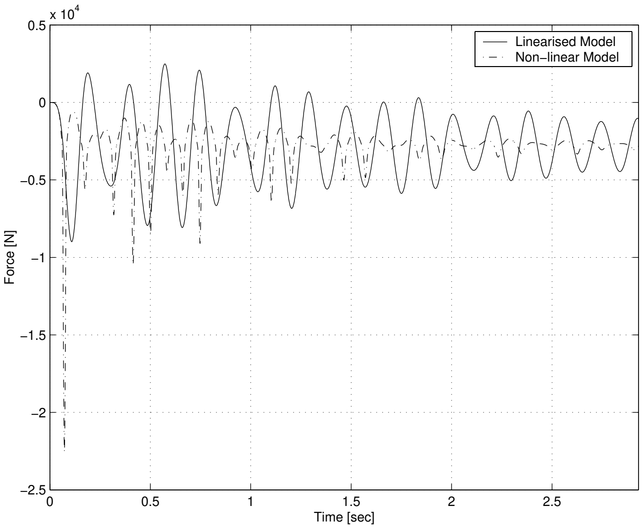

Figure 3.3 *The control object output at the torque rod due to the "Shunt and Shuffle" excitation applied to the non-linear physical model and a linearisation of it, demonstrating the poor agreement between the responses*

Designing a controller for a non-linear control object based on a linearised model according to (3.2), it should be evaluated with respect to the original model using closed-loop time domain simulations. The above-mentioned two software packages could be used to perform such an evaluation where data are interchanged between them during simulation. The multi-body system analysis and simulation software solves the equations of motion for the non-linear physical system (3.1) while the real-time simulation software solves the linear and possibly non-linear equations of the controller. This principle is here referred to as

- *co-simulation* or *software in the loop simulation* (SIL),

and is schematically shown in Figure 3.2. This closed-loop analysis, simulation, and verification environment has been identified as one of the most desirable and efficient ones when fulfilling the above mentioned demands.

The virtual environment for closed-loop simulation, analysis, and verification, has the advantage of accurate and time efficient managing of large physical models, broadband frequency characteristics, flexible structures, non-linear physical systems, generation of equations of motion, synthesis and analysis of control algorithms, general input/output relationship, and mathematical optimisation when dealing with development and verification of actively controlled structures using the same reference system model.

Even though this environment provides a good possibility to model the physical system very accurately, there will always be some discrepancies between the true physical system and the modelled one. Thus, it is necessary to consider the model uncertainties when dealing with control synthesis and analysis.

4

REQUIREMENT SPECIFICATION AND CLASSICAL CONTROL APPROACH

4.1 The Concept of Active Engine Suspension

The control object is described by (3.1) where m is a column vector having three elements and represents the internal engine excitation, i.e. the three components of the fluctuating torque, and u and z are the control object inputs and outputs respectively (both are 3x1 vectors). Those are presented as follows

$$m(t) = \begin{bmatrix} M_x(t) \\ M_y(t) \\ M_z(t) \end{bmatrix}, z(t) = \begin{bmatrix} F_{\text{tot}}^{\text{LHS}}(t) \\ F_{\text{tot}}^{\text{RHS}}(t) \\ F_{\text{tot}}^{\text{TR}}(t) \end{bmatrix}, u(t) = \begin{bmatrix} F_{\text{actuator}}^{\text{LHS}}(t) \\ F_{\text{actuator}}^{\text{RHS}}(t) \\ F_{\text{actuator}}^{\text{TR}}(t) \end{bmatrix} \tag{4.1}$$

The active inputs to the control object, i.e. the controller outputs, are two forces that act in z-direction (with respect to the engine local co-ordinate system) in parallel to the LHS and RHS engine mounts (called $F_{\text{actuator}}^{\text{LHS}}$ and $F_{\text{actuator}}^{\text{RHS}}$ respectively), and a force that acts in the longitudinal direction of the torque rod in parallel to its rear bushing (called $F_{\text{actuator}}^{\text{TR}}$), see Figure 4.1. These forces could in reality be generated by for example electrodynamic actuators. The outputs of the control object are the total resultant transmitted forces (also the sum of the controller outputs and the forces in the passive mounts) in the three clamped suspension points in the actuators direction: $F_{\text{tot}}^{\text{LHS}}$, $F_{\text{tot}}^{\text{RHS}}$ and $F_{\text{tot}}^{\text{TR}}$. The above chosen directions of actuators application are due to the fact that the body (also the receiver) is most sensitive in z-direction at the LHS and RHS mounts, and that the torque rod only transmits longitudinal forces.

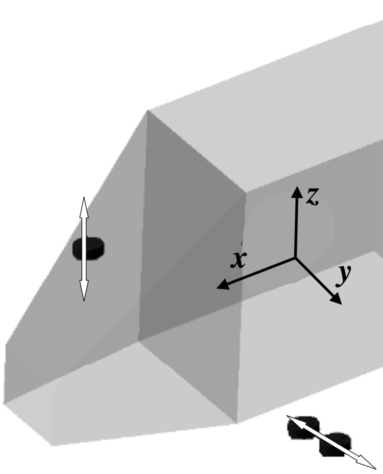

Figure 4.1 *Schematic picture of actuators location and directions of action*

As mentioned, the internal engine excitation M_x, M_y, and M_z, are applied to the model at the center of gravity.

4.2 Principle of the Active Engine Mounts

As mentioned, the AES system solution presented in this work is based on active engine mounts schematically shown using a simplified SISO model in Figure 4.2, where F_s is the actuator force and F_p corresponds to the internal and external engine excitation. M is the mass of the engine, K and C are the stiffness and damping of passive isolation elements in parallel to the actuator, i.e. representing a passive mount, x is the mass displacement relative the static equilibrium position, and F_y represents a feedback controller force. For an AES system with main objective to suppress spectral components of excitations at and above the natural frequencies of the passive engine suspension system, this configuration has certain good properties, e.g. low required actuator forces [12].

To illustrate the effects of force feedback and the chosen active principle of operation, we shall derive relations between the required actuator force F_s and displacement of the mass x due to an excitation F_p, for a one dimensional case. The receiver (representing the body and subframe) is assumed to be clamped. The

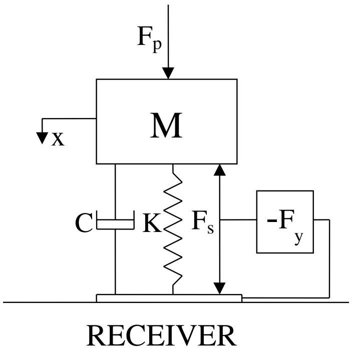

Figure 4.2 *Schematic picture of the principle of operation of the active engine mounts*

chosen feedback signal F_{tot}, is the total force applied to the receiver, i.e. the sum of the mount forces and the actuator force according to (4.2).

$$F_{tot} = (Kx + sCx + F_s) \tag{4.2}$$

The actuator force using negative feedback F_y is then

$$F_s = -F_y F_{tot} = -Fy(Kx + sCx + F_s) = \frac{-F_y\,(K + sC)\,x}{1 + F_y} \tag{4.3}$$

where s is the Laplace variable. Increasing F_y towards infinity, the required actuator force becomes

$$\lim_{F_y \to \infty} F_s = -\,(K + sC)\,x \tag{4.4}$$

which is equal to the force in the passive isolation stage except for having opposite phase, i.e. the active force will cancel the spring and damper forces.

Turning to the forced closed-loop response of the mass in Figure 4.2 when subjected to excitation F_p and the controller output F_s, it could be described by

$$Ms^2x + sCx + Kx = Fp - Fs \tag{4.5}$$

Equations (4.3) and (4.5) give

$$x = \frac{F_p}{\left(Ms^2 + \frac{sC+K}{1+F_y}\right)} \tag{4.6}$$

From Equation (4.6) it is clear that, when increasing the feedback gain, the poles of the transfer function from the primary force to the displacement move towards the origin and the closed-loop system will eventually reach the margin of stability, and also that, it is not possible to achieve complete cancellation of the transmitted forces at low frequencies. A cancellation of low frequency spectral components of the transmitted forces implies large displacements of the mass and consequently large actuator forces, see (4.4). Furthermore, the closed-loop effect of high feedback gain could also be described via the equation in terms of decreased equivalent stiffness and damping. This means lower natural frequency as well as higher amplitude of vibrations of the mass at low frequencies but lower at high frequencies, where high and low frequencies are relative to the natural frequency of the passive system.

As mentioned before the low frequency characteristics of the original passive engine suspension system have to be preserved since they already are satisfactory. Some of these desired low frequency characteristics are the ability of the engine suspension to deal with transient excitations, e.g “Shunt and Shuffle” excitation, without generating large engine displacements and also to maintain the handling characteristics of the vehicle. Beyond the possibility for large displacements to cause physical contact between the engine and other components inside the engine compartment, they also negatively affect the transmission.

Other reasons to preserve the passive engine suspension characteristics at low frequencies is what has been shown above, regarding the chosen principle of active mounts, where a controller attenuating low frequency excitation could cause large amplitude vibrations and will require very high power. Summing up, the controller designed in this paper for engine vibration isolation, should not introduce forces to the system at low frequencies. In other words,

- *the feedback law F_y must have low gain at low frequencies*

4.3 Excitation and Control Object Dynamics

To begin with, the equations of motion of the non-linear control object is linearised around static equilibrium position to obtain a suitable model for controller design.

Including sensor noise n in the linearised control object representation (3.2), it could also be written as

$$\begin{aligned} z &= Gu + w \\ y &= z + n \end{aligned} \tag{4.7}$$

where w represents the internal engine and external road excitations transformed to the output of the system, u represents the actuator forces (F_s in Figure 4.2) and z the total forces acting on the receiver (F_{tot} in (4.2)). From (3.2) and (4.7) it is clear that the relation between w and m is

$$w = G_m m \tag{4.8}$$

where

$$G_m(s) = C(sI - A)^{-1}N \tag{4.9}$$

In (4.9) s is the Laplace variable. The transfer function of the linearised control object G has nine elements according to (4.10). Those transfer function elements are given in Appendix A.3 together with the matrix N in (4.9).

$$G = \begin{bmatrix} G_{11} & G_{12} & G_{13} \\ G_{21} & G_{22} & G_{23} \\ G_{31} & G_{32} & G_{33} \end{bmatrix} \tag{4.10}$$

Figures 4.3 and 4.4 show a Bode diagram and an impulse response of the element G_{11}. The singular values [13] of G are presented in Figure 4.5. For a MIMO control object transfer function, the upper and lower gain boundaries are given by its singular values. The many peaks in the Bode Diagram and in the singular values plot correspond to the natural modes of the engine. Notice that, due to the chosen principle of the active engine mounts with actuators in parallel to passive ones, the gain is very low at low frequencies and equal to one at high frequencies.

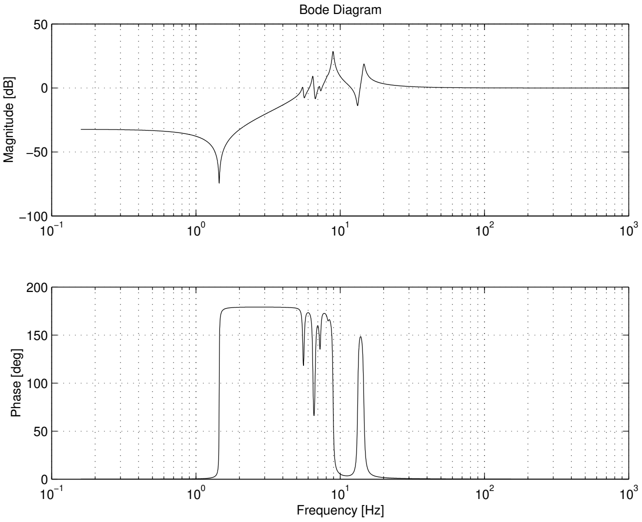

Figure 4.3 *Bode Diagram of G_{11} in (4.10)*

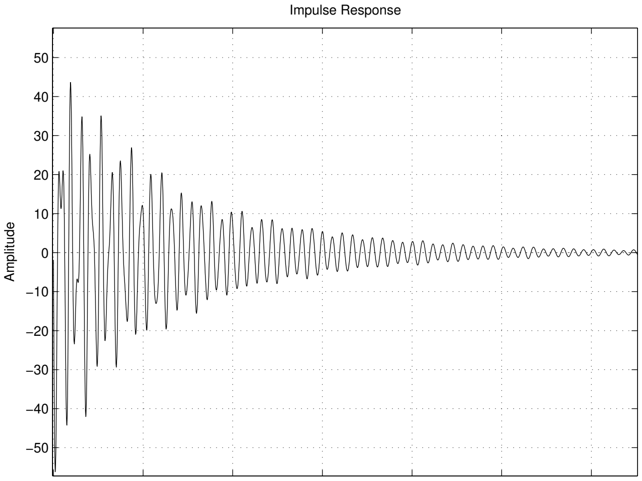

Figure 4.4 *Impulse response of G_{11} in (4.10)*

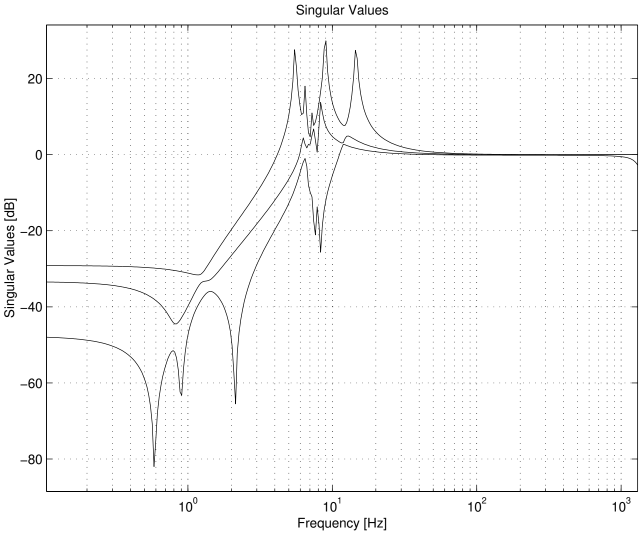

Figure 4.5 *The singular values of the transfer function of the control object G in (4.7)*

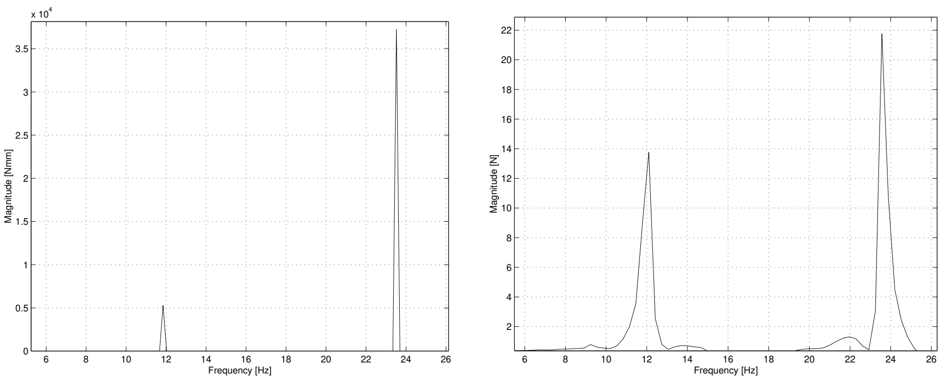

Figure 4.6 *Spectrum of M_y (left) and of the corresponding control object output at RHS (right)*

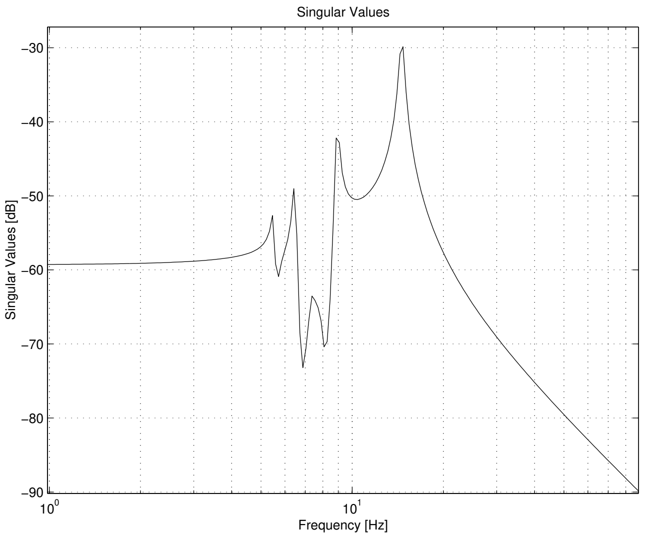

Figure 4.7 *Magnitude of the control object transfer function from excitation M_y to the RHS output, i.e. element (2,1) of G_m in (4.9)*

Consider the DFT (Discrete Fourier Transform) of M_y for excitation corresponding to engine idle operating condition and of resulting open-loop non-linear control object output at RHS, see Figure 4.6. The figure shows that the difference in magnitude between the excitation spectral components E and 2E is larger than the corresponding one of the response. This is due to the fact that, the frequency of both E and 2E is being close to some natural frequencies of the control object where the magnitude of its transfer function, see Figure 4.7, is higher at E than at 2E, reflecting the control object dynamics. Hence, engine excitation orders of importance to suppress could not be determined only by looking at the spectral contents of the excitation without considering the control object dynamics. Evaluating the response of the control object when subjected to internal engine excitations corresponding to idle and driving operating conditions shows that orders 1, 2, 2.5, and 5, are all important and have to be taken into consideration.

4.4 Closed-Loop System Requirements

We now introduce linear negative feedback control according to

$$u = -F_y y \tag{4.11}$$

(4.11) inserted into (4.7) gives the following relations for the closed-loop system

$$\begin{aligned} z &= Sw - Tn \\ u &= T_{uw}(w + n) \end{aligned} \tag{4.12}$$

Here S is the sensitivity function defined as

$$S = (I + GF_y)^{-1} \tag{4.13}$$

and T is the complementary sensitivity function denoted as

$$T = (I + GF_y)^{-1} GF_y \tag{4.14}$$

The definitions of the sensitivity and the complementary sensitivity are well known and could be found in e.g. [13]. Furthermore, the output of the controller due to w is determined by the transfer function from w to u, here denoted T_{uw} where

$$T_{uw} = -F_y (I + GF_y)^{-1} \tag{4.15}$$

The closed-loop requirements could be summarised in terms of the singular values of:

- **(R1)** S, determining the attenuation of the excitation. As mentioned earlier, the ability of the original passive suspension system to deal with large amplitude vibrations at low frequencies has to be preserved. This means that the low frequency characteristics have to be left unaffected implying that every singular value of S should be approximately equal to one below 1E for idle engine operation (frequency of first engine firing order), i.e. below approximately 11.7 Hz. Moreover, the singular values of S should ideally be very small in the frequency range where attenuation is needed, i.e. from approximately 11.7 Hz for 1E at idle operation to about 420 Hz. These requirements on S are pretty unusual, the singular values of S are normally required to be small for low frequencies up to some specific frequency determining the bandwidth of the closed-loop system.
- **(R2)** T, determining the propagation of sensor noise. These should ideally be small everywhere. T has to be small for high frequencies where the signal-to-noise ratio is low. The infinity norm of T also determines the degree of robust stability with respect to model uncertainties and should therefore be kept as small as possible.
- **(R3)** T_{uw}, determining the necessary control power. This requirement emerges from the fact that actuators and power sources are limited and that the low frequency characteristics should be preserved. The largest singular value of T_{uw} should therefore be very small for frequencies below 1E at idle engine operation. To begin with, the actuators are assumed ideal and therefore no bound is put on the control energy for frequencies above approximately 11.7 Hz. However, the singular values of T_{uw} should of course be kept as small as possible in the complete frequency range.

Figures 4.8, 4.9 and 4.10 visualise the closed-loop requirements in terms of the singular values of S, T and T_{uw}. The singular values of the open-loop transfer function G from u to z are superimposed.

4.5 Loop Gain Requirements

To make it easier to estimate the possibility of fulfilling the requirements, it is useful to convert the closed-loop requirements into requirements on the loop gain. For classical control synthesis as well as for modern control synthesis, it is also important to know approximately the ideal shape of the loop gain approximately. Since the control object has three inputs and three outputs, it is suitable to specify the requirements in terms of singular values. In order to guarantee that a specific loop gain implies the required closed-loop characteristics, it is also important to cluster the singular values. Due to the shape of the bounds for the singular values (see Figures 4.8, 4.9 and 4.10 for the closed-loop requirements), it is relevant to formulate the requirements for the open-loop gain with respect to the three frequency ranges defined according to Figure 4.11.

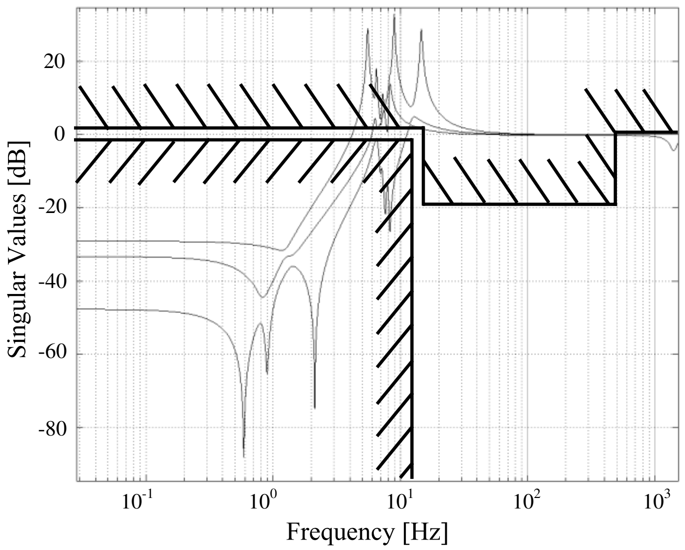

Figure 4.8 *Boundary for the singular values of S,* ▨ *= forbidden area*

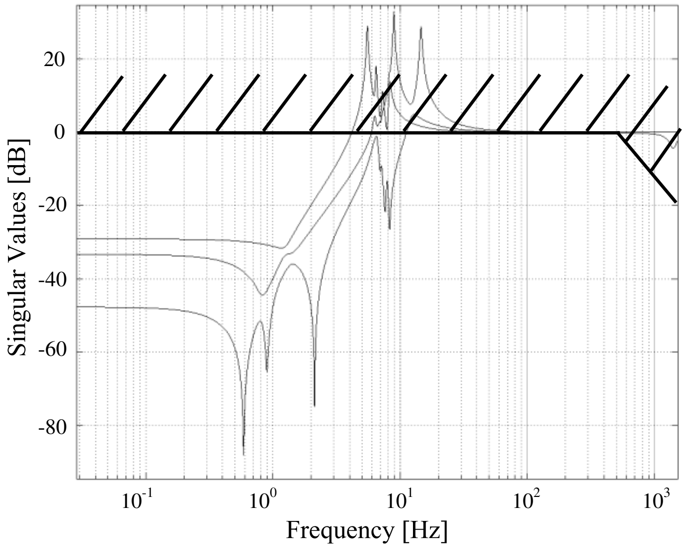

Figure 4.9 *Boundary for the singular values of T,* ▨ *= forbidden area*

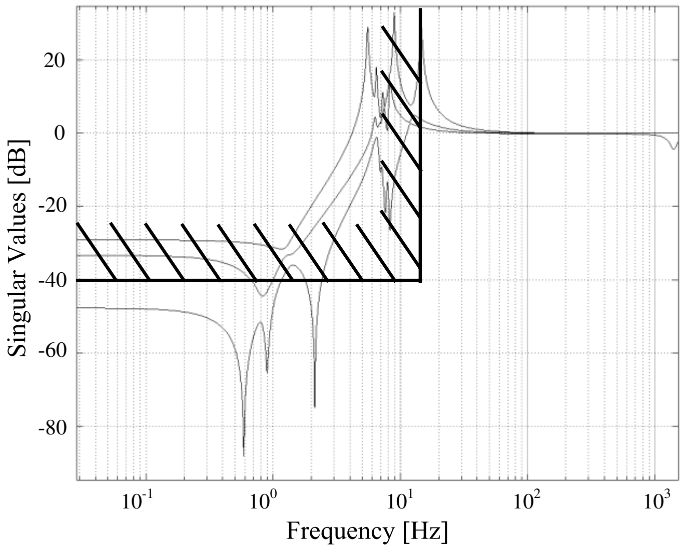

Figure 4.10 *Boundary for the singular values of T_{uw}, ▨ = forbidden area*

4.5.1 Frequency Region I

In frequency region I, the singular values of S should all be close to one. The largest singular value of S is

$$\overline{\sigma}(s) = \overline{\sigma}((I + GF_y)^{-1}) = 1/\underline{\sigma}(I + GF_y) \leq 1/(1 - \overline{\sigma}(GF_y)) \qquad (4.16)$$

The requirements on S (i.e. (R1)) and (4.16) imply that

$$\overline{\sigma}(GF_y) << 1 \qquad (4.17)$$

in this frequency range. To keep the singular values of T limited in consistency with requirement (R2) it is required that

$$\overline{\sigma}(T) = \overline{\sigma}(GF_y(I + GF_y)^{-1}) \leq \overline{\sigma}(GF_y)/(1 - \overline{\sigma}(GF_y)) << 1 \qquad (4.18)$$

is small. This corresponds to (4.17). Moreover, for the largest singular values of T_{uw} it holds

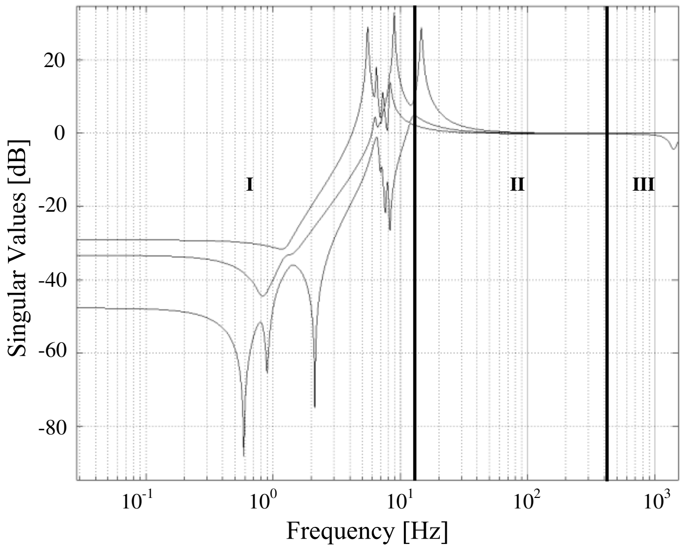

Figure 4.11 *Definition of the frequency ranges, I, II and III, to which the open and closed-loop requirements are defined with respect*

$$\overline{\sigma}(T_{uw}) = \overline{\sigma}(F_y S) \leq \overline{\sigma}(F_y)/\underline{\sigma}(I + GF_y) \leq \overline{\sigma}(F_y)/(1 - \overline{\sigma}(GF_y)) \tag{4.19}$$

(4.17) together with (4.19) and requirement (R3) give now an additional requirement for

$$\overline{\sigma}(F_y) << 1 \tag{4.20}$$

in region I.

4.5.2 Frequency Region II

In frequency region II, the requirements are different from the requirements in region I. (R1) gives

$$\overline{\sigma}(S) = \overline{\sigma}((I + GF_y)^{-1}) = 1/\underline{\sigma}(I + GF_y) \leq 1/(\underline{\sigma}(GF_y) - 1) \tag{4.21}$$

Equation (4.21) and (R1) imply

$$\underline{\sigma}(GF_y) >> 1 \tag{4.22}$$

From (4.18) it is clear that in order to keep the largest singular value of $T << 1$, condition (4.17) has to be fulfilled. Requirement (R2) is hence in conflict with (R1) in frequency region II. For the largest singular values of T_{uw}, taking the requirement (4.22) (since (R1) is the most important requirement in this frequency region) into account, the following holds

$$\begin{aligned} \overline{\sigma}(T_{uw}) = \overline{\sigma}(F_y S) \leq \overline{\sigma}(F_y)/\underline{\sigma}(I + GF_y) \leq (F_y)/(\underline{\sigma}(GF_y) - 1) \\ \approx \overline{\sigma}(F_y)/\underline{\sigma}(GF_y) \leq 1/\underline{\sigma}(G) \end{aligned} \tag{4.23}$$

From (4.23) it is clear that if the smallest singular value of S is far less than one, the largest singular value of T_{uw} depends mainly on the smallest singular value of G which of course is impossible to affect.

4.5.3 Frequency Region III

For frequency region III the main requirement (R2) concerns the largest singular value of T which is supposed to be kept less than one. From (4.18) it is known that this implies a condition according to (4.17). From (4.16) it is seen that this is consistent with requirement (R1) stating that the singular values of S should be close to one. From (4.19) and (4.20) it is known that in order to keep the control energy low during the circumstances specified by (R1) and (R2), it is needed that

$$\overline{\sigma}(F_y) << 1 \tag{4.24}$$

The loop gain requirements could now be summarised. In frequency region I, $\overline{\sigma}(GF_y)$ and $\overline{\sigma}(F_y)$ are required to be far less than one. In region II, there has to be a trade-off between good excitation attenuation ($\underline{\sigma}(GF_y) >> 1$) and satisfactory sensor noise propagation ($\overline{\sigma}(GF_y) << 1$). For frequencies in region III, $\overline{\sigma}(GF_y)$ is again required to be less than one. From (4.17) and (4.20) it is seen that the largest singular value of the open-loop gain must be less than the largest singular value of G in order to utilise small control energy in frequency region I. This could be realised through noticing that $\overline{\sigma}(F_y) << 1$ and moreover

$$\overline{\sigma}(GF_y) \leq \overline{\sigma}(G)\overline{\sigma}(F_y) \tag{4.25}$$

and thus $\overline{\sigma}(GF_y) << \overline{\sigma}(G)$. Furthermore it is desired to keep $\overline{\sigma}(F_y)$ small everywhere in order to minimise the control energy. The requirement for the open-loop gain is visualised in Figure 4.12, showing the bounds for the ideal open-loop gain.

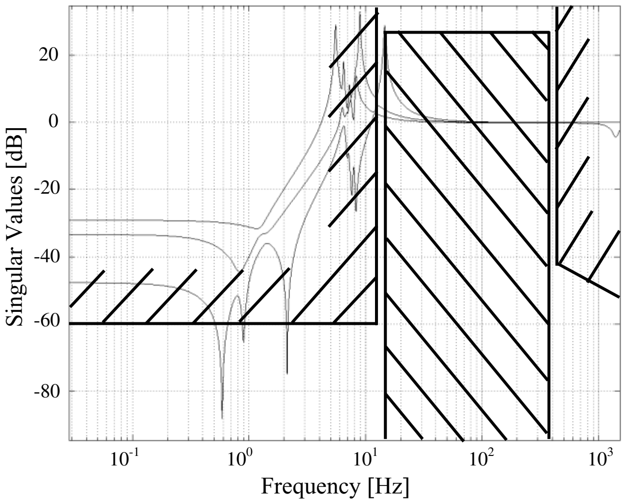

Figure 4.12 *The requirements on the singular values of the loop gain,* GF_y*,* ▨ *= forbidden area*

4.6 Closed-loop Limitations

From Figure 4.12 it is clear that the requirements put on the singular values of the open-loop gain GF_y, are not realistic. For example, the sharp transitions between the different frequency regions (defined by Figure 4.11) are not possible without a very high order controller. As mentioned earlier, there is also a trade-off between attenuation of excitation (from road and engine) and measurement noise propagation (since $S + T = I$). Moreover, if the largest singular value of S is less than one in some frequency range it must be larger than one elsewhere. The model of the engine (3.2) contains two zeros in the RHP, i.e. a so called non-minimum phase system. These zeros imply even stronger limitations on S. Such discussion about limitations can be formalised by some well known relations, e.g. Bode's sensitivity integral relation and Poisson integral formula (see, for instance, [13] and [44]).

4.7 Classical Control

Dealing with feedback control design, the techniques associated with the *classical control* theory should be tried first. Those techniques were originally developed for design of simple SISO feedback controllers and implies working with the loop gain to achieve certain closed-loop characteristics. Knowing the required characteristics of the loop gain, the design is normally carried out in two stages: first a controller $F_y(s)$ is chosen so that the desired loop gain, $|G(s)F_y(s)|$, is achieved and then, sufficient gain and phase margins are guaranteed by adjusting the phase of $F_y(s)$. Usually, the two steps interfere with each other, and the design becomes iterative, including repeated assessments based on visualisations of $G(s)F_y(s)$ using Nyquist and Bode diagrams.

The SISO classical control techniques have been generalised for the MIMO case and two common methods for MIMO feedback control design using the SISO classical control approach are [19]:

- the characteristic-locus method
- the Nyquist-array method

Both methods are based on the generalised Nyquist stability criterion and rely on the success of a preliminary decoupling stage with objective to convert the MIMO problem to a set of independent SISO problems. The next step consists of designing SISO controllers for those independent SISO loops. Visual inspection is used to identify the appropriate SISO controllers for both methods. The names of the methods indicate the diagrams used to assess the design, i.e. the characteristic-locus plot [19] and Nyquist arrays with Gershgorin bands [19], respectively. The Nyquist arrays with Gershgorin bands is a way to describe the characteristic-locus approximately, which means that the Nyquist array method is likely going to generate a more conservative design.

The classical control techniques mentioned above are useful when the main objectives is to guarantee closed-loop stability, but show severe limitations when the required loop gain varies strongly with frequency, which is the case for the problem of interest (see Figure 4.12). It is not possible to pay attention to the closed-loop stability when shaping the loop gain, and since adjustment of the phase also affect the loop gain, the design process becomes iterative and difficult. Moreover, the initial decoupling can only be done for one specific frequency which affects the performance and the closed-loop stability in an unpredictable way.

A MIMO feedback control design has been attempted using the classical control techniques. However, many of the drawbacks associated with the classical techniques were soon revealed. Consider the singular values of transfer function of the control object (G in (4.7)) shown in Figure 4.13. To achieve 20 dB attenuation in the major part of frequency region II (see Figure 4.11), the gain of the controller F_y, must be approximately 10. Figure 4.14 shows the sensitivity S, when using a diagonal feedback controller with constant gain 10, i.e. $F_y = -10I$. Clearly, a lot of frequency dependency has to be built in to the feedback controller to achieve the desired closed-loop requirements. It turns out to be extremely hard to select frequency dependant SISO controllers that gives closed-loop stability together with acceptable performance. Even if it is possible to manually choose a feedback controller using the classical control techniques, the process is extremely time consuming. For this particular problem it seems to be impossible to design a MIMO feedback controller without support to achieve stability while shaping the loop gain within a reasonable time period.

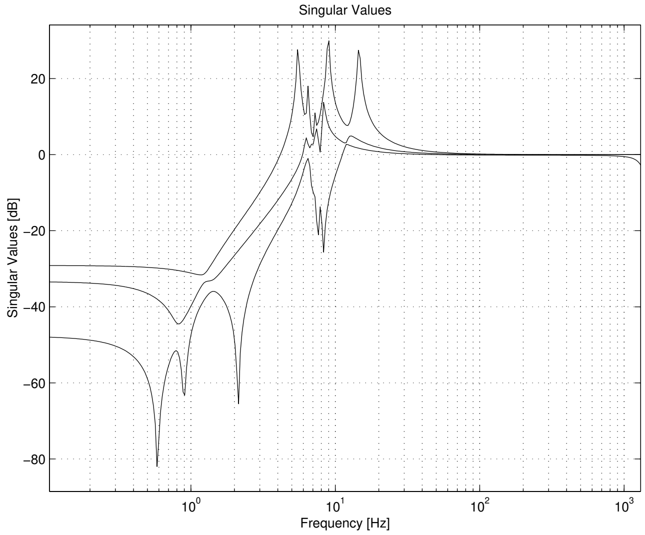

Figure 4.13 *The singular values of the transfer function of the control object G in (4.7)*

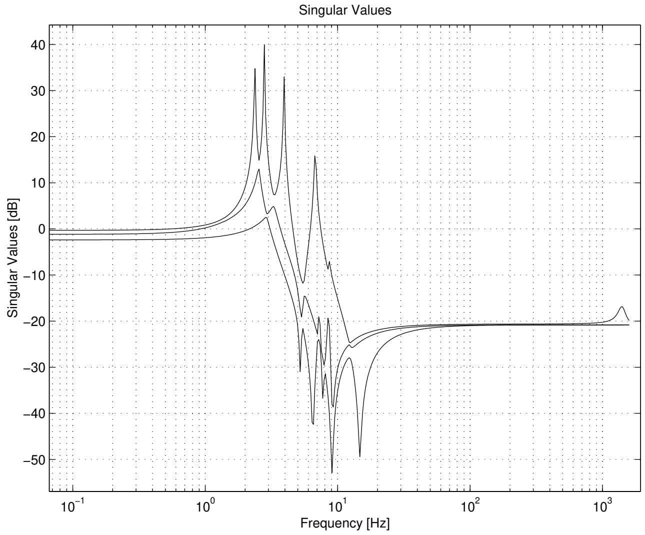

Figure 4.14 *The singular values of S when $F_y = -10 * I$*

5

LQG Control of the Linearised Control Object

5.1 General LQG Theory

Linear Quadratic Control (LQG) theory is well known and described in text books on control theory [13, 19]. In contrast to the classical control methods, involving graphical manipulation of frequency responses, e.g. the characteristic locus or the Nyquist arrays with Gershgorin bands, LQG methodology is based on certain time domain criteria. Moreover, this method, part of the *modern control* theory, allows loop gain shaping to achieve required performance and robustness while providing stability automatically. The set-up for LQG control synthesis and analysis is presented in Figure 5.1 where the control object G is represented by

$$\begin{aligned} \dot{x} &= Ax + Bu + Nm \\ z &= Cx + Du \\ y &= Cx + Du + n \end{aligned} \tag{5.1}$$

or equivalently

$$\begin{aligned} z &= Gu + w = Gu + G_m m \\ y &= z + n \end{aligned} \tag{5.2}$$

where G_m is described by (4.9). The only difference between (5.1) and (5.2), and the previously introduced representation of the linearised model of the control object (3.2) is the noise n, introduced by measurements of z.

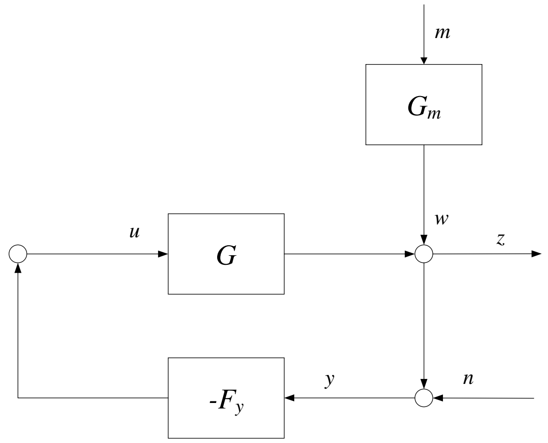

Figure 5.1 *General feedback configuration and set-up for LQG control synthesis*

Assuming normally distributed white noise excitation m and measurement noise n with constant spectral densities R_m and R_n, respectively, the LQG controller is then the feedback controller F_y in Figure 5.1 which minimises the cost function

$$\begin{gathered} J = \|z\|_Q^2 + \|u\|_R^2 = \\ \lim_{T\to\infty} \frac{1}{2T} \int_{-T}^{T} \left(z^T(t) Q z(t) + u^T(t) R u(t) \right) dt \end{gathered} \tag{5.3}$$

The tuning parameters R_m, R_n, Q, and R are used to achieve desired closed-loop characteristics, where the most basic LQG design uses constant parameters. Yet, frequency dependent parameters could be applied using augmentation. Thus, introducing

$$Q(i\omega) = W_z^T(i\omega)W_z(i\omega) \tag{5.4}$$

$$R(i\omega) = W_u^T(i\omega)W_u(i\omega) \tag{5.5}$$

(5.3) could be expressed as [19]

$$J = \frac{1}{2\pi}\int_{-\infty}^{\infty} \mathrm{Tr}\,(W_z\Phi_z(i\omega)W_z^* + W_u\Phi_u(i\omega)W_u^*)d\omega \tag{5.6}$$

where $\Phi_z(i\omega)$ and $\Phi_u(i\omega)$ are the spectral densities of z and u, respectively. Furthermore, m and n could be modelled as outputs of transfer functions W_m and W_n driven by noise as

$$m = W_m(i\omega)v_1 \tag{5.7}$$

$$n = W_n(i\omega)v_2 \tag{5.8}$$

where v_1 and v_2 are normally distributed uncorrelated white noise processes having spectral densities R_1 and R_2, respectively. Then, by theory for linear signal processing [13], the spectral densities of m and n could be expressed as

$$\Phi_m = W_m R_1 W_m^* \tag{5.9}$$

$$\Phi_n = W_n R_2 W_n^* \tag{5.10}$$

which together with (5.2) imply that the spectral density of w, i.e. the excitation m transformed to the output of the control object, is

$$\Phi_w = G_m W_m R_1 W_m^* G_m^* \tag{5.11}$$

Returning to the closed-loop equations (4.12) the spectral densities for u and z could be expressed as

$$\begin{aligned} \Phi_u &= T_{uw}\left(\Phi_w + \Phi_n\right) T_{uw}^* \\ \Phi_z &= S\left(\Phi_w\right) S^* + T\left(\Phi_n\right) T^* \end{aligned} \tag{5.12}$$

Using (5.6), (5.10), (5.11) and (5.12), the cost function J could then be expressed equivalently as

$$\begin{aligned} J = \tfrac{1}{2\pi} \int\limits_{-\infty}^{\infty} \operatorname{Tr}(&W_z S G_m W_m R_1 W_m^* G_m^* S^* W_z^* + W_z T W_n R_2 W_n^* T^* W_z^* + \\ &W_u T_{uw} G_m W_m R_1 W_m^* G_m^* T_{uw}^* W_u^* + W_u T_{uw} W_n R_2 W_n^* T_{uw}^* W_u^*) d\omega \end{aligned} \tag{5.13}$$

Introducing the H_2-norm notation of a transfer function $F(s)$ as

$$\|F\|_2^2 = \frac{1}{2\pi} \int\limits_{-\infty}^{\infty} \operatorname{Tr}[F^*(j\omega)F(j\omega)] d\omega \tag{5.14}$$

(5.13) could be equivalently expressed as

$$J = \left\| \begin{bmatrix} W_z S G_m W_m R_1^{1/2} \\ W_z T W_n R_2^{1/2} \\ W_u T_{uw} G_m W_m R_1^{1/2} \\ W_u T_{uw} W_n R_2^{1/2} \end{bmatrix} \right\|_2^2 \tag{5.15}$$

Considering (5.13) and (5.15), it is clear that the four transfer functions W_z, W_u, W_m, and W_n, could be used to shape the singular values of S, T, and T_{uw} and, thus, desired closed-loop characteristics could be achieved.

5.2 Controller Design

Dealing with the requirements specification according to Chapter 4, it is not relevant to use constant matrices for W_z, W_u, W_m, and W_n. Instead, frequency dependent transfer functions have to be used to achieve desired loop gain. Considering the desired shape of S and (5.15) it is clear that W_m and $R_1^{1/2}$ have to be large at frequencies where S is required to be small. Choosing W_m according to Figure 5.2

and W_u, W_z, W_n, R_1, and R_2 to be real constant diagonal matrices gives singular values of S according to Figure 5.3. These singular values are hence affected in consistency with W_m, however, it seems to be impossible to achieve clustered singular values. The design parameters used in this chapter could be found in Appendix A.4.

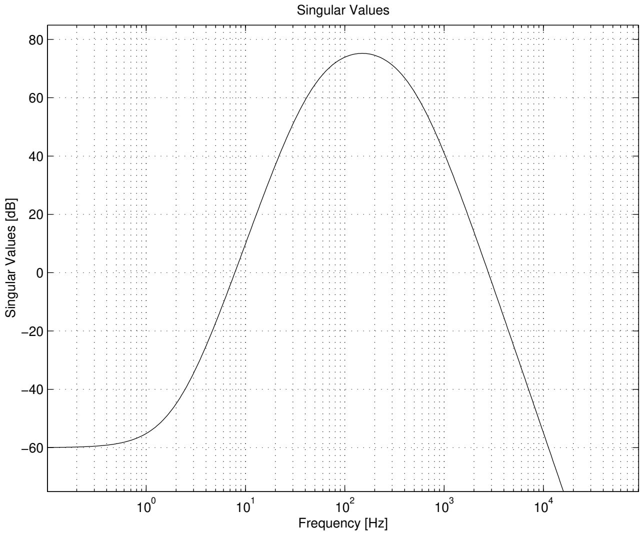

Figure 5.2 *Singular values of the transfer function W_m used to model the excitation m*

A method to adjust one of the singular values of $S(i\omega)$ using singular value decomposition of $G_m W_m$ is presented in [19] where only one singular value at a specific frequency could be affected at a time. For the particular problem of interest this means that it is not possible to cluster the singular values of S at 100 Hz, and at 10 Hz simultaneously.

The result of using this method to cluster the singular values of S at 100 Hz is shown in Figures 5.4 and 5.5. The shape of S is rather close to the desired one but the singular values of the transfer function T_{uw} are far to large for frequencies below 10 Hz with respect to the requirements specification.

To lower the level of the singular values of T_{uw} W_u should be increased, see (5.15). Moreover, increasing W_u is equivalent with decreasing W_z and since it is easier to augment the control object model with W_z than with W_u, W_z has been modelled according to Figure 5.6. The result is presented in Figures 5.7 and 5.8 showing the singular values of S and T_{uw}, respectively. From the figures it does not seem possible to achieve small singular values of T_{uw} uniformly below 10 Hz as well as well clustered ones of S at 100 Hz, simultaneously.

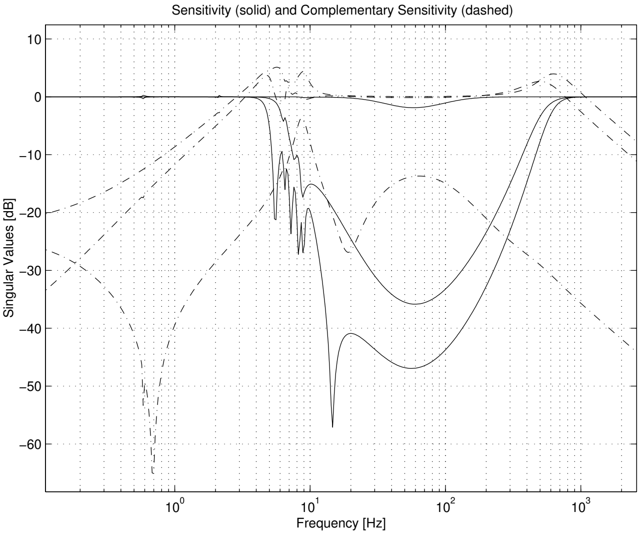

Figure 5.3 Singular values of S (solid) and T (dashed) using W_m according to Figure 5.2. The singular values are not well clustered

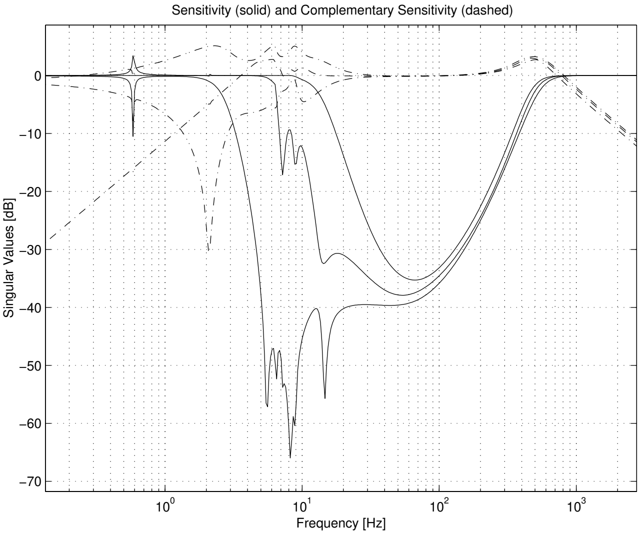

Figure 5.4 Singular values of S (solid) and T (dashed) using W_m according to Figure 5.2 with singular value clustering at 100 Hz

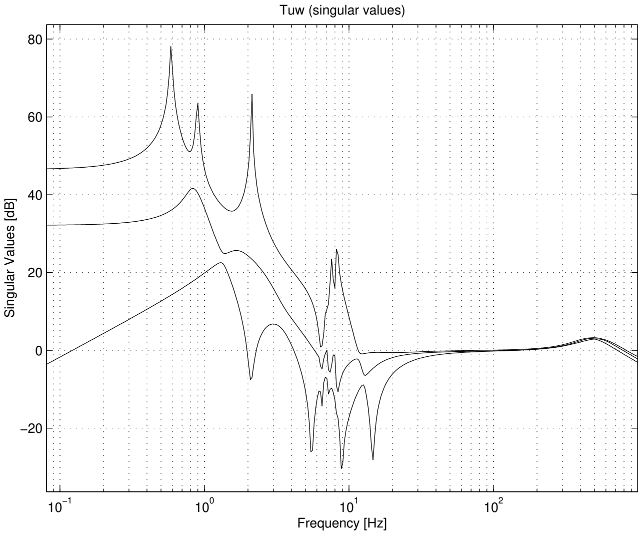

Figure 5.5 *Singular values of T_{uw} with controller corresponding to S shown in Figure 5.4. The controller requires large control forces for excitation below 20 Hz*

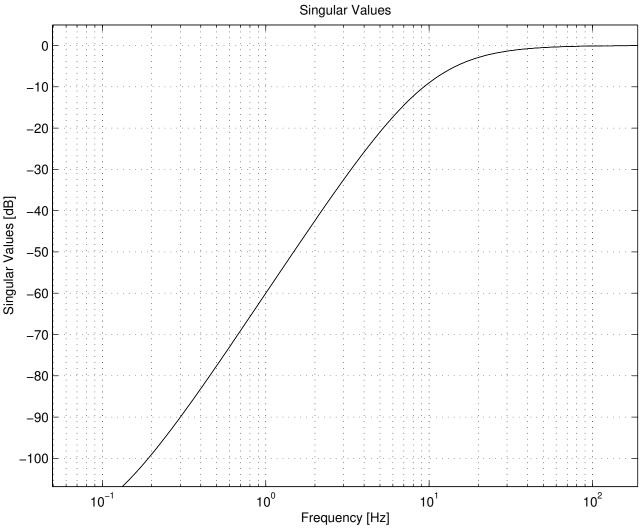

Figure 5.6 *Singular values of W_z used to decrease the singular values of T_{uw} below 10 Hz*

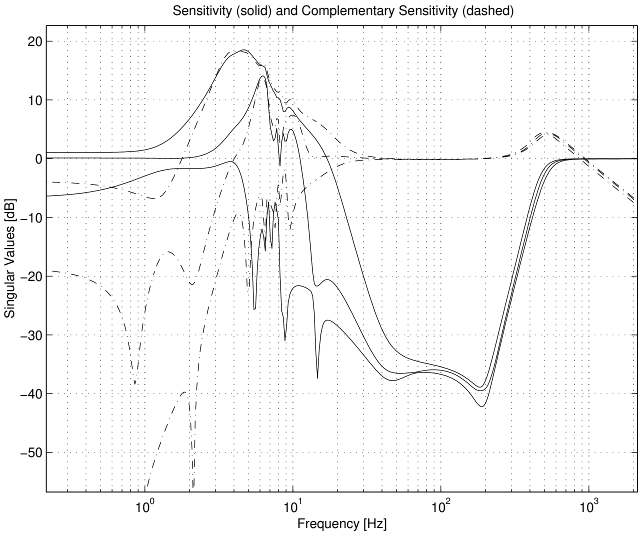

Figure 5.7 *Singular values of S using W_m and W_z shown in Figures 5.2 and 5.6, respectively, and singular value clustering at 100 Hz*

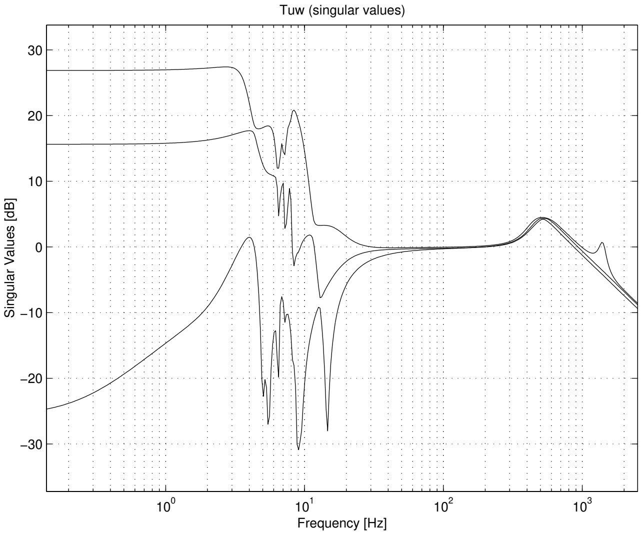

Figure 5.8 *Singular values of T_{uw} with controller corresponding to S shown in Figure 5.7. The controller could still require large control forces for excitation below 20 Hz*

5.3 Comments

To improve the design of the controller using LQG methodology, the transfer function W_n, used to model the characteristics of the measurement noise n, should be increased at frequencies below 10 Hz. However, the specific requirements for this particular problem implies that the LQG method starts looking like frequency domain loop gain shaping and for such problems other more suitable methods exist. In the next three chapters, the results of designing a feedback controller using one of those methods (H_2-method) are presented.

6

H_2 CONTROL OF THE LINEARISED CONTROL OBJECT

The control object is a non-linear dynamic system with potential for large angular displacements and non-linear material characteristics, see Figure 6.1. However, configuration, design and validation of a H_2 controller is first carried out based on the linearisation (3.2) of the non-linear object, which is assumed to be a good approximation (see [13, 44] for literature on H_2 control). The linearisation is only likely to be valid close to the static equilibrium point around which the control object is linearised. Thus, the validity of the assumption made above has to be investigated using the non-linear model and co-simulation. Chapter 8 presents a study of the non-linear effects of the control object.

6.1 General H_2 Theory

From Chapter 4 it is clear that the objectives of the active engine system are suitably expressed in terms of frequency dependant requirements on the singular values of the desired loop gain. The requirements on the loop gain could equivalently be converted to closed-loop requirements and expressed in terms of the sensitivity, etc. These are the conditions when H_2 theory is to be preferred.

H_2 is the process of choosing a feedback controller in order to minimise the H_2-norm, see (5.14), of some frequency weighted closed-loop transfer function, i.e. to chose F_y in Figure 6.2 such that the H_2-norm of the transfer function from w

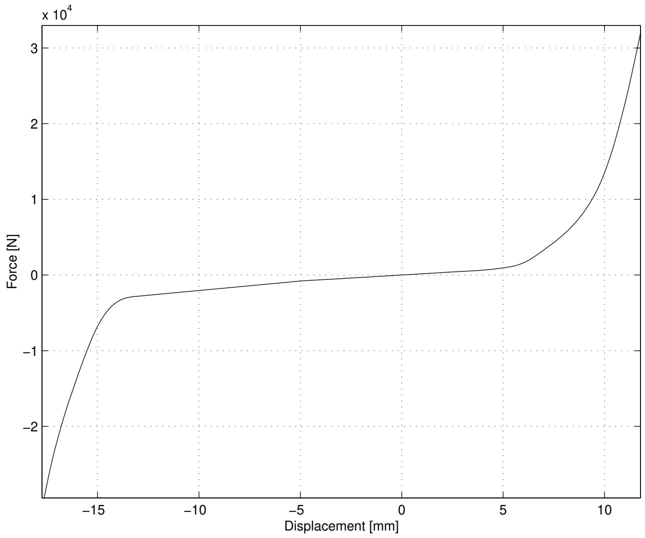

Figure 6.1 *Non-linear static stiffness in the x-direction (global co-ordinate system) of the bushing connecting the torque rod and the sub-frame*

to z is minimised, see [13, 44]. The system P in Figure 6.2 represents the original control object augmented with some dynamics in order to reflect the design requirements. Specifically, minimising the H_2-norm of the transfer function from w to z ($z = [z_1\ z_2\ z_3]^T$) in Figure 6.3 over all F_y's means that the following norm is minimised:

$$\|T_{zw}\|_2^2 = \left\| \begin{bmatrix} W_u T_{uw} \\ -W_T T \\ W_S S \end{bmatrix} \right\|_2^2 \tag{6.1}$$

Minimising the above transfer function means that the weighted closed-loop transfer functions S, T, and T_{uw} will be small in "H_2-sense", i.e. the corresponding H_2-norms will be small.

6.2 On the Choice of Weighting Functions

The order of a H_2 controller is equal to the sum of the order of the control object model, and the number of states needed in order to realise the weighting functions in (6.1). As a high order controller is computationally more demanding than a low order one, weighting functions with as low order as possible should be used to shape the closed-loop transfer functions.

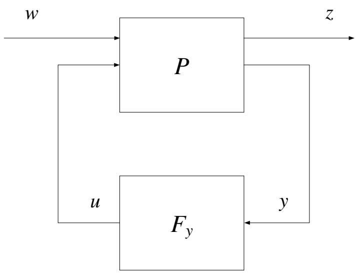

Figure 6.2 *General set-up for H_2-design. The augmented system P reflects the design requirements.*

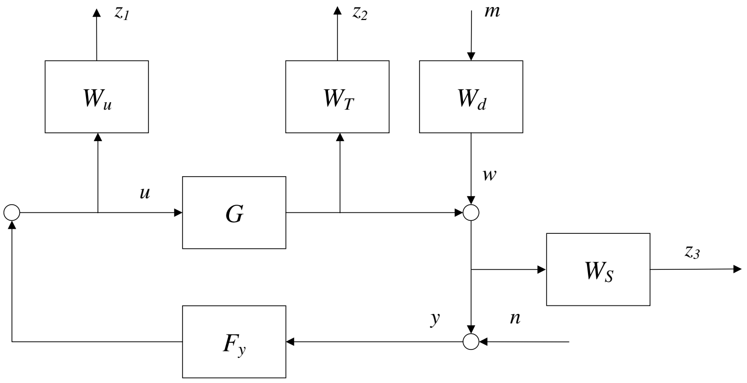
z_1
z_2
m
W_u
W_T
W_d
w
u
G
W_S
z_3
y
n
F_y

Figure 6.3 *Feedback configuration with weights, a specific set-up for H_2-design*

Since the control object has three inputs and three outputs, the sensitivity weighting function should have a diagonal structure according to (6.2).

$$W_S(s) = \begin{bmatrix} w_s(s) & 0 & 0 \\ 0 & w_s(s) & 0 \\ 0 & 0 & w_s(s) \end{bmatrix} \tag{6.2}$$

Here w_s is a SISO frequency dependant weighting function. Notice that no other structure of W_S gives possibility to equal effectively shaping the sensitivity function. Since the same requirements apply to all three channels, identical diagonal elements should be used. The transfer functions W_T and W_u are also required to be diagonal with three inputs and three outputs for effectively shaping T and T_{uw}.

The weighting functions for S, T and T_{uw} should be selected to reflect the closed-loop requirement specifications. This could however be quite tricky due to the limitations mentioned in Section 4.6. For example, when selecting the weighting functions for S and T, the trade-off between suppression of the excitation (internal and external) and noise propagation, has to be taken into account. Choosing conflicting weighting functions generally implies unpredictable closed-loop characteristics. The process of weighting functions selection is inevitably iterative but could considerably be sped up by carefully choosing the weighting functions.

6.3 Broad Band Control

It is clear from the requirements specification that it is desired to suppress excitations in a frequency range from approximately 12 Hz to about 420 Hz. Furthermore, the closed-loop system should exhibit a good robust performance with respect to excitation frequency content variations, including time varying excitations. This requires S to have a shape similar to the one presented in the specifications, see Figure 4.8. A controller that gives such a sensitivity function is here referred to as a *broad band* controller.

6.3.1 Initial Design

Initially only W_S has been used to achieve the required sensitivity shape. Using the structure of W_S according to (6.2) and the SISO weighting function w_s shown in Figure 6.4, gives S according to Figure 6.5 (see Appendix A.5.1 for details about the weighting function). Hence, it is possible to achieve singular values of S very near the ideal shape. Furthermore, the desired low frequency characteristics of the closed-loop system are presented in Chapter 2 and Section 4.4. Considering the singular values of T_{uw} shown in Figure 6.6, it is clear that the low frequency specifications below 12 Hz are not at all fulfilled. Low frequency excitation would imply high required control power and, moreover, the energy used by the actuators has to be produced by the engine affecting the fuel consumption negatively. The shape of T_{uw} is hence not satisfactory.

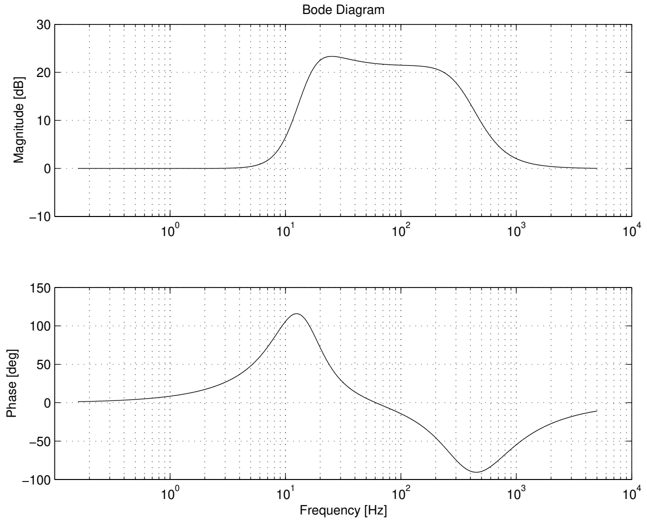

Figure 6.4 *Frequency characteristics of the diagonal elements w_s of the weighting function W_S*

Ideally, the controller should fulfill the requirements specification at all frequencies, i.e. at frequencies corresponding to regions I, II and III, defined in Figure 4.11. To meet the specifications in frequency region I (see Section 4.5), the largest singular values of the loop gain and the controller, have to be small. On the other hand, good attenuation in frequency region II, requires the smallest singular values of the loop gain to be large. Considering the expressions for S, (4.13), and T_{uw}, (4.15), and the singular values of the transfer function of the control object (G in (4.7)) shown in Figure 6.7, the largest and smallest singular values are much separated close to the desired zero dB loop gain cross-over frequency (see Section 4.5). Thus, at this frequency it is not possible to achieve well clustered singular values for both S and T_{uw}. Together with the requirement on the loop gain to have a sharp transition between frequency regions I and II, it is clear that it will not be possible to meet the specifications close to the boundary between frequency region I and II. Hence, there has to be a design trade-off.

6.3.2 Final “Trade-Off” Design

Considering (6.1), a weighting function W_u has to be introduced in order to decrease the levels of the singular values of T_{uw} shown in Figure 6.6. The gain of this weighting function should be high where T_{uw} has to be small, i.e. especially at frequencies in frequency region I.

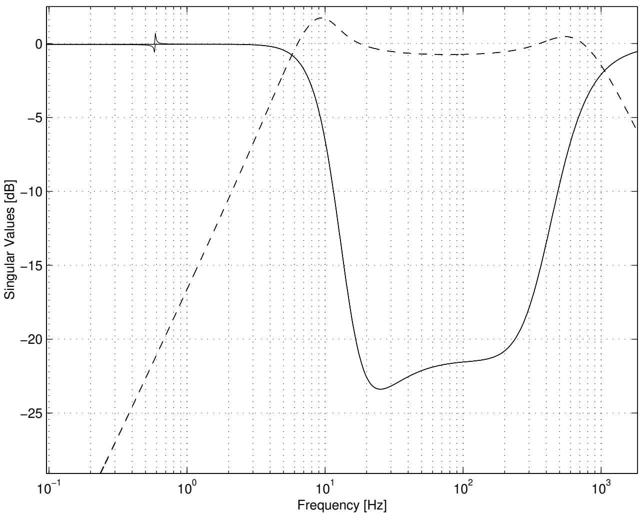

Figure 6.5 *Singular values of S (solid) and T (dashed) for a H_2 controller using broad band weighting function for S according to Figure 6.4 where both W_T and W_u set to zero. Thus, the shape of S is very close to the desired one*

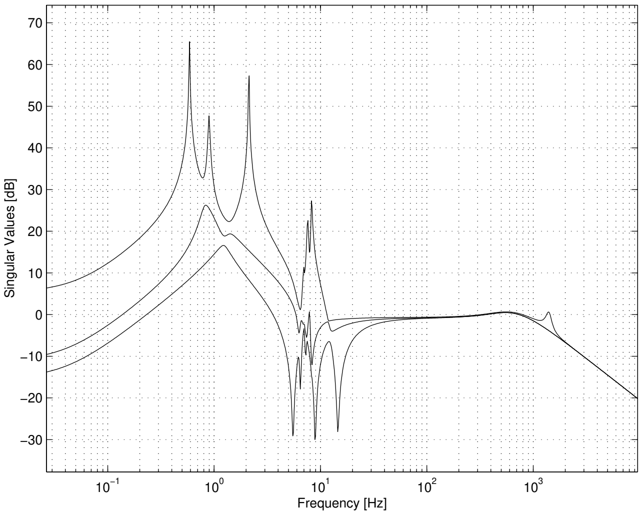

Figure 6.6 *Singular values of T_{uw} corresponding to Figure 6.5. The corresponding controller will generate large undesired control forces for low frequency excitation*

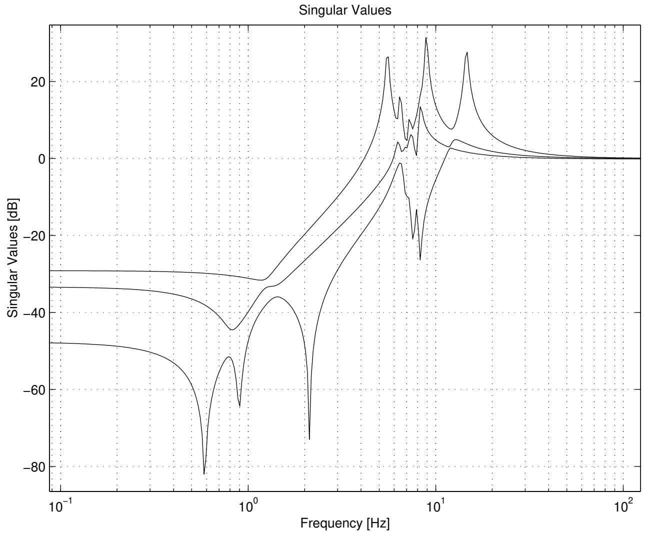

Figure 6.7 *Singular values of the transfer function of the control object, G in (4.7)*

The sensitivity and the complementary sensitivity corresponding to a trade-off design are shown in Figure 6.8. This figure reveals that the controller still provides very nice attenuation in the frequency range from 12 to about 500 Hz, and also that the total forces transmitted to the body and subframe may be amplified by approximately 4 dB, i.e. with a factor of 1.6, for frequencies between 1 Hz and 8 Hz.

Figure 6.9 shows the singular values of T_{uw} and one of the identical diagonal elements of W_u^{-1} (see Appendix A.5.3). Compared to the preliminary design, the singular values of T_{uw} have been somewhat decreased in frequency region I, see Figures 6.9 and 6.6. The weighting function W_S from the preliminary design for S was unaltered.

As expected it is difficult to fulfill the requirements specification in frequency regions I, II and III, simultaneously. Furthermore, it is a rather hard task to achieve small and well clustered singular values of S and, at the same time, fulfilling the requirements on T_{uw}, close to the loop gain '0 dB cross-over' frequency.

Moreover, since no model can respond exactly like the true physical system, the closed-loop system has to be robustly stable to modelling errors, including non-modelled time delays, introduced, for instance, by the sampling process in a digital implementation. Time delays as well as poor signal-to-noise ratio, cause primarily problems at high frequencies. As mentioned in Chapter 4, the singular values of T determine the noise propagation and the degree of robust stability to modelling errors. Therefore, the singular values of T have to decrease with fre-

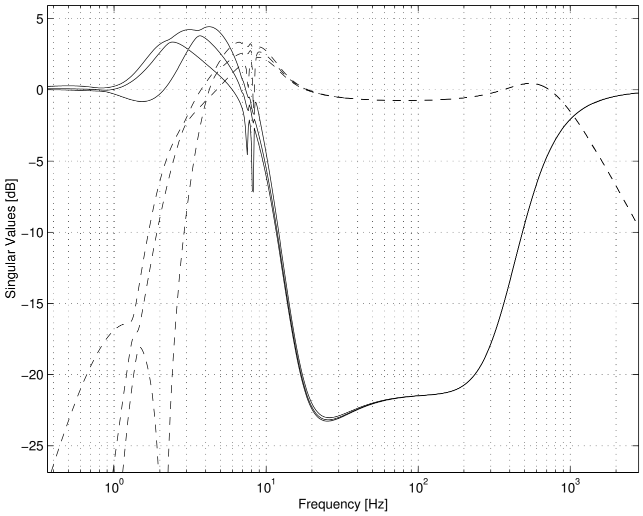

Figure 6.8 *S (solid) and T (dashed) for a design with trade-off made between good low and good high closed-loop frequency characteristics. The requirements on the shape of S have been balanced against reduced singular values of T_{uw} at frequencies below 10 Hz*

quency and consequently also the loop gain. However, good suppression of the excitation requires high loop gain and, as a result, good attenuation of the transmitted forces has to be balanced against sensor noise propagation and tolerance to modelling errors.

Figure 6.10 shows the singular values of the loop gain corresponding to the trade-off design, where the high frequency balancing and the relatively sharp transition between low loop gain in frequency region I and high loop gain in frequency region II, are demonstrated.

6.3.3 Simulations

The control object considered in this chapter is completely linear, implying that the superposition principle applies. For excitations that represent driving operating condition consisting of a fluctuating torque superimposed on a nominal one, the superposition principle means that the effects of the fluctuating and the nominal torque could be investigated separately. As mentioned in Chapter 2, two principally different fluctuating torques corresponding to constant (idle operating condition) and varying engine speed (driving operating condition) exist. Hence, three load cases have to be used for control design and validation. Those are

- the fluctuating torque corresponding to idle operating condition at constant

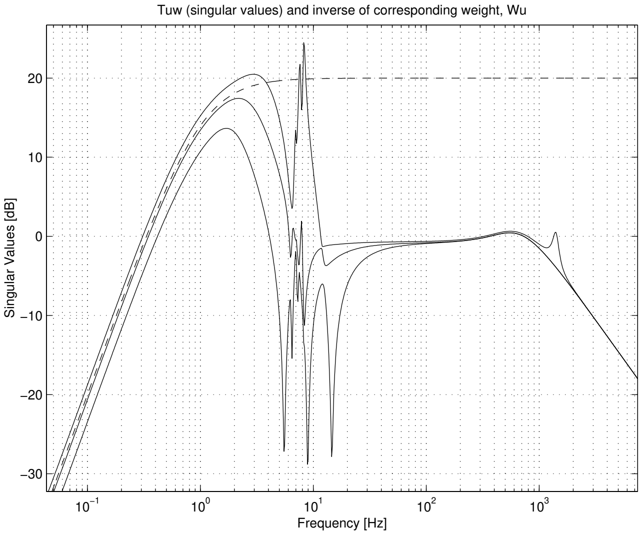

Figure 6.9 *Singular values of T_{uw} for a design with trade-off made between good low and good high closed-loop frequency characteristics. Compared to the preliminary design, see Figure 6.6, the singular values have been somewhat reduced at frequencies below approximately 10 Hz. One of the diagonal elements of W_u^{-1} is also shown*

700 rpm engine speed

- the fluctuating torque corresponding to driving operating condition for a rotational speed 4-seconds sweep from 700 rpm to 5000 rpm
- the transient “Shunt and Shuffle” excitation corresponding to a dropped clutch operation

The main objective of the active engine isolation system is to suppress the fluctuating torque from the engine excitation. To begin with, the two principally different fluctuating torques have therefore been applied. Figure 6.11 demonstrates the performance of the trade-off design when the engine is subjected to the stationary fluctuating torque and the AES system performance is noticeably good. From Figures 6.12, 6.13 and 6.14, it is also clear that the suppression of the time varying excitation is excellent in the whole speed range, where the trade-off controller was validated using a fluctuating torque corresponding to a 4-second sweep from 700 rpm to 5000 rpm.

Turning to validation of the closed-loop low frequency characteristics corresponding to the trade-off design, a simulation has been run using the linearised model for control synthesis subjected to the transient “Shunt and Shuffle” exci-

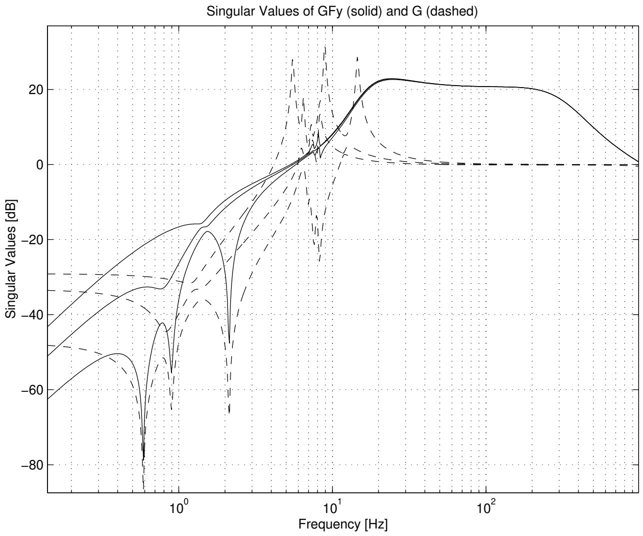

Figure 6.10 *Singular values of the loop gain for a design with trade-off made between good low and good high closed-loop frequency characteristics*

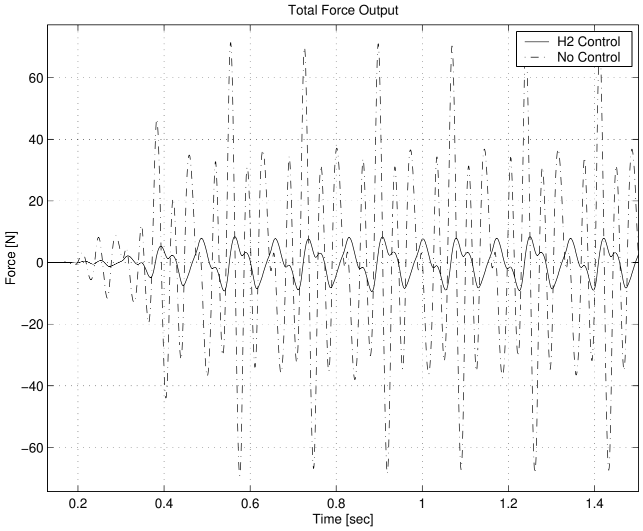

Figure 6.11 y^{RHS} *due to the fluctuating torque corresponding to engine idle operating condition, with the trade-off controller corresponding to Figure 6.8, and without control. Hence, good attenuation is achieved*

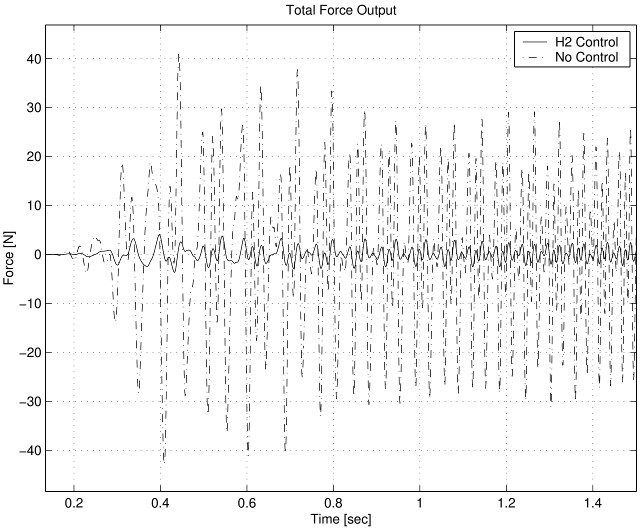

Figure 6.12 *y^{RHS} due to the fluctuating torque corresponding to the sweep excitation, with the trade-off controller corresponding to Figure 6.8, and without control. The performance is very good*

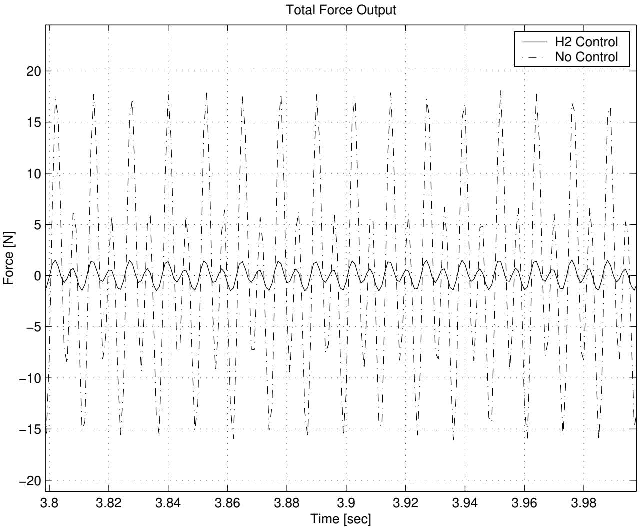

Figure 6.13 *As Figure 6.12, demonstrating the good performance also at high frequencies*

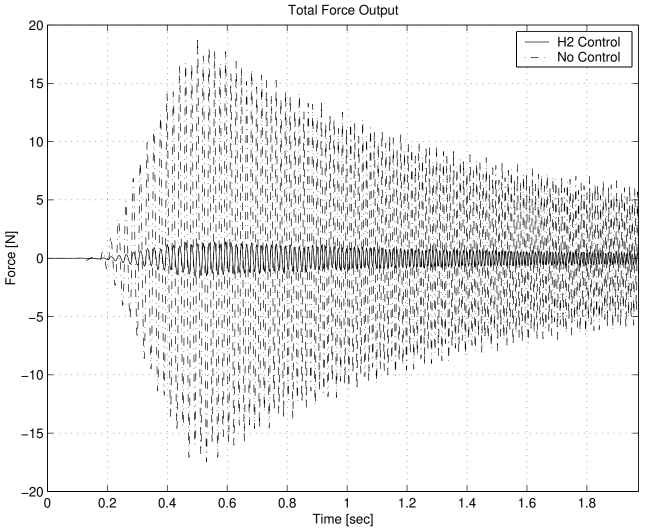

Figure 6.14 *y^{TR} due to the fluctuating torque corresponding to the sweep excitation, with the trade-off controller corresponding to Figure 6.8, and without control*

tation originating from a dropped clutch operation, see Figure 2.8. As expected, and consistent with Figure 6.8, the transmitted forces are somewhat increased at low frequencies, see Figure 6.15. Furthermore, the controller output shown in Figure 6.16 is quite high but compared with the preliminary H_2 design, the ability to deal with the “Shunt and Shuffle” excitation has been improved, see Figures 6.6 and 6.9. The singular values of T_{uw} in frequency region I could not be further decreased to reduce the low frequency control energy without unacceptably affect the shape of S.

The “Shunt and Shuffle” excitation load case is principally similar to a nominal torque one, although it is more extreme with respect to ramping angle (reflecting the ramping speed) and peak load. Consequently, if a controller could handle the “Shunt and Shuffle” excitation, it should also be able to deal with all other transient nominal loads.

To sum up, the controller corresponding to the final design (see Figures 6.8, 6.9, and 6.10) shows good performance and is able to attenuate the transmitted forces with approximately 20 dB for excitations in frequency region II. However, the necessary actuator forces are quite high when dealing with high load low frequency excitation, and therefore, saturation of the actuators is most likely to occur in reality. For this reason, the effect of input saturation has to be investigated. The results from such an investigation are presented in Chapter 7.

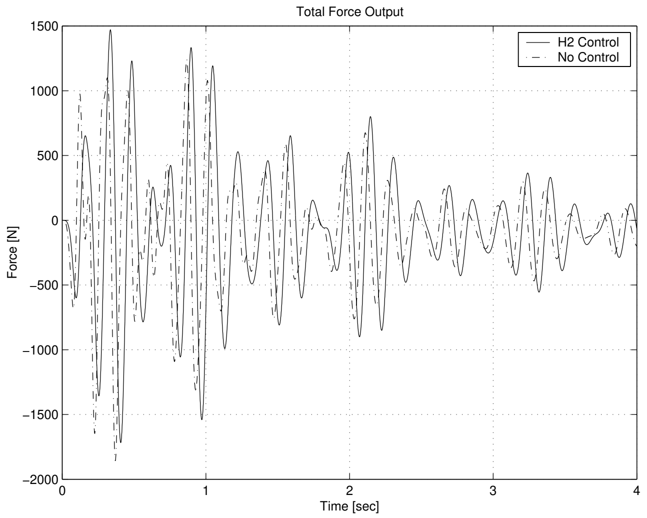

Figure 6.15 *y^{RHS} due to the "Shunt and Shuffle" excitation with the controller corresponding to Figure 6.8 and without control. The transmitted forces should ideally be the same but the difference is not considerable*

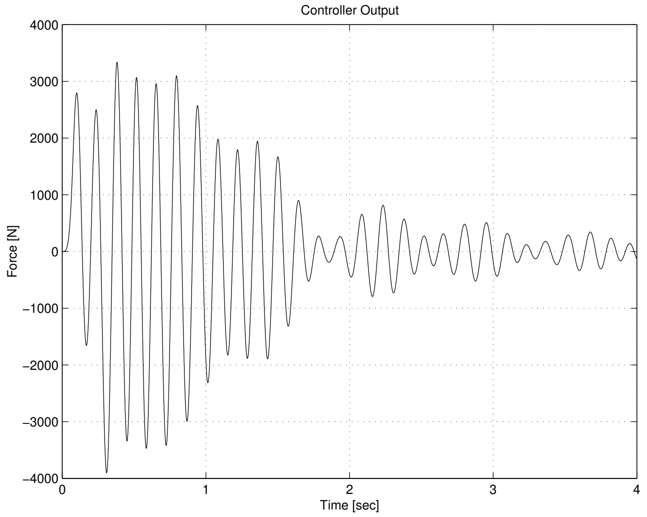

Figure 6.16 *u^{RHS} due to the "Shunt and Shuffle" excitation with the controller corresponding to Figure 6.8. It should ideally be zero at frequencies below 10 Hz which is clearly not the case*

6.4 Narrow Band Control

Suppression of only a few excitation spectral components requires the loop gain to be high only at those frequencies. This is what is here referred to as *narrow band* control. From the design of the broad band controller in Section 6.3, it was found difficult to achieve a good compromise between low and high frequency requirements, especially for frequencies close to the 1^{st} engine order, 1E, at idle engine operation. However, it is expected to be easier to acheive an acceptable narrow band controller than a broad band one due to the limitations presented in Section 4.6, but also owing to the fact that it is easier to construct narrow band weighting functions using, for instance, so called “notch filters”. Furthermore, a narrow band controller could not only be used for idle (or stationary) engine operation, but also in a Gain Scheduling scheme to suppress several spectral components of a time varying excitation. All in all it is interesting to investigate the potential of H_2 theory for narrow band control.

Consider Figures 2.2, 2.3 and 2.4, in Section 2, showing the spectral components of the stationary fluctuating torque corresponding to idle engine operation. It is expected to obtain good overall attenuation if the two most dominating orders of M_x together with the single most dominating order of M_y and M_z are suppressed. Hence, reducing the singular values of the sensitivity at these four frequencies (i.e. at 1E, 2E, 2.5E and 5E) should be enough. Dealing with idle engine operation, the rotational frequency of the engine is E= 700/60 Hz, i.e. approximately 11.7 Hz (see (2.1)).

6.4.1 Initial Design

In a first attempt to construct a narrow band controller, W_S is built up using three SISO transfer functions, each consisting of four narrow band, 2^{nd} order filters connected in series. The peaks of those four notch filters are located at frequencies corresponding to the four engine orders identified above, see Figure 6.17. The result of using this weighing function is presented in Figure 6.18, showing the singular values of S and T. All the weighting functions used in this section could be found in Appendix A.6.

Although S and T look satisfactory, this particular design is not acceptable. Contrary to the specifications, Figure 6.18 reveals that the controller will suppress excitation in frequency range I, in addition to the four main frequencies in frequency region II (see Figure 4.11 for definition of regions I, II, and III). Furthermore, from inspection of the singular values of the transfer function T_{uw}, see Figure 6.19, it is clear that low frequency excitation would cause the controller to generate large control forces. Hence, the requirement specifications are not fulfilled since the low frequency characteristics have been affected and the preliminary narrow band design is therefore rejected.

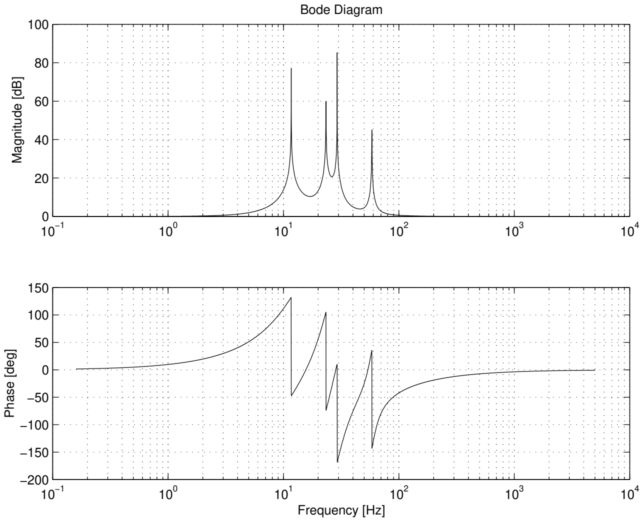

Figure 6.17 *The frequency characteristics of the filters used to construct the weighting function W_S, i.e. the inverse of the diagonal elements of W_S*

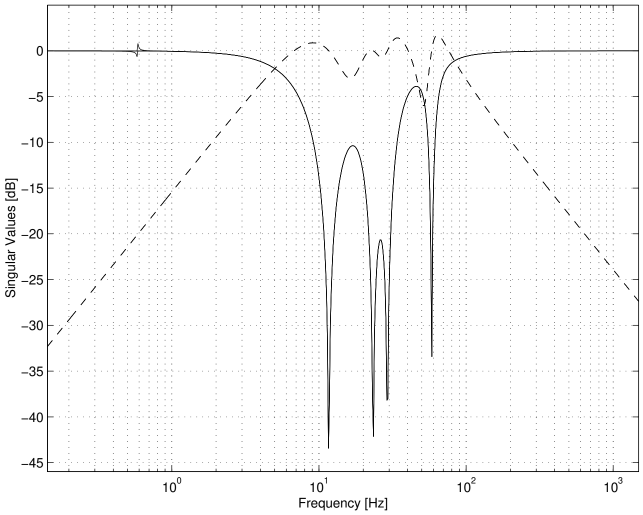

Figure 6.18 *Singular values of S (solid) and T (dashed) for the preliminary narrow band H_2 controller. In addition to excitation suppression at frequencies in region II, this controller will, in conflict with the requirements, also suppress excitation in frequency region I*

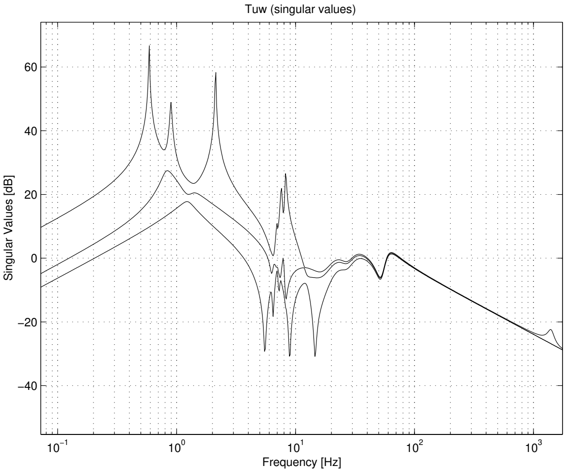

Figure 6.19 *Singular values of T_{uw} for the preliminary narrow band H_2 controller. The controller will require large undesired control forces for excitation below 10 Hz*

6.4.2 Final Design

To leave the low frequency characteristics unaffected, a weighting function W_u had to be introduced to achieve loop gain low enough in frequency region I, see Figure 6.21. In this frequency region, T_{uw} and hence F_y should ideally be zero according to the requirements specification, which makes S equal to one. Furthermore, F_y should be large at 1E in order to suppress order one at idle engine operation. This requires a rapid change of the loop gain at the transition from frequency region I to frequency region II and therefore W_u had to be based on high order filters. Moreover, the weight W_u has been set to increase at high frequencies in order to attain a 40 dB/decade roll-off rate.

Using W_s from the preliminary narrow band design, and W_u according to Figure 6.21, an acceptable “final” design was obtained. The sensitivity presented in Figure 6.20 reveals that the dominating orders of the engine excitation are attenuated with approximately 20 dB. However, some degradation of the performance in certain frequency bands (i.e. singular values of S above one) have to be accepted to get a good enough attenuation at those orders. Furthermore, in consistency with the requirements, Figure 6.25 indicates that the output from the controller will be insignificant for excitations in frequency region I. Finally, Figure 6.22 shows the corresponding loop gain, demonstrating the rapid change of the loop gain at the border between frequency region I and II.

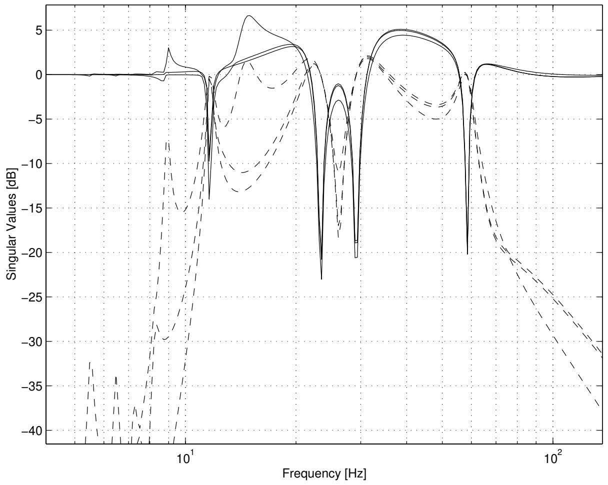

Figure 6.20 *Singular values of S (solid) and T (dashed) for the final narrow band H_2 controller with objective to fulfill the requirements at all frequencies (i.e. using both W_S and W_u). Some degradation of the performance has to be accepted at frequencies other than the ones corresponding to the dominating engine orders*

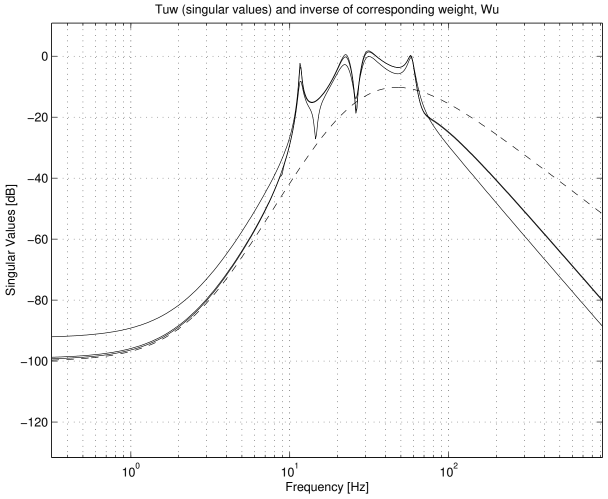

Figure 6.21 *The inverse of one of the diagonal elements of the weighting function W_u (dashed) and the singular values of the corresponding transfer function T_{uw} (solid)*

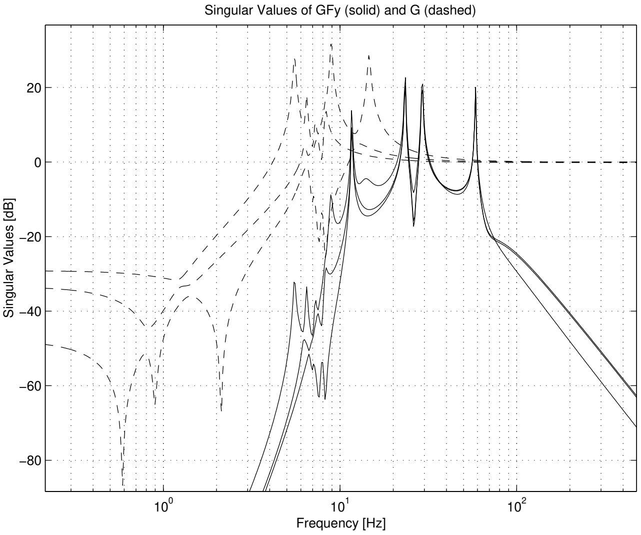

Figure 6.22 *The final loop gain GF_y corresponding to Figures 6.20 and 6.21*

6.4.3 Simulations

To validate the main objective of the active engine isolation system to suppress the fluctuating torque from the engine excitation, a simulation with the engine subjected to a fluctuating torque corresponding to idle operating condition, has been performed. Figures 6.23 and 6.24 present the results from this simulation, demonstrating the excellent attenuation of the total transmitted forces.

For validation of the low frequency characteristics, a simulation with the "Shunt and Shuffle" excitation (see Figure 2.8) has been carried out. Figure 6.25 shows the total transmitted forces at the RHS y^{RHS} with and without control, and Figure 6.26 the corresponding actuator force u^{RHS}. Clearly and as desired, the total transmitted forces are practically unaffected by the controller when the engine is subjected to such excitation.

To sum up, narrow band feedback control has proved to be a very efficient way to deal with engine idle operating condition excitation. Moreover, the controller corresponding to the final design leaves the low frequency characteristics practically unaffected. On the other hand, it seems to be very difficult to achieve drops in sensitivity to cover broader frequency ranges without deteriorating the performance beyond desired bandwidth, i.e. in frequency region I and at frequencies between the ones corresponding to the four dominating orders of engine excitation. Thus, a controller based on Gain Scheduling using multiple narrow band feedback controllers is not suitable for broad band engine vibration isolation.

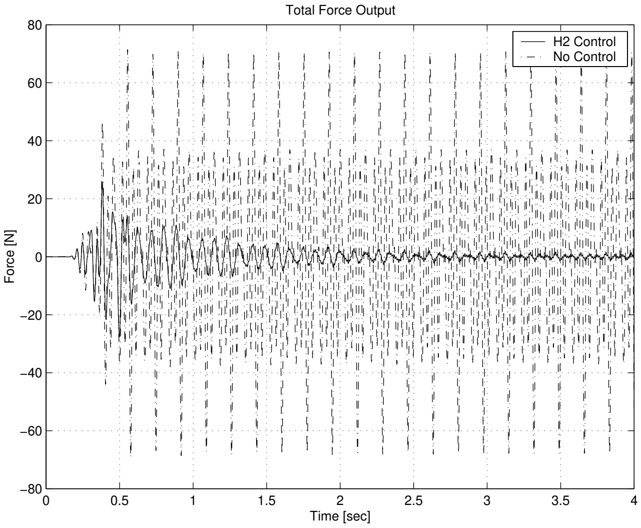

Figure 6.23 *y^{RHS} when the engine is subjected to a fluctuating torque corresponding to idle operating condition. The attenuation is very good*

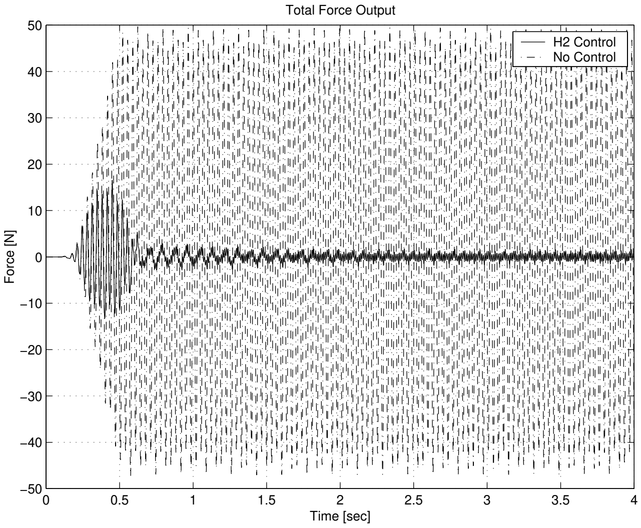

Figure 6.24 *y^{TR} when the engine is subjected to a fluctuating torque corresponding to idle operating condition. The attenuation is excellent*

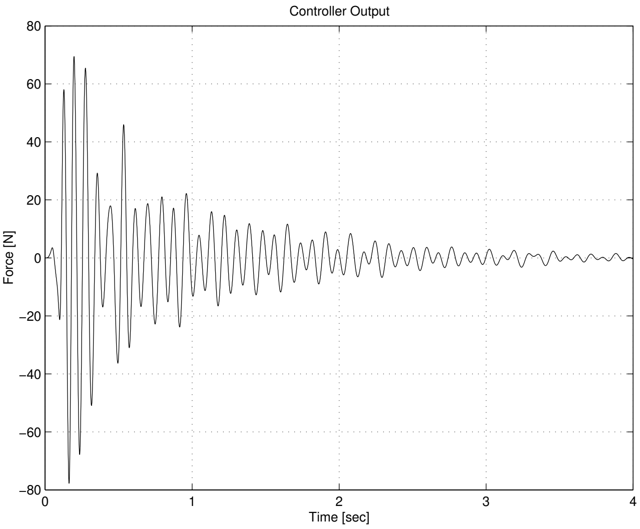

Figure 6.25 *u^{RHS} due to the transient "Shunt and Shuffle" excitation for a controller corresponding to Figures 6.20, 6.21 and 6.22. The controller output would ideally be zero. However, it is moderate and acceptable*

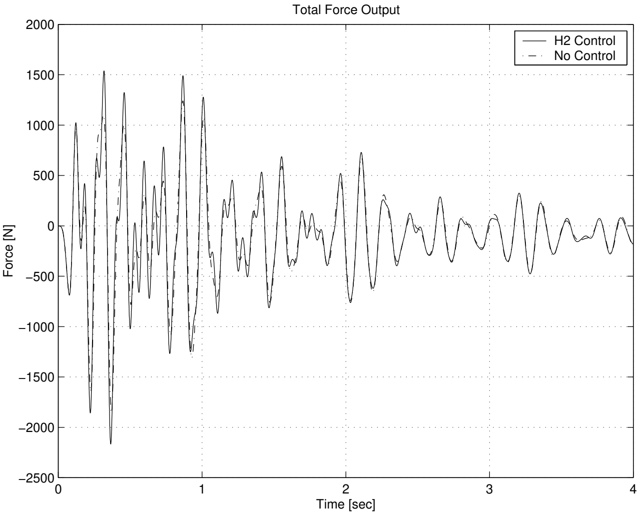

Figure 6.26 *y^{RHS} due to the transient "Shunt and Shuffle" excitation with control corresponding to Figures 6.20, 6.21 and 6.22, and without control. As desired, the transmitted forces are nearly unaffected by the control*

6.5 Model Order Reduction

H_2 control theory gives a controller with an order equal to the sum of the order of the control object model and the number of states in the realisation of the weighting functions. Generally, controllers should always be as little computationally demanding as possible, and therefore a low order controller is to prefer compared to a high order one. There are two main approaches to arrive at a low order controller. First, a high order controller could be designed with a subsequent reduction of the controller. This is what is commonly referred to as controller reduction. The other approach is to first reduce the order of the control object model, and then based on this reduced order model, a lower order controller could be designed. Combinations of both approaches are also possible. In this section, both approaches have been used based on balanced realisations which is described in most literature on control theory, see e.g. [44].

As a consequence of the specific closed-loop requirements presented in Section 4.4, the realisation of the “trade-off” controller developed in Section 6.3 required 66 states. These are 36 states from the weighting function W_S (see Figure 6.4), 6 states from W_u (see Figure 6.9), and 24 states from the linear model of the control object. Thus, the objective of this section is to reduce the order of the broad band trade-off controller, i.e. to reduce the number of those states.

To begin with, ordinary balanced model truncation has been carried out. It was found that the controller could be reduced from 66 to 40 states with satisfactory performance degradation and perceived closed-loop stability. Figures 6.27 and 6.28 correspond to a controller with an order of 40. Further reduction leads to unsatisfactory performance, especially close to 5 Hz, see Figure 6.29. A reduction to less than 33 states leads to closed-loop instability.

To proceed, the model of the control object has been reduced from 24 to 16 states and subsequently used for designing the controller. Using the weighting functions from the trade-off design in Section 6.3, a H_2 controller was designed based on the reduced model of the control object. However, applying balanced truncation to the controller achieved this way does not give a lower order controller than without the preceding model order reduction.

Furthermore, balanced truncation with matched DC gain has been carried out. The result is similar to state truncation, where 40 states are still required, to achieve closed-loop characteristics close enough to the requirement specifications. Figures 6.30 and 6.31 correspond to a controller reduced to 40 states. For controllers of orders lower than 40 the performance degradation are noticeable and the sensitivity function exhibit unwanted peaks in the frequency range from 1 to 10 Hz, see Figures 6.32 and 6.33. Figure 6.33 shows also that, eventually, the controllers start to exhibit unacceptable roll-off rates. Anyhow, closed-loop stability is perceived in all cases.

Finally, frequency weighted balanced truncation according to [44] has been evaluated. Given an original full order controller F_y, the objective is to find a lower order one F_y^{Red} such that

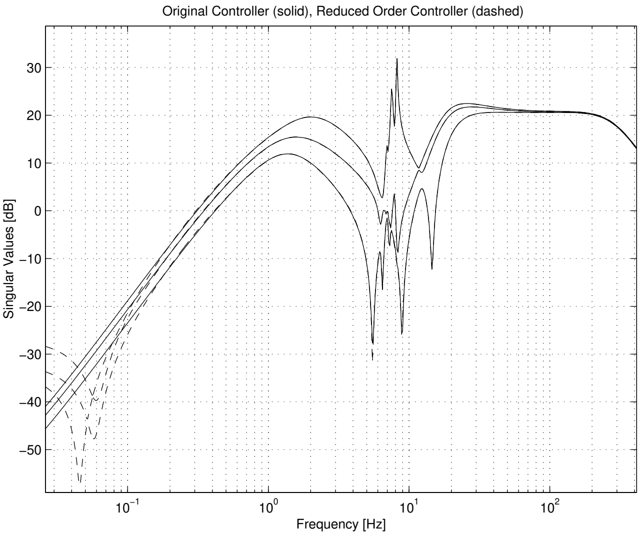

Figure 6.27 *Singular values of the controller before reduction (solid) and after reduction to 40 states (dashed) using balanced state truncation. The controller is only slightly affected at very low frequencies*

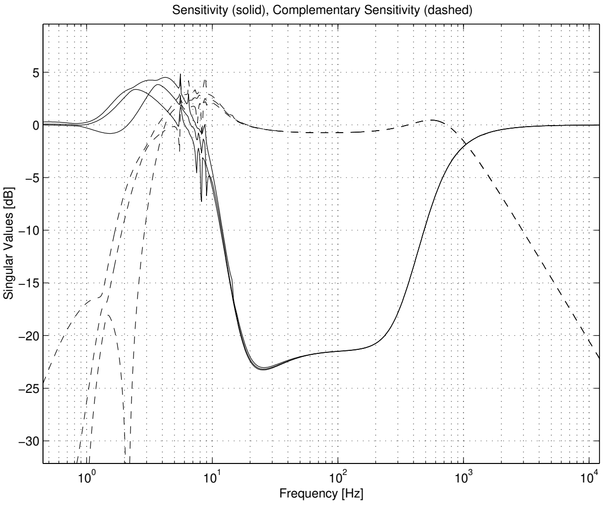

Figure 6.28 *Singular values of S and T for the controller reduced to 40^{th} order using balanced state truncation. The corresponding controller shows characteristics very similar to the original one*

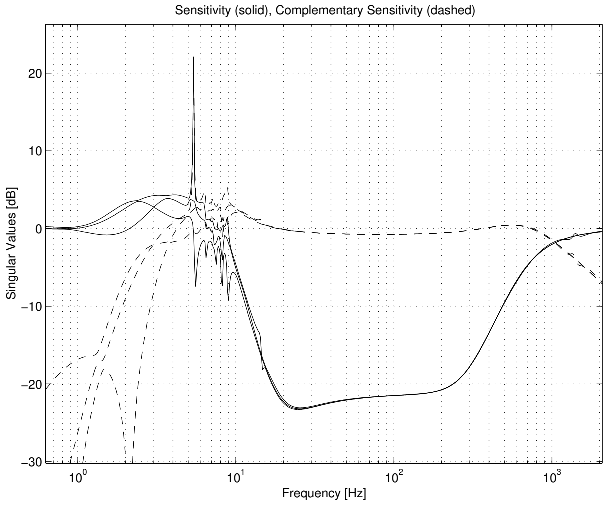

Figure 6.29 *Singular values of S and T for the controller reduced to an order of 36 using balanced state truncation. The performance is unacceptable below 10 Hz*

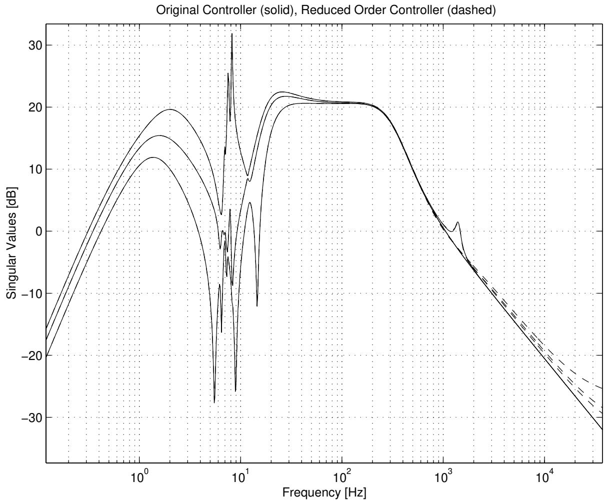

Figure 6.30 *Singular values of the controller before reduction (solid) and after reduction to 40 states (dashed) using balanced state truncation with matched DC gain. The corresponding controller has about the same characteristics as the original one*

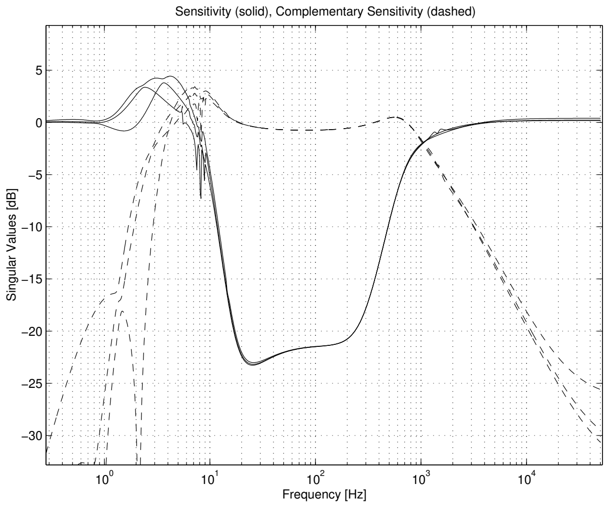

Figure 6.31 *Singular values of S and T for the controller reduced to an order of 40 using balanced state truncation with matched DC gain. The corresponding controller has about the same characteristics as the original one*

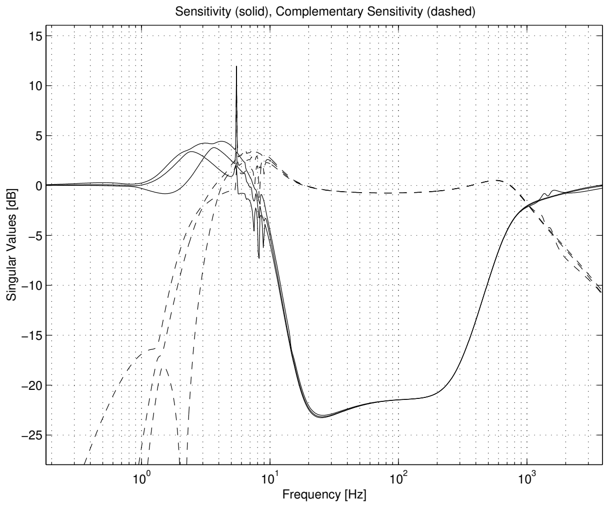

Figure 6.32 *Singular values of S and T for the controller reduced to an order of 38 using balanced state truncation with matched DC gain. Once again, the performance is unacceptable below 10 Hz*

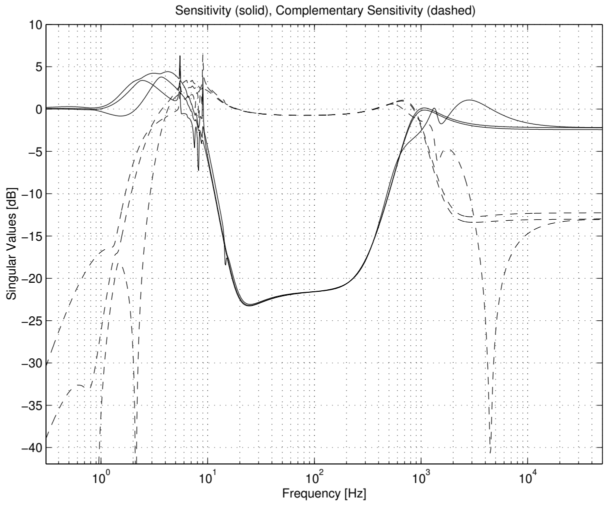

Figure 6.33 *Singular values of S and T for a controller reduced to an order of 32 using balanced state truncation with matched DC gain. In addition to the drawbacks demonstrated in Figure 6.32, the roll-off rate is also unacceptably affected*

$$\|W_o(F_y - F_y^{Red})W_i\|_\infty \tag{6.3}$$

is as small as possible. The “Balanced Truncation with Stability Weighting”-method [44] uses $W_i = I$ and

$$W_o = (I - P_{22}F_y)^{-1}P_{22} \tag{6.4}$$

where P_{22} is the state space realisation that would have been used in a controller implementation with an internal LQG structure, i.e. with a state observer and state feedback. P_{22} is also the subsystem from u to y in the augmented system P in Figure 6.2. Figure 6.34 shows the singular values of W_o. Besides focusing on preservation of closed-loop stability, the frequency weighted controller reduction using W_o according to Figure 6.34 should give a better agreement between the original controller and the reduced order controller at frequencies around 10 Hz, i.e. frequencies where the previous methods showed degradation.

Figures 6.35 and 6.36 correspond to a controller reduced to an order of 30 using stability weighted balanced truncation. The result is consistent with Figure 6.34,

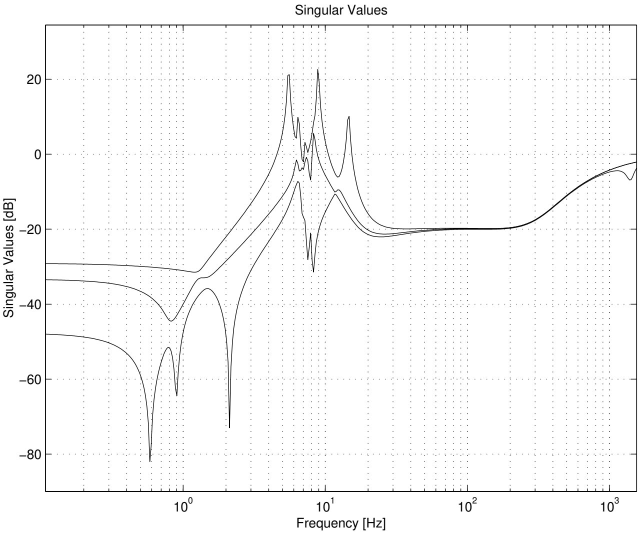

Figure 6.34 *Singular values of W_o according to (6.4)*

showing good agreement around 10 Hz and worse below 1 Hz. This controller has been evaluated using simulations with both harmonic and transient excitation, and the performance degradation for frequencies below 1 Hz does not cause any problems.

Hence, the order of the controller could be reduced from 66 to 30 states with satisfactory closed-loop characteristics. Considering the desired shape of the loop gain with the sharp transition between frequency region I and II, see Figure 4.12, and also the many natural modes of the control object close to 10 Hz, see Figure 6.7, it is not surprising that as many states as 30 are required. Considering the evaluated methods for controller order reduction with respect to this particular case, balanced truncation with stability weighting is the most effective one.

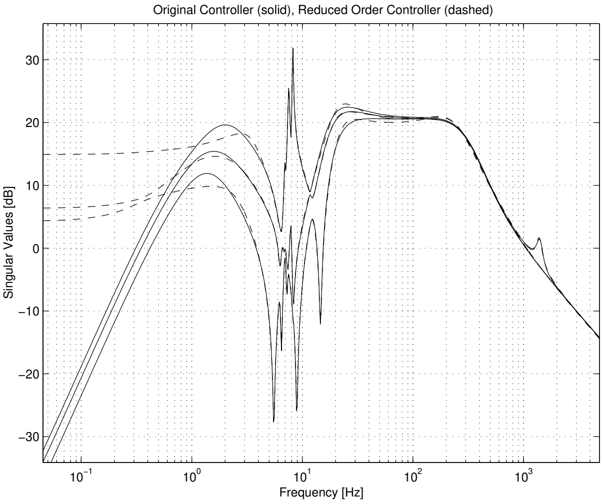

Figure 6.35 *Singular values of the controller before reduction (solid) and after reduction to 30 states (dashed) using balanced state truncation with stability weighting. The changes of the controller below 10 Hz do not considerably affect the closed-loop stability and performance*

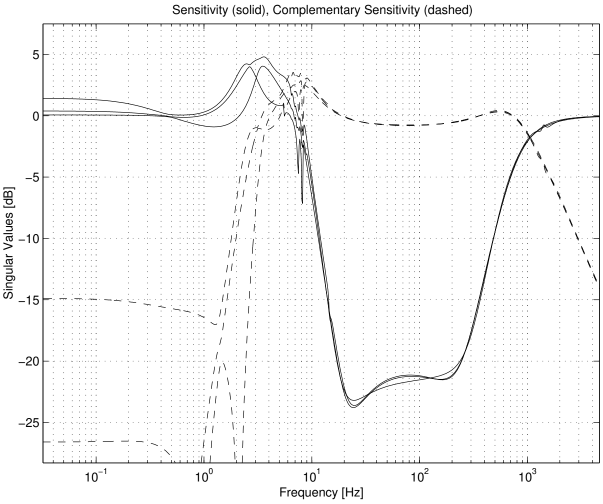

Figure 6.36 *Singular values of S and T for a controller reduced to an order of 30 using balanced state truncation with stability weighting. The closed-loop stability is preserved and the controller does still perform well in closed-loop simulations*

6.6 Robust Stability Analysis

The control design in this report is model based. Any model of a physical system is equipped with modelling errors and the closed-loop system must be able to deal with this. Modelling errors affect the performance of the controller and, what is worse, the closed-loop stability. The effect of model uncertainties on the closed-loop stability is here validated using a perturbation model according to:

$$P_\Delta = (1 + \Delta)P \tag{6.5}$$

where P is the model of the control object used for control design and P_Δ the true physical control object. Conditions for closed-loop stability under the presence of modelling errors described by (6.5) are mentioned in most literature on control theory. For robust stability the following criterion holds [13, 44]:

$$\|\Delta T\|_\infty < 1 \tag{6.6}$$

where T is the complementary sensitivity. The perturbation model (6.5) could be used to describe output errors, covering, for instance, non-modelled high frequency dynamics and time delays. Assume for example that the true system is delayed T_d seconds, then the relation between the true control object and its model used for control design is

$$P_\Delta = e^{i\omega T_d} P \tag{6.7}$$

The perturbation model (6.5) could be used to describe this with

$$\Delta = e^{i\omega T_d} - 1 \tag{6.8}$$

Note also that

$$0 < \left|(e^{i\omega T_d} - 1)\right| < 2 \tag{6.9}$$

which implies that for complementary sensitivity $T < 0.5$, the closed-loop system tolerates any phase delay.

Returning to Figures 6.9 and 6.21 where the complementary sensitivity for the broad band trade-off design and the successful narrow band design are shown respectively. It is clear that the narrow band design is much more robust to modelling errors. The tolerance of the closed-loop system to time delays could be observed from the figures of T. However, it is more easily obtained using a first order Padé approximation in series with the controller. From such an investigation the narrow band design and the broad band trade-off one are found to tolerate maximum delays of 4.2 ms and 0.23 ms, respectively. This is not surprising since the singular values of T at high frequencies is much larger for the broad band design than for the narrow band one. Moreover, a given value of $\overline{\sigma}(T(i\omega))$ corresponds to a specific maximum phase lag α, which in turn is equivalent to a maximum time delay $T_d = \alpha/\omega$.

6.7 Comments

This chapter has been dealing with H_2 controller design for vibration isolation of a linearised model of the control object. The objective has been to design

- one fixed broad band controller that alone achieves broad band vibration isolation
- narrow band controllers to be used in a gain scheduling scheme to achieve broad band vibration isolation

The designed broad band controller (see Figures 6.8, 6.9, and 6.10) has shown good performance and ability to attenuate the transmitted forces with approximately 20 dB for excitations in frequency region II. However, quite high actuator forces are required when the engine is subjected to the transient “Shunt and Shuffle” excitation. The corresponding effect of the controller on the low frequency characteristics is acceptable but the required high actuators forces could lead to saturation of the actuators.

Turning to narrow band H_2 control, it appears to be an excellent way to deal with engine excitation corresponding to idle operating condition. However, it does not seem to be suitable to achieve broad band control based on Gain Scheduling using multiple narrow band controllers since it appears to be very difficult to achieve drops in sensitivity to cover broader frequency ranges without deteriorating the performance beyond desired bandwidth, i.e. in frequency region I and at frequencies between the ones corresponding to the four dominating orders of engine excitation. Such a solution would hence require a very large number of controllers. Therefore, the narrow band solution for vibration isolation will not be treated here any further.

The desired shape of the loop gain (see Figure 4.12) and the large number of control object natural modes close to 10 Hz have been found to require a high order controller. The final broad band design resulted in a controller of order 66. Using model order reduction, the order of the controller has been reduced to 30 states with satisfactory closed-loop characteristics. Further reduction leads to unsatisfactory performance degradation and eventually closed-loop instability.

Since the required actuator forces are quite high when the engine is subjected to the “Shunt and Shuffle” excitation, the effect of input saturation has to be investigated. The results from such an investigation are presented in Chapter 7. It also remains to evaluate the broad band controller developed in Section 6.3 against the non-linear control object model. Chapter 8 deals in details with the non-linearity effects.

7

LINEAR CONTROL OBJECT AND INPUT SATURATION

The actuators have so far been considered ideal and able to generate any forces instantaneously. However, in reality the actuators will be limited with respect to generated forces and if the H_2 controller requires forces higher than this limit the actuators will saturate, i.e. *input saturation*. As seen before, the broad band controller corresponding to the trade-off design requires high control forces of the actuators when the engine is subjected to high transient nominal torque and saturation is therefore likely to occur.

In order to study the basic effects of such phenomena, the actuators have been assumed to saturate at ±300 N. First input saturation is studied on the MIMO system where some interesting occurrences appeared and to closely investigate them, they were re-created using a SISO system with similar characteristics. Finally, the existence of those saturation effects have been explained and confirmed using *describing function analysis*.

7.1 On Controller Implementation

First of all, it is important to notice that a H_2 controller can be implemented with an internal structure identical to the structure of an LQG controller, i.e. with a state observer and state feedback. There are two principally different ways to implement a H_2 controller when the control system is subjected to input saturation.

These two H_2 controller implementations use either the computed control force or the applied (possibly saturated) control force for state estimation. Figures 7.1 and 7.2 describe schematically those principally different ways of implementing the controller. Here, $f(\overline{u})$ is a function describing the saturation, K is the state feedback gain and L is the state estimator gain. Using frequency dependant weighting functions in the H_2 synthesis leads to an extended state space model described by the real matrices $\overline{A}$, $\overline{B}$, $\overline{C}$ and $\overline{D}$. Those matrices are also a realisation of the augmented transfer function from u to y in Figure 6.2.

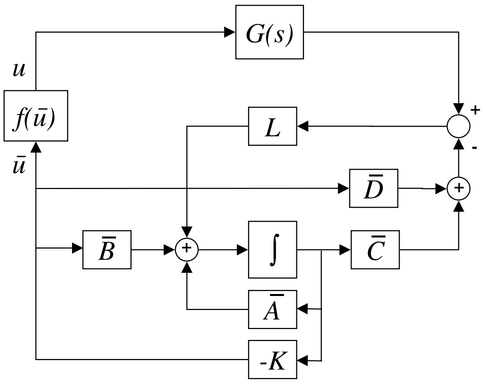

Figure 7.1 *Implementation of a H_2 controller using the computed control force for state estimation*

7.2 The MIMO Case

The two controller implementations described above have been evaluated using the trade-off controller design from Section 6.3 corresponding, e.g. to Figure 6.8. Figures 7.3 to 7.5 show the results from input saturation when the computed control force is used for state estimation, i.e. when using an implementation according to Figure 7.1. The corresponding effects of using the applied control force for state estimation according to Figure 7.2, are shown in Figures 7.6 to 7.8. In both cases, the engine is subjected to the transient “Shunt and Shuffle” excitation corresponding to a dropped clutch operation. Clearly there is saturation using either controller implementations but self-oscillations only when using the applied control force for state estimation.

The effects of input saturation identified above are most easily investigated using a SISO systems. Therefore it would be useful to re-create the results from the MIMO system simulations using a SISO system with similar characteristics. Next chapter describes such a SISO system.

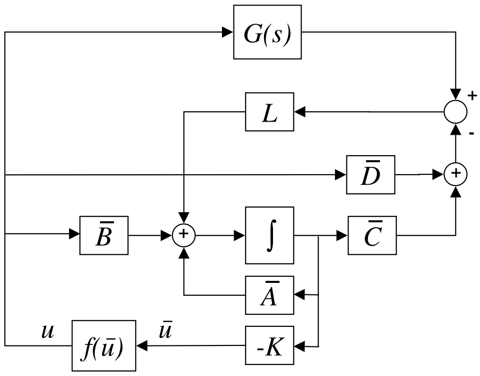
G(s)
L
+
-
$\bar{D}$
+
$\bar{B}$
+
∫
$\bar{C}$
$\bar{A}$
u
$\bar{u}$
$f(\bar{u})$
-K

Figure 7.2 *Implementation of a H_2 controller using the applied control force for state estimation*

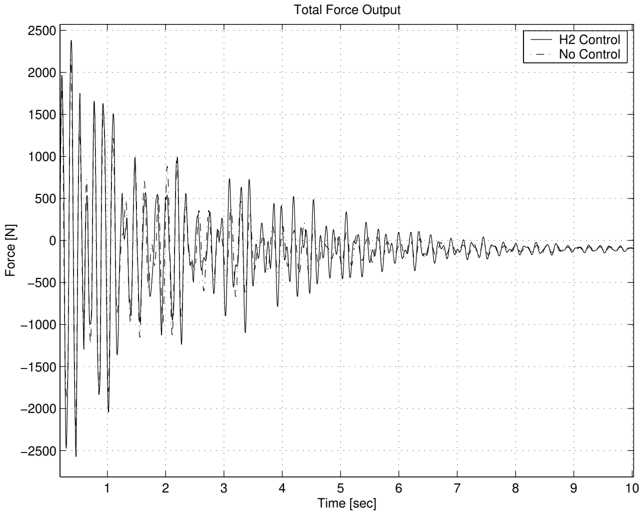

Figure 7.3 y^{LHS} *due the "Shunt and Shuffle" excitation when the state estimator uses the computed control force. There is no self-oscillation in this case*

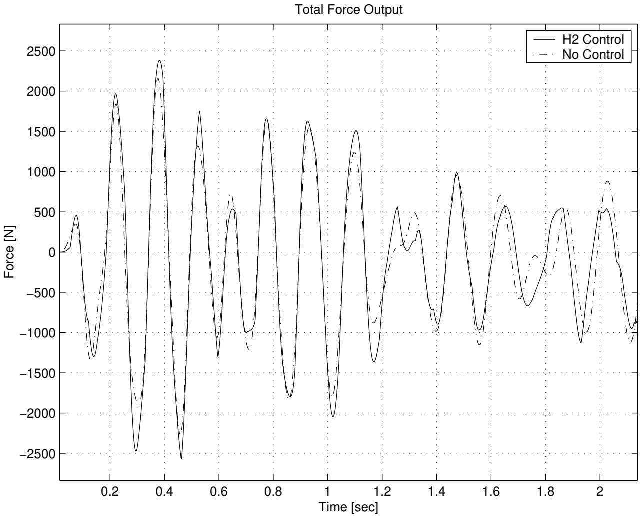

Figure 7.4 *Close-up of Figure 7.3. The effects of saturation is acceptable*

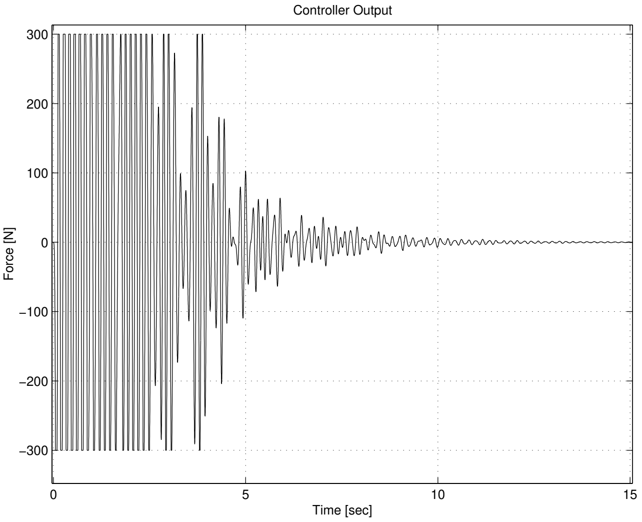

Figure 7.5 *The saturated controller output not used for state estimation at LHS, corresponding to Figure 7.3*

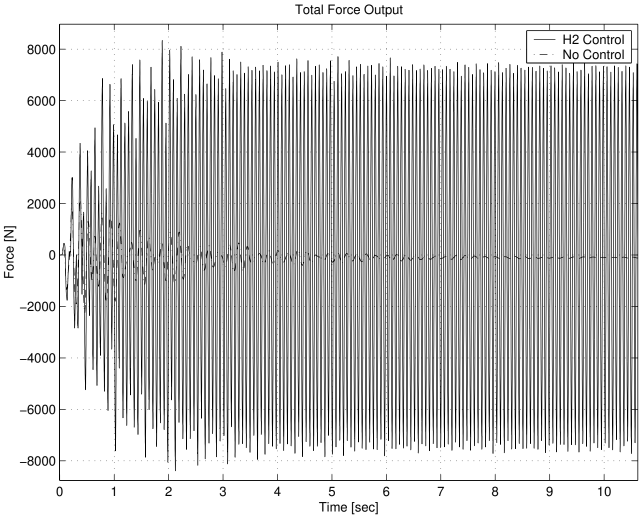

Figure 7.6 *y^{LHS} due the "Shunt and Shuffle" excitation when the applied control force, i.e. the saturated control force, is used for state estimation. There is clearly self-oscillation in this case*

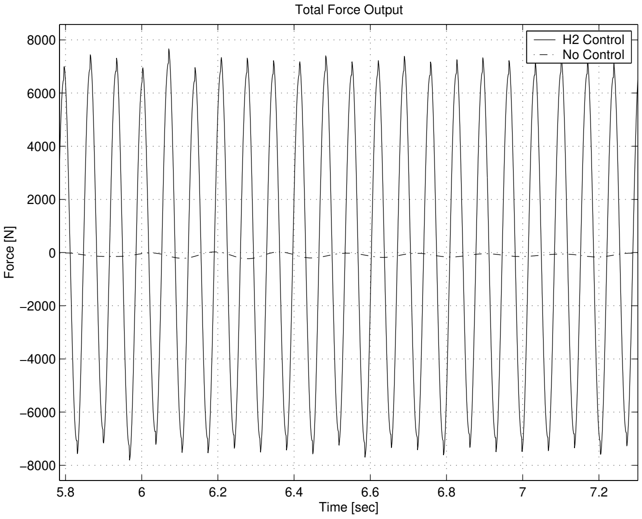

Figure 7.7 *Close-up of Figure 7.6. The transmitted forces are considerable increased which is very unfortunate*

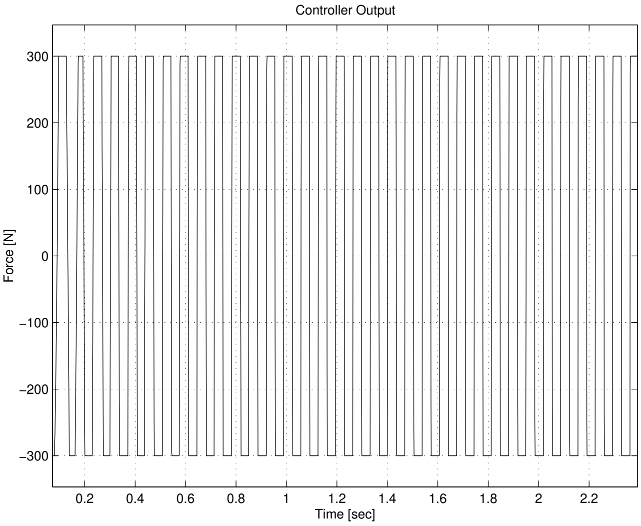

Figure 7.8 *The control force at LHS corresponding to Figure 7.6, i.e. the control force also used in the state estimator*

7.3 A SISO Case Study

Using only the actuator and the sensor at LHS yields a SISO control object with dynamics identical to the ones of the MIMO control object. The frequency characteristics are presented in Figure 7.9. Using the weighting functions from the "trade-off" design in Section 6.3 gives closed-loop characteristics similar to the ones of the corresponding MIMO closed-loop system, see Figures 7.10 and 7.11. The SISO closed-loop system described above is particularly interesting to study if it exhibits similar phenomena as the MIMO closed-loop system in the case of input saturation.

Simulations have once again been performed using the two principally different controller implementations with the engine subjected to the "Shunt and Shuffle" excitation originating from a dropped clutch operation. Figures 7.12 and 7.13 show the results from a simulation where the computed control force is used for state estimation, where Figures 7.14 and 7.15 show the corresponding results when the applied control force is used in the state estimator. Since the effects from the SISO simulations clearly correspond very well to the effects from the MIMO simulations, these phenomena should be further investigated. Such an investigation is presented in the next section.

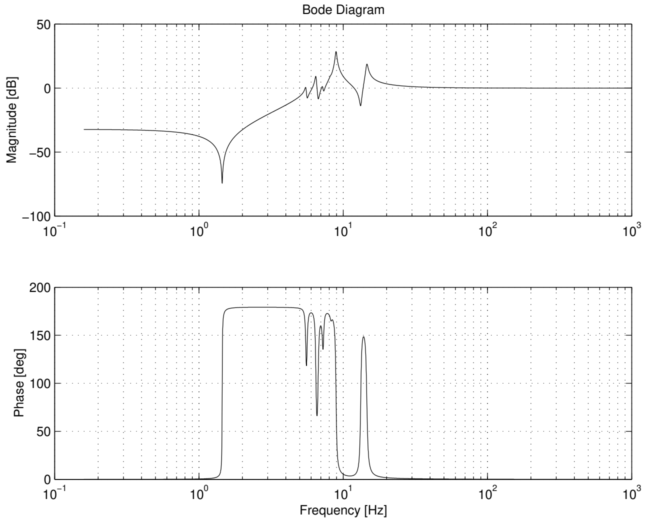

Figure 7.9 *The Bode Diagram of the SISO control object used to re-create the effects of input saturation for the MIMO system*

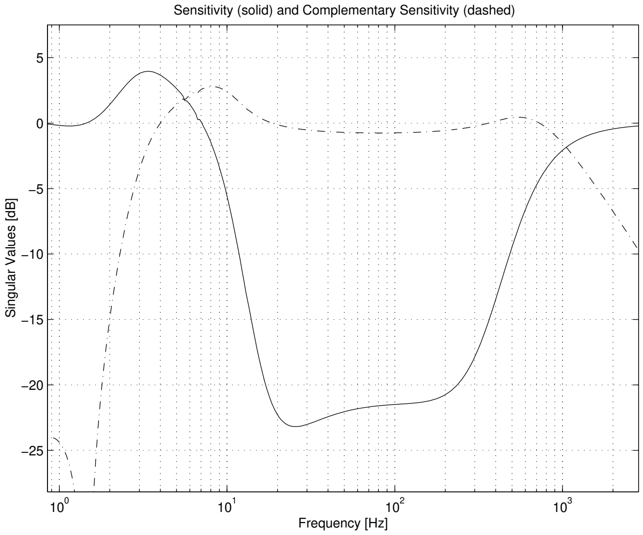

Figure 7.10 *The sensitivity corresponding to a H_2 design using the SISO control object according to Figure 7.9 and the weights from the trade-off design presented in Section 6.3*

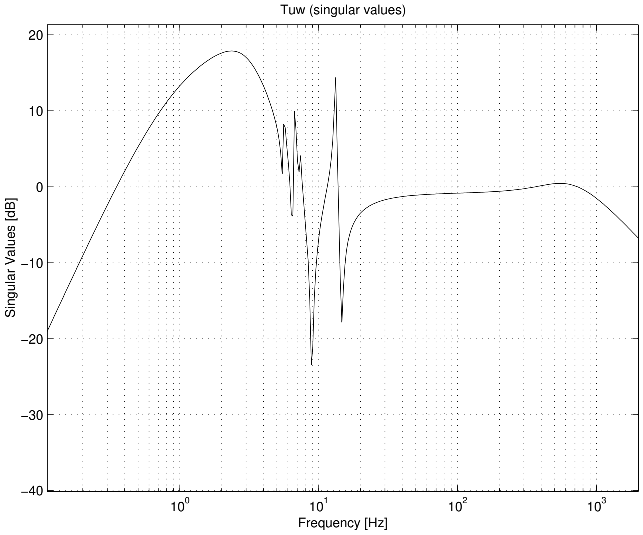

Figure 7.11 *The magnitude of the transfer function T_{uw} corresponding to S in Figure 7.10*

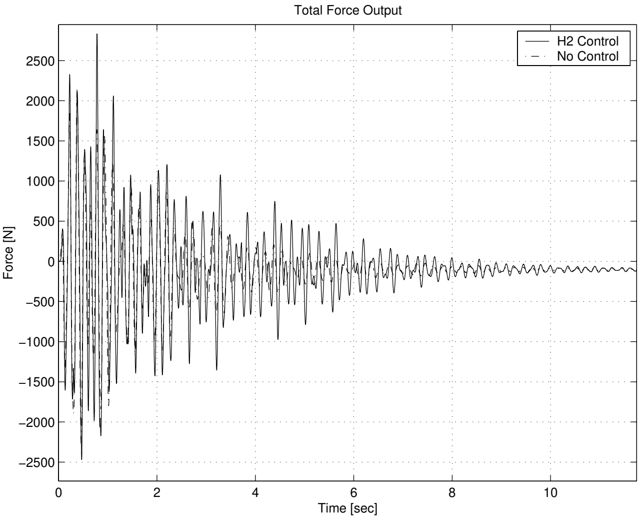

Figure 7.12 *y^{LHS} due the "Shunt and Shuffle" excitation when the state estimator uses the computed control force. There is no self-oscillation and the level of the transmitted force is acceptable*

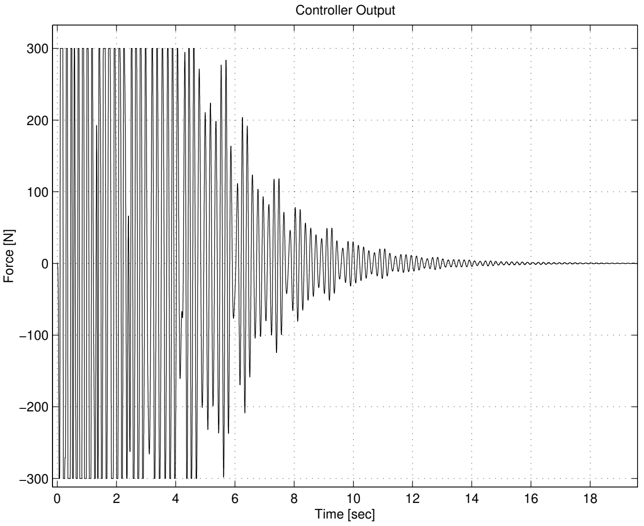

Figure 7.13 *The saturated controller output not used for state estimation at LHS, corresponding to Figure 7.12*

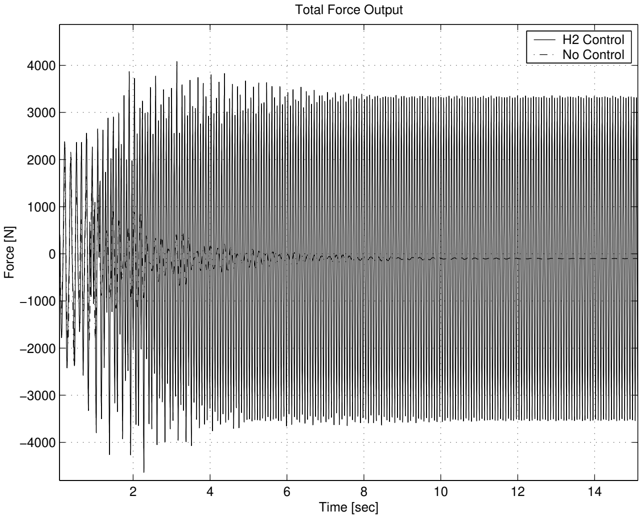

Figure 7.14 y^{LHS} *due the transient excitation when the applied control force is used for state estimation. There is clearly self-oscillation in this case*

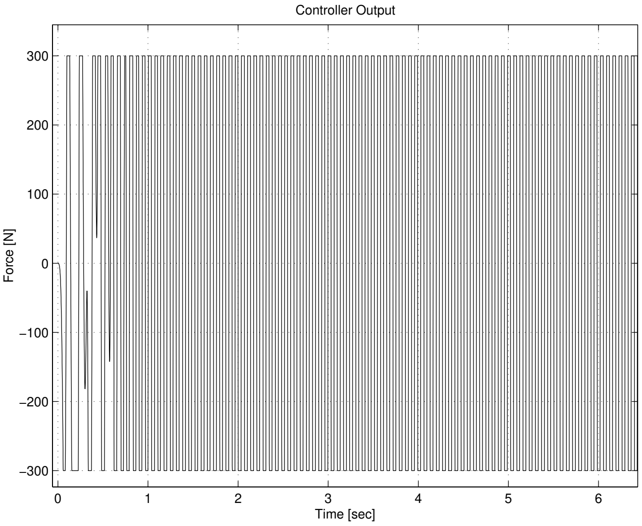

Figure 7.15 *The control force used in the state estimator at LHS, corresponding to Figure 7.14*

7.4 Describing Function Analysis

In this section the phenomena of input saturation is investigated using describing function analysis [2, 13]. This method is used to predict the presence of self-oscillations in a feedback system containing static non-linearity. It is an approximate method and can not be used to prove the presence of self-oscillations but is normally used to give an indication of the closed-loop system behaviour. The set-up for describing function analysis is shown in Figure 7.16.

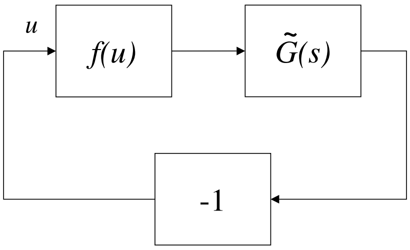

Figure 7.16 *The set-up for describing function analysis. The block $f(u)$ represents the non-linearity*

The describing function theory could be summarised as follows [13]: If there is a linear system ($\widetilde{G}(s)$) and a static non-linearity in a closed-loop negative feedback system, the conditions for self-oscillation is given by

$$Y_f(C)\widetilde{G}(i\omega) = -1 \tag{7.1}$$

where $Y_f(C)$ is the describing function for the non-linearity $f(u)$ in Figure 7.16, C is the amplitude of the oscillating signal u, and ω is the oscillation frequency. The amplitude and frequency of a self-oscillation could also be identified graphically since (7.1) correspond to the intersection between $\widetilde{G}(i\omega)$ and $-1/Y_f(C)$.

As mentioned before it is assumed that the actuators saturate at ±300 N, which means that the expression for the corresponding describing function becomes [13]

$$Y_f(C) = \begin{cases} \frac{2}{\pi}(\arcsin\frac{300}{C} + \frac{300}{C}\sqrt{1-(\frac{C}{300})^{-2}} & C > 300 \\ 1 & C \leq 300 \end{cases} \tag{7.2}$$

Applying the graphical describing function analysis on the SISO systems using the two different controller implementations, require the Nyquist diagram of $\widetilde{G}(s)$.

However, the linear system $\widetilde{G}(s)$ will be different for the two implementations described in Section 7.1. $\widetilde{G}$ has been derived for the two cases from Figures 7.1 and 7.2. The function $f(u)$ in Figure 7.16 is the same as $f(\overline{u})$ in Figure 7.1 and Figure 7.2. For state estimation using the computed control signal according to Figure 7.1, $\widetilde{G}$ is

$$\widetilde{G}(s) = K(sI - \overline{A} + \overline{B}K - L\overline{D}K + L\overline{C})^{-1}LG(s) \tag{7.3}$$

where $G(s)$ is the transfer function of the SISO control object. For an implementation according to Figure 7.2 (i.e. using the applied control force for state estimation), $\widetilde{G}$ is

$$\widetilde{G}(s) = G_1(s) + G_2(s)G(s) \tag{7.4}$$

where

$$\begin{aligned} G_1(s) &= K(sI - \overline{A} + L\overline{C})^{-1}(\overline{B} - L\overline{D}) \\ G_2(s) &= K(sI - \overline{A} + L\overline{C})^{-1}L \end{aligned} \tag{7.5}$$

The Nyquist diagram corresponding to (7.3) is shown in Figure 7.17, and for (7.4) the Nyquist diagram is shown in Figures 7.18 and 7.19. Noticing that the locus of $-1/Y_f(C)$ is a line from -1 to $-\infty$, it is clear that there is intersection between the Nyquist diagram of $\widetilde{G}$ and $-1/Y_f(C)$ only when the applied control force is used for state estimation. Moreover, at the intersection, ω is approximately equal to 91rad/sec. and C is approximately equal to 22700. The signal u in Figure 7.16 could therefore be expected to self-oscillate with a frequency of 91rad/sec (approximately 14.8 Hz) and with an amplitude of approximately 22700N. Since the Nyquist diagram corresponding to $\widetilde{G}$ given by (7.4) is quite complicated, the same diagram without the reflection with respect to the real axis is shown in Figure 7.20. Another way of determining if and where $\widetilde{G}$ crosses the negative real axis is using a traditional Bode diagram. This is presented in Figures 7.21 and 7.22. The alternative presentations of $\widetilde{G}$ may not make it more easy to identify the intersection between $\widetilde{G}$ and $-1/Y_f(C)$, but they confirm the previous observation.

Figure 7.23 shows the signal u from Figure 7.16 corresponding to the simulation using the applied control force for state estimation (see Figures 7.14 and 7.15), where Figure 7.24 shows the magnitude of its Fourier transform. The indications from the describing function analysis are hence very consistent with the simulation results shown in Section 7.3.

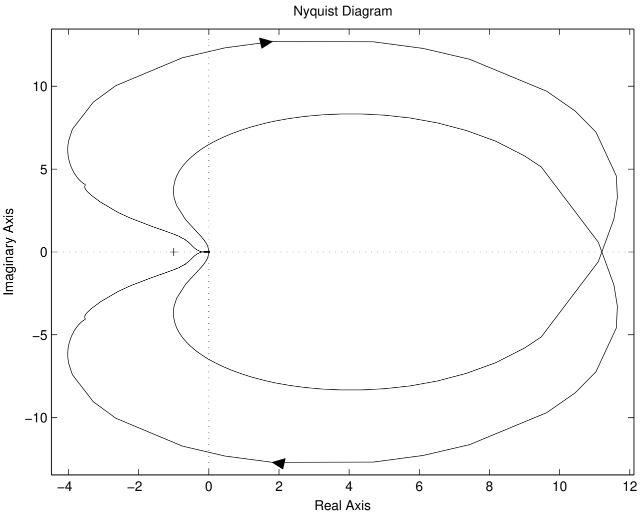

Figure 7.17 *The Nyquist diagram corresponding to* $\widetilde{G}$ *described by (7.3)*

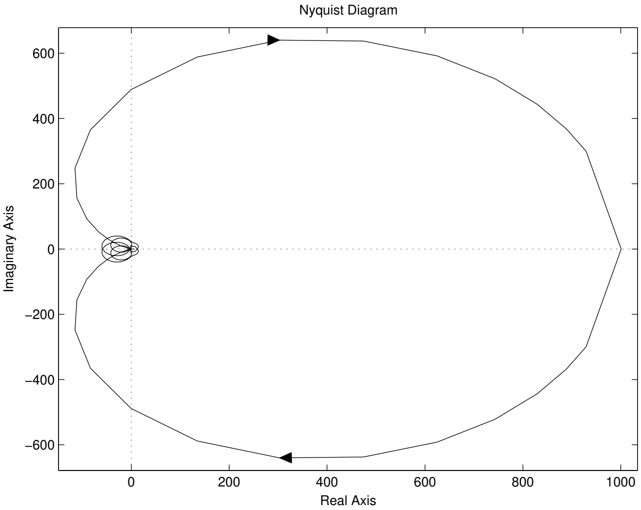

Figure 7.18 *The Nyquist diagram corresponding to* $\widetilde{G}$ *described by (7.4)*

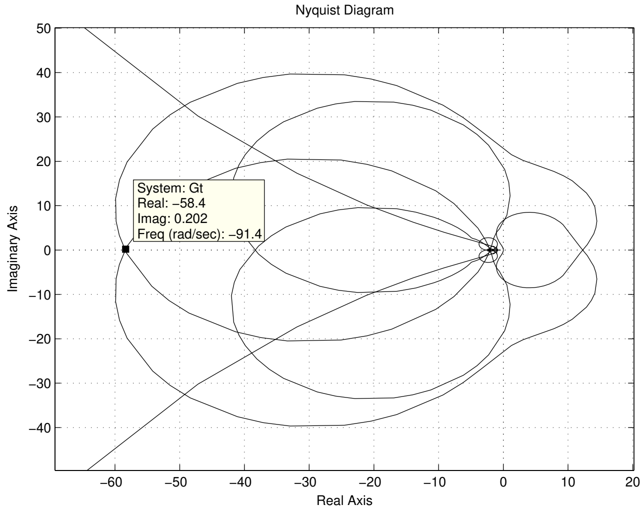

Figure 7.19 *Close-up of Figure 7.18*

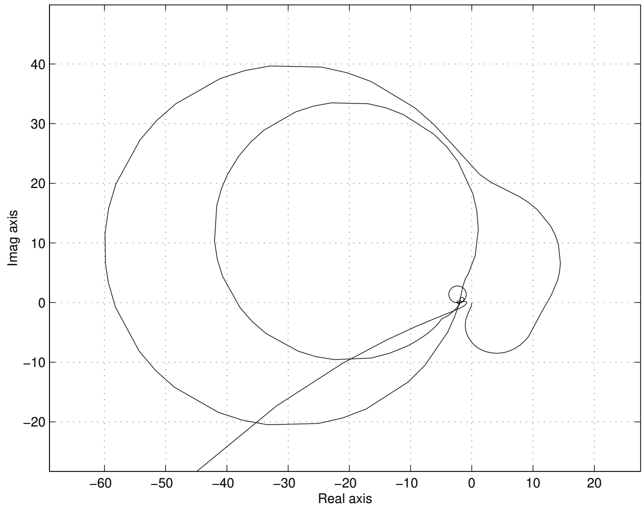

Figure 7.20 *Nyquist diagram for* $\widetilde{G}$ *given by (7.4) without the reflection with respect to the real axis*

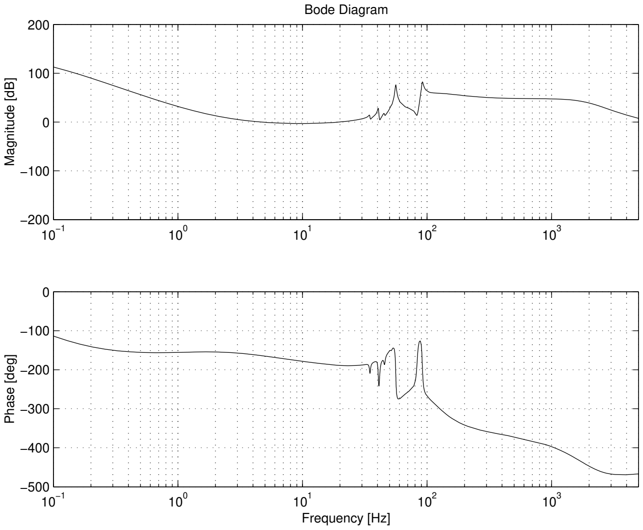

Figure 7.21 *Bode Diagram of the transfer function $\widetilde{G}$ given by (7.4)*

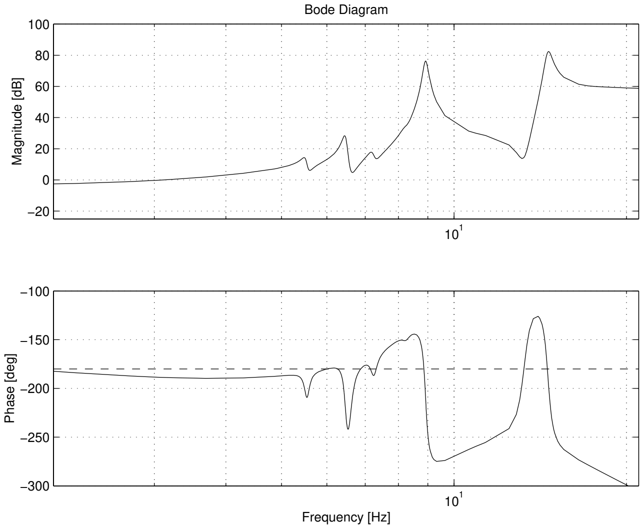

Figure 7.22 *Close up of Figure 7.21*

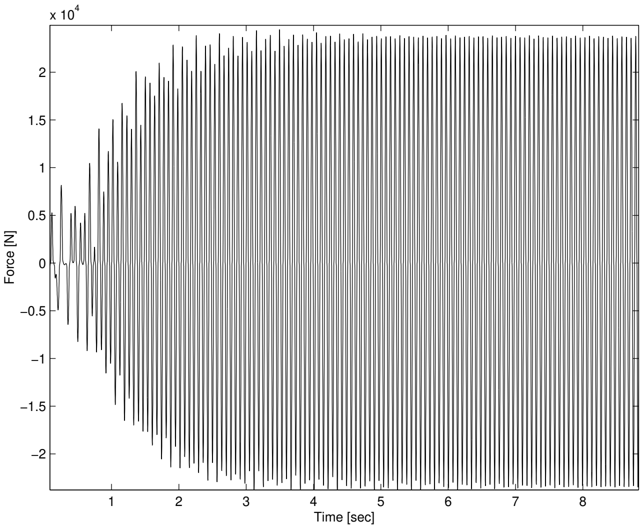

Figure 7.23 *The signal u for the SISO simulation with state estimation using the applied control force*

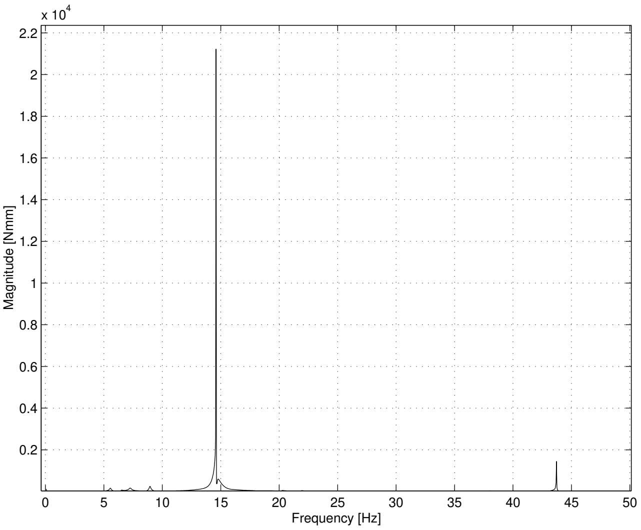

Figure 7.24 *Magnitude of the Fourier transform of the signal u*

7.5 Comments

In this chapter, the actuators forces have been assumed limited to ±300 N. Consequently, when the engine is subjected to the “Shunt and Shuffle” excitation, the broad band controller developed in Section 6.3 causes the actuators to saturate. The effects of input saturation are still found to be acceptable where the closed-loop system remains stable. Unexpectedly it has been found that the computed control signal has to be used in the controller to avoid self-oscillations. This conclusion is a bit surprising but supported by the results from describing function analysis. Since, the conclusion from the simulations and analysis carried out in this chapter are rather unusual, it is an issue for further investigations which is beyond the scope of this work.

8

Control of the Non-linear Control Object

Using H_2 control theory guarantees stability even though the stability margins could be arbitrarily small [5]. Furthermore, differences between the model used for controller design and the true physical control object, might lead to performance degradation. For this particular problem, the linear model previously used for design in Chapter 6 is known to have modelling errors due to linearisation. Therefore, an investigation of those designs using the non-linear model of the physical control object and closed-loop simulations, will be considered in this chapter.

The two broad band designs developed based on the linearised model of the control object in Section 6.3, were first validated using co-simulation, i.e. using the non-linear control object model (see Chapter 3 and Figure 3.2), with the engine subjected to the "Shunt and Shuffle" excitation. In both cases, closed-loop instability occurred. However, this is not surprisingly when considering the large discrepancy between the two open-loop responses (see Figures 8.1 and 8.2), presenting the control object output at the RHS engine mount and torque rod, i.e. y^{RHS} and y^{TR}, respectively.

To estimate the size of the output error, the two outputs have been transformed using DFT-analysis. This shows that the low frequency contribution from zero to about 30 Hz dominates the differences between the outputs of the two models. For linear systems, the condition for robust stability (6.6) could then have been used to specify the required shape of the complementary sensitivity T in order to achieve stability. However, this analysis is not valid when dealing with non-linear systems. Despite that, it will here be used to possibly give an approximate estimate of requirements on T. Thus, the singular values of the complementary sensitivity T should be small for frequencies below 30 Hz to achieve closed-loop stability.

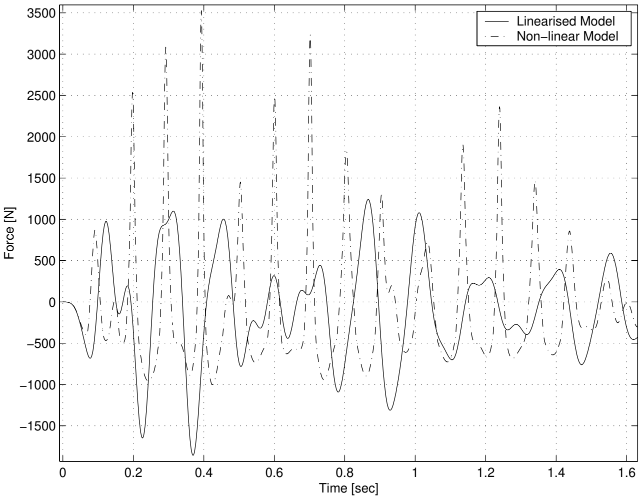

Figure 8.1 *y^{RHS} due to the "Shunt and Shuffle" excitation applied to the non-linear model and its linearisation used for control synthesis (i.e. open-loop responses). For this excitation, the linear model is hence a rather poor description of the control object*

8.1 Stability Trade-off Design

To be able to deal with the identified model discrepancy originating from unmodelled non-linearity, the above mentioned analysis indicates that the controller should have small singular values of T below 30 Hz. This additional requirement contradicts the desired closed-loop characteristics in region II (see Chapter 4 and Figure 4.12), starting at approximately 11.7 Hz. Hence, it is expected to be a difficult task to find a satisfactory broad band controller.

In fact, it seems to be impossible to find an acceptable controller that suppresses the excitation in the complete engine speed range, due to the additional requirement on T. This is simply because the loop gain cannot be both high and low at the same time. Thus, another control design approach has to be sought for when considering the mentioned circumstances. There could be two reasons for this which are related to the linearisation errors originating from

- non linear material characteristics
- large angular displacements of the engine

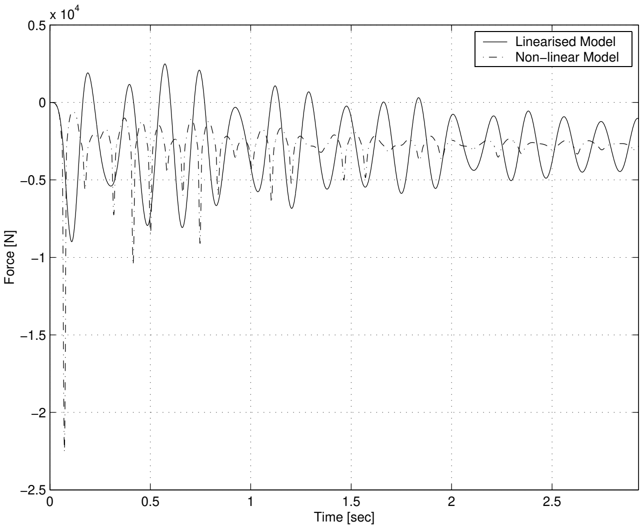

Figure 8.2 *y^{TR} due to the "Shunt and Shuffle" excitation applied to the non-linear physical model and its linearisation used for control synthesis (i.e. open-loop responses), demonstrating the poor agreement between the responses*

It must be sorted out if the models differences are due to non-linear material characteristics or even large angular displacements, since this might restrict the region of operating conditions that a linear controller could possibly deal with. This will be the topic of the following two sections.

8.2 Non-linear Material Effects

Carefully studying the stiffness characteristics of the mounts and bushings of the passive engine suspension system, it is seen that the stiffnesses are locally reduced for some directions, close to the engine static equilibrium position corresponding to the engine working point for idle operating condition. An example of this is shown in Figures 8.3 and 8.4, presenting the static stiffness in the global x-direction of the torque rod rear bushing connecting it to the subframe. The reason for those local reductions is to minimise the transmitted forces at idle operating condition while providing higher stiffnesses at driving operating conditions.

The stiffness of mounts and bushings used in an AES system do not have to be locally reduced for the above reason, presumed that the closed-loop system could suppress the excitation corresponding to idle operating condition. Consequently, those stiffnesses have been linearised for future investigations, see Appendix A.2. Figure 8.5 shows the stiffness in the global x-direction of the torque rod rear bushing

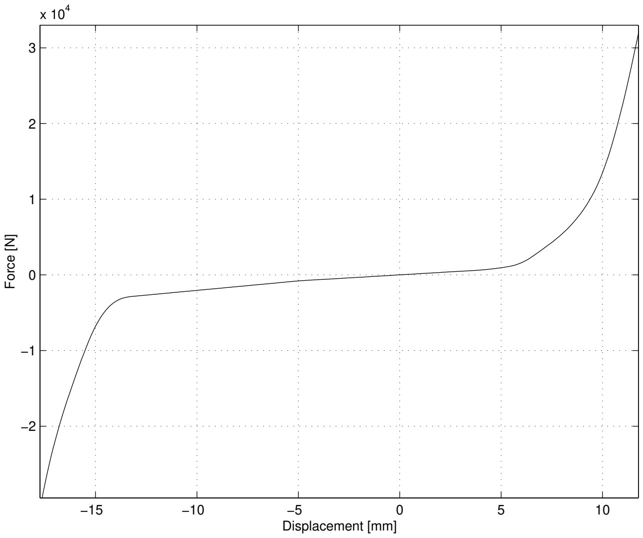

Figure 8.3 *Static stiffness in the global x-direction of the torque rod rear bushing*

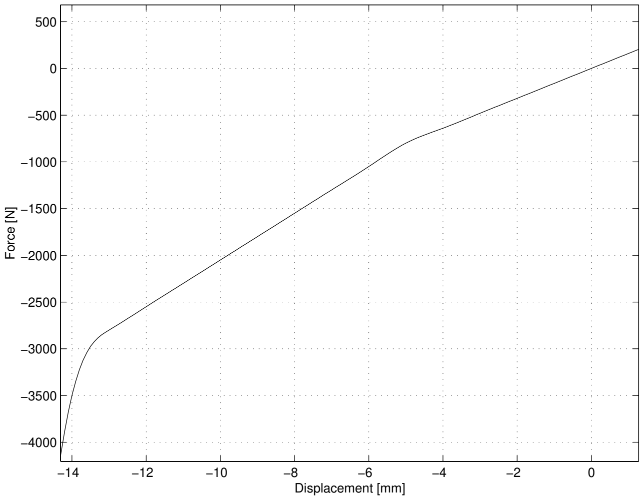

Figure 8.4 *Close-up of Figure 8.3*

connecting it to the subframe, before and after linearisation.

From Chapter 2 and Figure 2.8, it is mentioned that the excitation corresponding to driving operating condition consists of a fluctuating torque superimposed on a nominal one. Since the engine working point is insignificantly affected by the fluctuating torque, it is neglected when investigating the effects of the nominal torque level.

With completely linear stiffnesses about the static equilibrium position and increased stiffnesses for large displacements, the stiffness elements exhibit non-linear characteristics dependant on the level of the nominal torque. To simplify the control synthesis, it is suitable to distinguish between the suppression of excitations corresponding to low and high levels of nominal torque causing the mounts and bushings to exhibit:

- linear material characteristics
- non-linear characteristics

, respectively. Figure 8.6 presents the load case used to simulate the low level together in comparison to the "Shunt and Shuffle" excitation. Relating to driving operating conditions, the low level nominal torque arises from normal acceleration of the car.

To proceed, closed-loop simulations have been carried out with linearised stiffnesses when the engine is subjected to the low level load case. Those simulations still show closed-loop instability even though an investigation of the forces in the bushings show that they are all well within the intervals with linear stiffnesses. The conclusion of this study is that the discrepancy between the non-linear and the linearised model is not only due to the non-linear material properties, but also due to large angular displacements. This will be further investigated in next section.

8.3 Large Angular Displacements Effects

When the engine is subjected to a nominal torque corresponding to certain driving operating conditions, then its most dominating displacement is the rotational one around the global y-axis. Figure 8.7 shows schematically the angular displacement α of the engine when subjected to a constant nominal torque, M_x, applied in the x-direction with respect to the local engine co-ordinate system (see Figure 2.1). Considering the control object output at LHS, i.e. the z-component of the transmitted force with respect to the global co-ordinate system, the mount stiffness contribution due to the angular displacement is

$$\Delta F_z = k_z L(\cos\alpha - 1) \tag{8.1}$$

where k_z is the stiffness of the LHS mount in the global z-direction and L is the

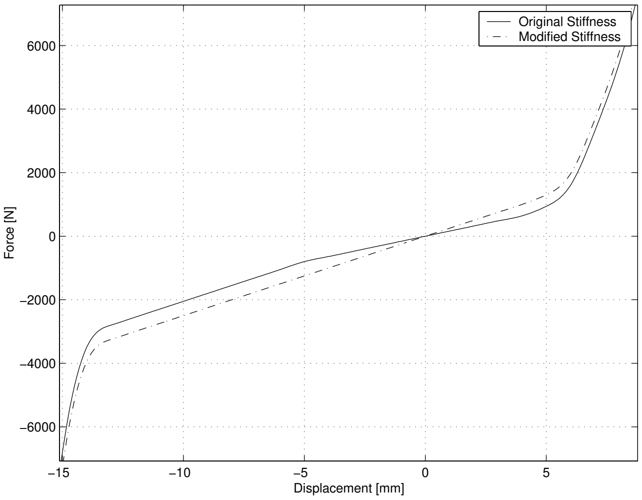

Figure 8.5 *Translational stiffness in the x-direction (global co-ordinate system) of the bushing connecting subframe and torque rod, before and after linearisation*

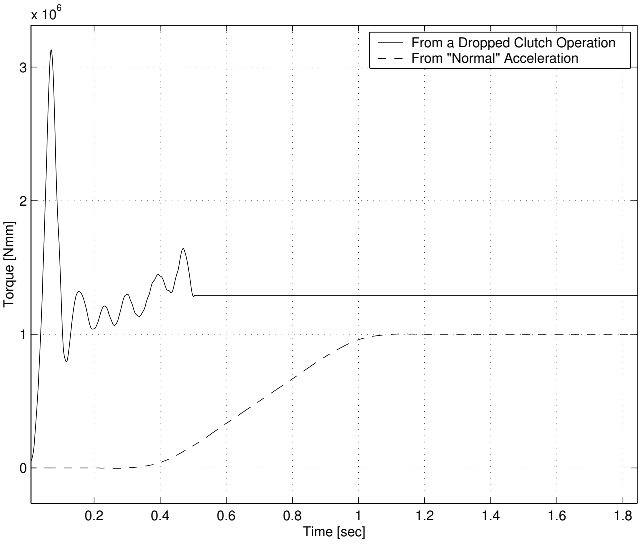

Figure 8.6 *The nominal load corresponding to a normal acceleration of the car together with the "Shunt and Shuffle" excitation.*

distance from the engine rotational center to its position. Linearising the equations of motions about the static equilibrium position ($\alpha = 0$), the *cosine*-term in (8.1) could then be approximated with a constant equal to 1. Thus, the force contribution according to (8.1) is equal to zero for all angular displacements around the global y-axis. Such a linearisation effect is believed to be the reason why closed-loop instability occurs when the engine is subjected to the low level nominal torque according to Figure 8.6.

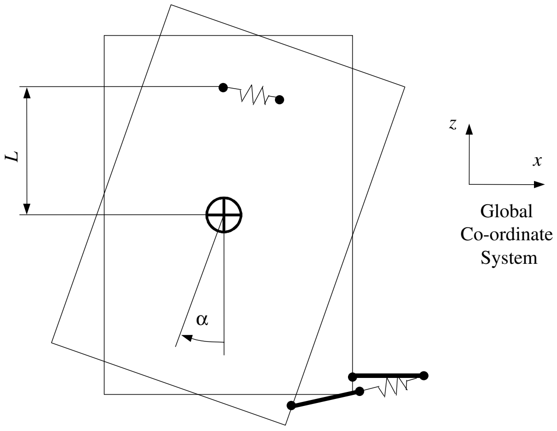

Figure 8.7 *Angular displacement of the engine alpha around the global y-axis and the distance from the engine rotational center to its position L*

A linearisation of the non-linear control object about an equilibrium operating point, could be represented as

$$\begin{aligned} \delta\dot{x} &= A(m_e)\delta x + N(m_e)\delta m \\ \delta z &= C(m_e)\delta x \end{aligned} \tag{8.2}$$

where $\delta m = m - m_e$, $\delta z = z - z_e$, and m_e describes the operational equilibrium point about which the non-linear model is linearised and represents a nominal torque M_x. Equation (8.2) is also used to represent the linear model of the control object in (3.2) where $m_e = 0$Nm.

To closely investigate if the model discrepancies originate from a non-linearity due to large angular displacements, three simulations have been performed to investigate the differences in the open loop responses. In all cases M_x is equal to a ramp from 1000Nm to 1050Nm where the three different control objects correspond to:

- the non-linear model
- the original model linearisation about $m_e = 0\text{Nm}$
- a model linearised about $m_e = 1000\text{Nm}$

Figures 8.8, 8.9, and 8.10 show the responses, i.e. the transmitted forces at LHS (y^{LHS}), RHS (y^{RHS}), and torque rod (y^{TR}), of the three models, respectively. As expected, the response of the linearisation about $m_e = 1000\text{Nm}$ is much more consistent with the response of the non-linear model than the one corresponding to the linearisation about $m_e = 0\text{Nm}$, where both level and dynamic contents are well correlated.

To conclude, the reason for model discrepancy between the non-linear model and its linearisation is not only due to non-linear material characteristics, but also large angular displacements. A controller that takes the effects of those two non-linearity types into consideration is hence desired. Section 8.4 deals with this problem.

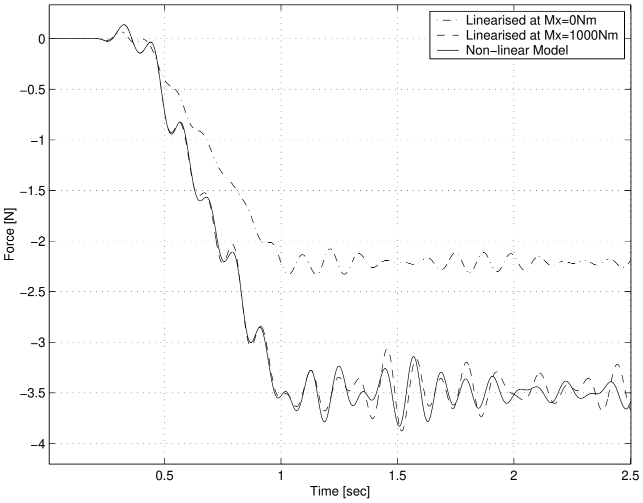

Figure 8.8 *y^{LHS} for the three different models when subjected to a nominal torque from 1000Nm to 1050Nm*

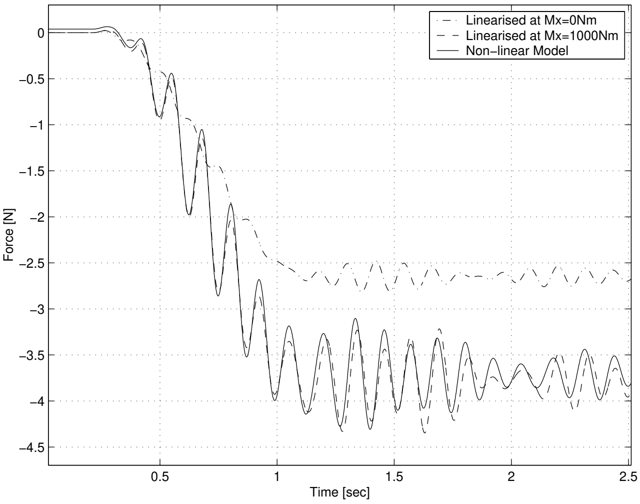

Figure 8.9 *As Figure 8.8 but for* y^{RHS}

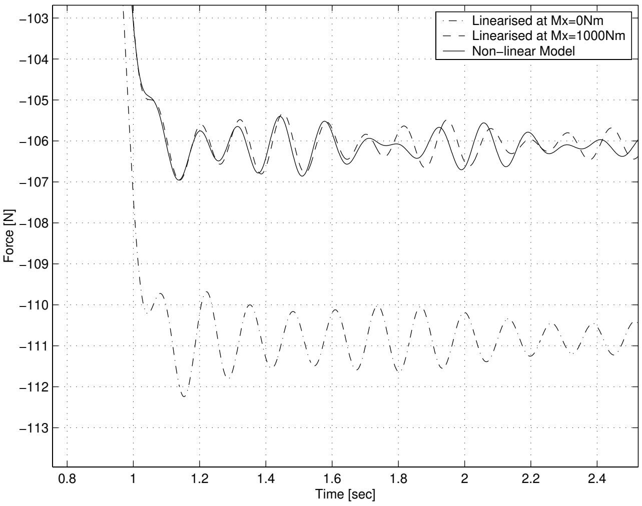

Figure 8.10 *As Figure 8.8 but for* y^{TR}

8.4 Gain Scheduling and Non-linearities

In the previous section it is stated that model discrepancy due to large angular displacement, is the reason for closed-loop instability, when the engine is subjected to the low level nominal torque excitation (see Figure 8.6). One way to take this phenomenon into account is to let the controller change with the variation of the engine angular displacement, i.e. with variation of nominal torque level. This can be done using a *Gain Scheduling* [34] scheme consisting of H_2 controllers based on several linearisations about different equilibrium operating points.

Gain Scheduling to deal with the low level nominal torque is first investigated where linearisations about four equilibrium operating points, $m_e = 0$, 500, 1000, and 1500Nm have been considered. To proceed, H_2 controllers for each of the points were designed and implemented in a Gain Scheduling scheme with linearly interpolated parameters scheduled on the LHS mount force in the global x-direction, since this parameter has been identified to accurately describe the engine angular displacement around the global y-axis.

Figure 8.11 shows the transmitted force at LHS, y^{LHS}, when the engine is subjected to the low level nominal torque, where the three different curves correspond to an open-loop simulation using the non-linear model and two closed-loop co-simulations. The two closed-loop simulations make use of the original trade-off controller discussed in Section 6.3 and the non-linear controller based on Gain Scheduling.

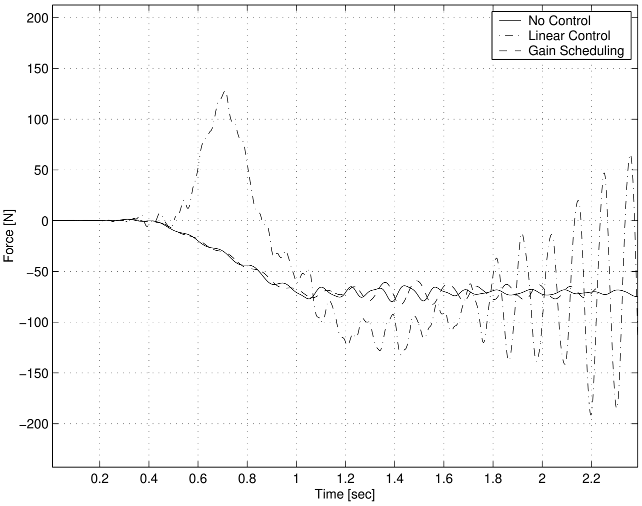

Figure 8.11 *y^{LHS} due to the low level nominal torque. Without control, with H_2 control based on a linearisation at static equilibrium ($m_e = 0$), and with Gain Scheduling. Thus, closed-loop stability is achieved using Gain Scheduling*

Closed-loop stability achieved when using Gain Scheduling further confirms the fact that non-linearities due to large angular displacements are the reason for model discrepancy.

The Gain Scheduled controller is the only one of the controllers considered so far that is able to deal with the low level nominal torque. However, it still remains to validate its ability to deal with excitation corresponding to driving operating conditions, where the fluctuating torque according to Figures 2.2, 2.3 and 2.4 are superimposed to the low level nominal torque.

Simulations bring forward that it is necessary to low pass filter the scheduling parameter to achieve good performance and closed-loop stability. Figures 8.12 and 8.13 show the control object output at LHS and at torque rod when using Gain Scheduling to deal with excitation corresponding to driving operating conditions. The curves represent the responses with and without low pass filtered scheduling parameter as well as the open-loop response. Clearly, the Gain Scheduled controller with low pass filtered scheduling parameter is to a large extent able to suppress the excitation. Without low pass filtering the scheduling parameter strongly depends on the actuator forces, especially the one at LHS, implying that a closed-loop is generated in addition to the main feedback loop. This feedback loop has the potential to become unstable which also occurs for the case without low pass filtered scheduling parameter.

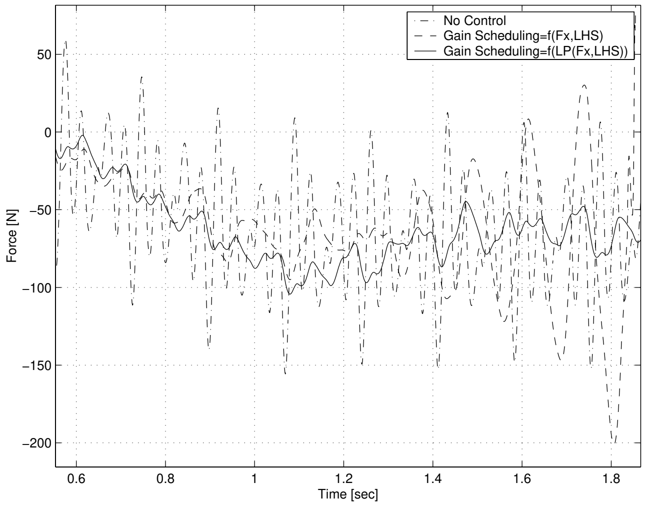

Figure 8.12 *y^{LHS} due to the driving operating condition corresponding to the low level nominal torque in the case of no control and when using Gain Scheduling with and without low pass filtered scheduling parameter. The performance is pretty good when using low pass filtering, and otherwise, there is closed-loop instability*

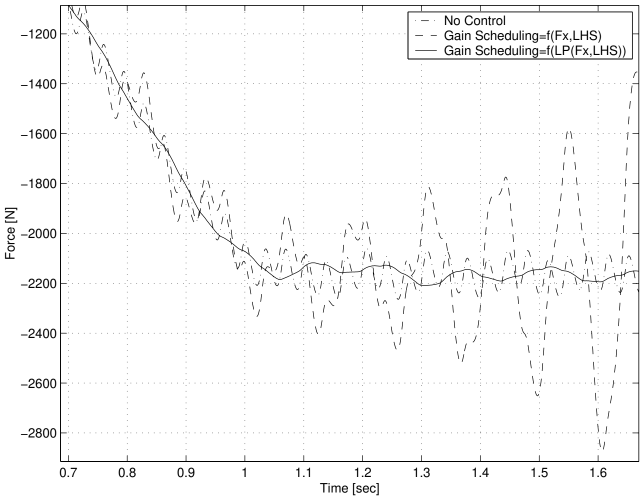

Figure 8.13 *As 8.12 but for* y^{TR}

What remains to investigate is the potential of using Gain Scheduling to deal with excitation causing the mounts and bushings to exhibit non-linear material characteristics. As mentioned, the mounts and bushings exhibit linear or non-linear stiffness characteristics depending on the level of the nominal part of M_x where high nominal levels arise, for instance, from rapid accelerations. Figure 8.14 presents, among others, a time history of such a high level nominal torque.

It seems to be impossible to achieve closed-loop stability for excitations that cause the mounts and bushings to exhibit non-linear stiffness characteristics. Gain Scheduling requires a scheduling parameter accurately describing the equilibrium operating point of the non-linear control object. Since this parameter has to be low pass filtered, it cannot reflect the operating point for rapidly changing control object dynamic characteristics. This is what occurs when the engine is subjected to excitation causing the control object to show its quickly changing non-linear material characteristics. However, it could also occur for rapid changes in the level of the nominal torque, i.e when dealing with high ramping speeds. Consequently, Gain Scheduling is limited to low level nominal torque excitations and low to moderate ramping speeds.

8.5 Gain Scheduling and Input Saturation

In the previous section, it has been shown that closed-loop stability and satisfactory suppression of excitations corresponding to driving conditions with a low level nominal torque, can be achieved using Gain Scheduling. However, the actuators were assumed to be ideal and, hence, the effect of their limitation remains to be investigated.

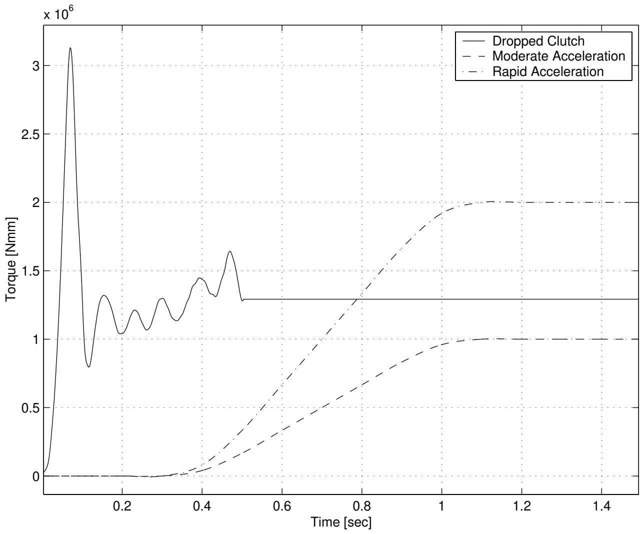

Figure 8.14 *The nominal part of M_x corresponding to a moderate and a rapid acceleration. The measured 1st gear engine torque during a dropped clutch operation is also shown*

Figure 8.15 shows the actuator forces calculated by the Gain Scheduled controller corresponding to the stable simulation presented in Figures 8.12 and 8.13. Using assumptions from the investigation of the effects of input saturation in Chapter 7, i.e. with the actuators limited to ±300N, the actuator force at the torque rod will clearly cause input saturation. To validate input saturation effects in this case the simulation has been repeated with actuators limited to ±300N. The result is presented in Figures 8.16 to 8.18 showing the transmitted forces at LHS, y^{LHS}, with and without control, as well as the saturated actuator one at the torque rod, u^{TR}, respectively. From the figures it is clear that input saturation seems to be rather harmless for excitations corresponding to driving operating conditions with low level nominal torque, i.e. when dealing with moderately rapid changes of control object dynamic characteristics.

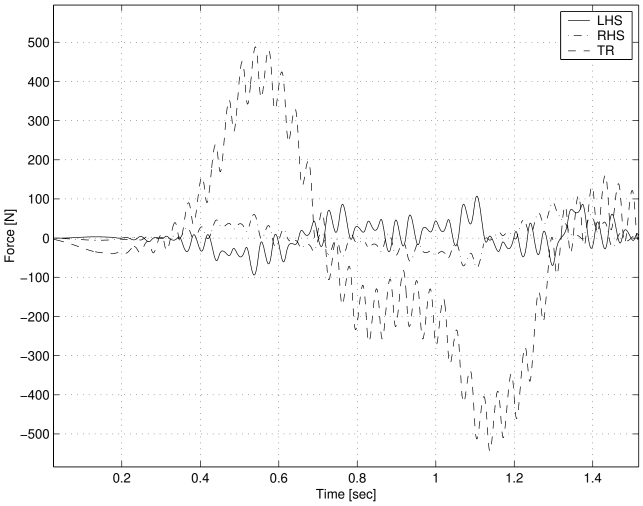

Figure 8.15 *The actuator forces, u^{LHS}, u^{RHS} and u^{TR}, corresponding to the stable suppression of the driving operating excitation presented in Figures 8.12 and 8.13*

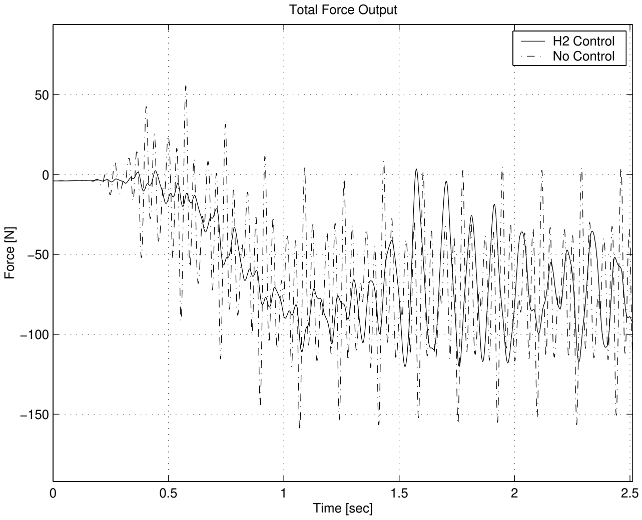

Figure 8.16 *y^{LHS} with Gain Scheduling control and without control when the engine is subjected to the excitation corresponding to the driving operating condition with the low level nominal torque where actuators are assumed to be limited to ±300 N. Thus, the effects of input saturation is acceptable*

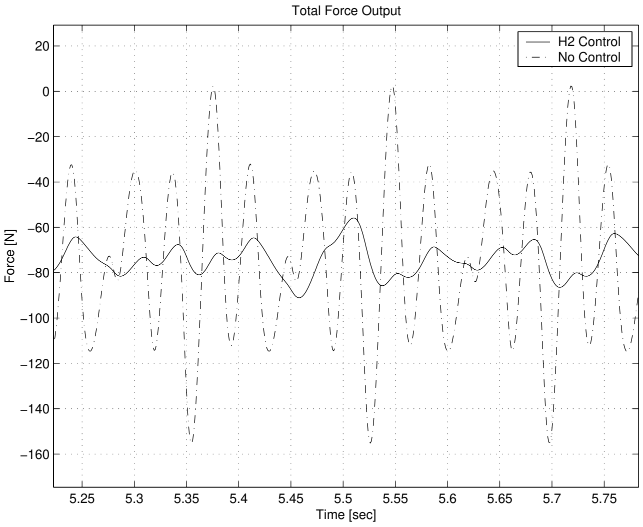

Figure 8.17 *As Figure 8.16, demonstrating the nice steady-state performance*

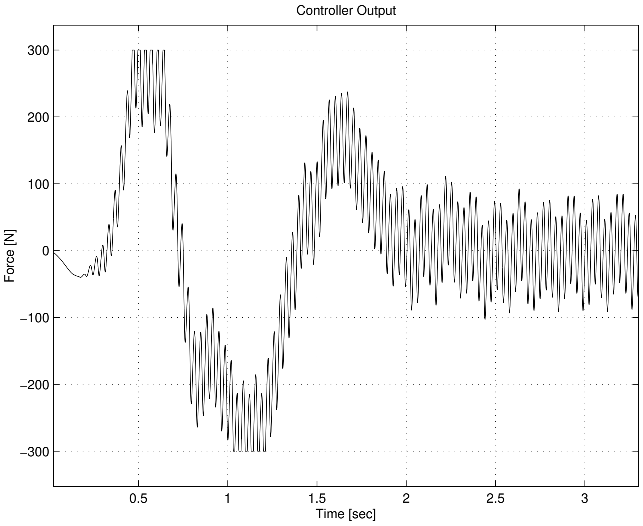

Figure 8.18 *The actuator force, u^{TR}, corresponding to the simulation result presented in Figures 8.16 and 8.17*

8.6 Comments

This chapter handlers non-linearities of the control object. It has been shown that there are two different errors that occurs due to linearisation that have to be considered. Those are

- linearisation errors due to large angular displacement of the engine
- linearisation errors due to non-linear material characteristics

Using Gain Scheduling, a non-linear controller has been obtained that deals with non-linearities corresponding to low and moderate transient load levels and ramping speeds, i.e. only non-linearities originating from large angular engine displacements. Moreover, for driving operating conditions corresponding to such conditions, the fluctuations in the control object output are acceptably suppressed.

9

General Discussion

9.1 Engine Excitation Characteristics

In Chapters 6 and 8 it has been shown that the conditions for control synthesis change with engine excitation characteristics, mainly due to the non-linearities of the control object, where the load cases used in the evaluation of the control design correspond to:

- engine idle operating condition
- engine driving operating condition with nominal part of $M_x = 1000\text{Nm}$
- engine driving operating condition with the nominal part of $M_x = 2000\text{Nm}$
- a dropped clutch operation, i.e. a “Shunt and Shuffle” excitation

The dynamics of the control object depend on the level of the nominal part of M_x, see Chapter 8. At moderate levels, the control object exhibits non-linear characteristics due to large angular displacements and at higher levels even due to non-linear material properties.

Gain Scheduling is useful when the operating point changes slowly with respect to the control object dynamics. Thus, this technique is suitable when dealing with excitations corresponding to low and moderate levels of ramping speeds and nominal part of M_x.

For this particular problem, it is clear that the excitation characteristics determining the possibilities of using Gain Scheduling could be described by two parameters α and L, according to Figure 9.1, representing ramping speed and nominal torque level, respectively. The control object dynamics changes too fast relative to the speed of change of the operating point when α is large and when L is high. In the case of non-linear material characteristics, the dynamics of the control object changes more rapidly at high levels nominal torques than at low ones for a specific ramping speed due to varying stiffnesses of mounts and bushings.

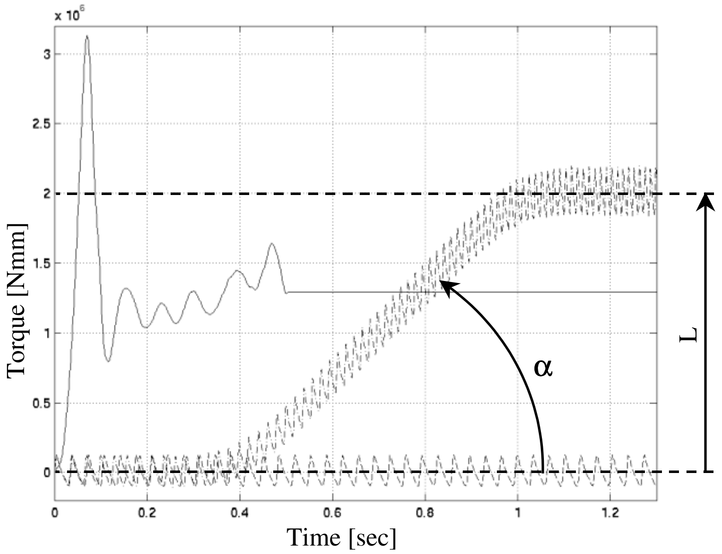

Figure 9.1 *The ramping speed α and nominal torque level L determining the speed of change of the control object dynamics. The curves represent measured 1st gear engine torque during a dropped clutch operation, as well as the torque M_x corresponding to engine idle ($\alpha = 0$) and driving operating conditions, respectively*

The broad band external road excitation which have manifold effects, have not yet been discussed. For frequencies around the natural frequencies of the passive engine suspension system, road excitation will excite the engine modes to resonances possibly causing large engine displacements. In this case, high mount damping are desired implying high dynamic stiffnesses which is in conflict with the main objective of the AES system to attenuate the forces transmitted to body and subframe. The developed feedback controller deals with this situation by leaving the low frequency mount characteristics unchanged.

As mentioned before, the objectives of the AES system is to reduce body and chassis structural vibration and, consequently, decreasing structure borne noise inside the car compartment. AES systems achieve this by reducing the engine transmitted forces to neighboring subsystems. However, when dealing with road excitation, this could actually increase the noise and vibration inside the compartment since the forces acting on body and chassis originating from road and combustion process, might cancel each other.

To closely deal with external road engine excitation, an extended control object model including at least the car front-end and its subsystems, has to be considered. Moreover, evaluation of the performance of AES system should be based on body and subframe accelerations in stead of transmitted forces. These are all important issues for future investigation.

9.2 Feedback Signal Choice

Transmitted forces is a natural feedback signal choice when the mounts are assumed clamped at one side. However, in general the choice of feedback signal is not obvious. Displacement, velocity, and acceleration of the receiver as well as the linear momentum with respect to the transmitted force, are other possible alternatives. It has been pointed out that the receiver dynamics will to a greater extent influence the transfer function from the actuator force to the feedback signal, in the case of acceleration feedback than in the case of total force feedback [33, 38]. However, acceleration feedback has been successfully used for active vibration isolation enhancement [16], where the natural frequencies of the flexible receiver were well above the passive stage corner frequency.

Effects of acceleration feedback have, to some extent, been investigated in this work. The body and subframe have been modelled using 6DOFs stiffness and damping elements and, thus, 18 DOFs (i.e. 36 states) were added to the control design model. Using stiffnesses approximately ten times higher than the ones of the mounts, the transfer function between the control force and the feedback signal, i.e. the control object dynamics, has been noticed to have about the same complexity in both cases and, thus, the measurement of the total force should not considerably simplify control synthesis. Consistently with the above discussion, closed-loop simulations comprising acceleration feedback showed results similar to the ones corresponding to total force feedback.

To conclude, the objectives together with the problem prerequisites determine the most suitable choice of feedback signal. For every unique problem, this choice has to be carefully considered.

9.3 AES System Characteristics

In Section 4.2 it was shown that when dealing with AES systems using active engine mounts consisting of actuators in parallel with passive elements, the actuators forces will cancel the fluctuating forces in the passive elements. This has been verified using closed-loop simulations, see Figure 9.2. The figure shows the forces in the LHS active mount corresponding to a closed-loop simulation when the engine is subjected to excitation corresponding to its idle operating condition.

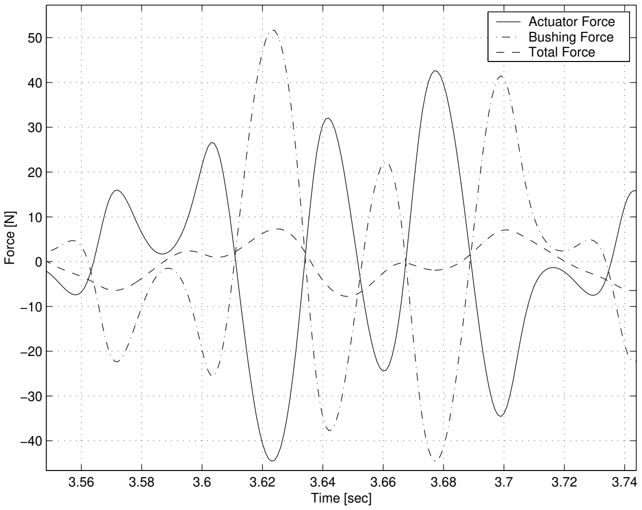

Figure 9.2 *Forces in the LHS mount*

Furthermore, as expected from the investigation done in Section 4.2, the engine vibration amplitudes are reduced when using feedback control with high gain at frequencies above 11 Hz. Figure 9.3 shows the accelerations in the z-direction at LHS with and without control when the engine is subjected to excitation corresponding to its idle operating conditions. Since the displacements of the engine are reduced, the forces in the passive elements are also decreased, see Figure 9.4. However, in reality stiffness and damping contributions from other, to engine, coupled subsystems such as the drive shafts, the subframe, etc., would also affect the engine vibrations. These effects are important issues for further investigations.

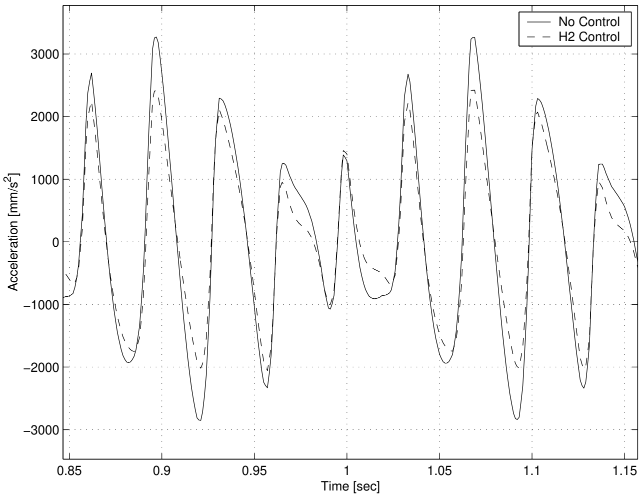

Figure 9.3 *Engine acceleration in z-direction at LHS. Hence, the corresponding displacement is somewhat reduced due to the AES system which is highly desirable*

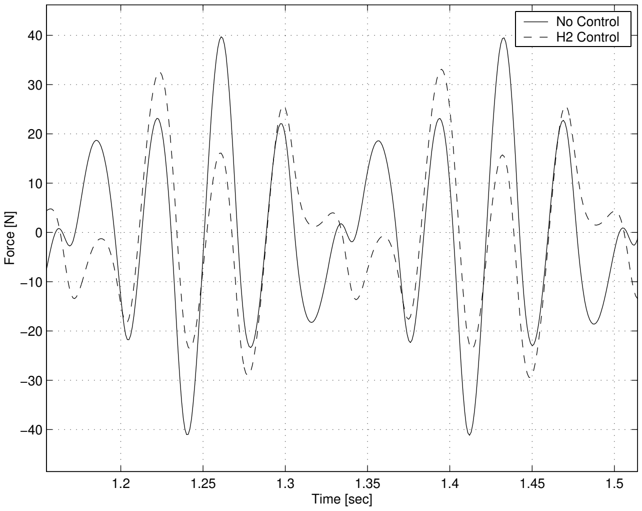

Figure 9.4 *Force in z-direction at LHS, with and without control. The result is consistent with the ones presented in Figure 9.3*

10

CONCLUDING REMARKS

A MIMO AES system controller for broad band attenuation of transmitted forces from the engine to chassis and body has been developed using feedback control. The proposed solution deals with system non-linearities and all possible engine excitations except those corresponding to very high ramping speed or extremely high nominal engine torque for which the controller has to be turned off.

The desired closed-loop characteristics is pointed out to require a specific and rather unusual loop gain shape. Classical control methods and LQG theory have been evaluated but found to be deficient. Instead, H_2 frequency domain loop shaping technique has been used which proved to be a powerful method, where desired closed-loop characteristics and stability have found to be easily achieved when dealing with a linearised model of the control object. However, due to the desired loop gain and the properties of the control object dynamics, an implementation of the feedback controller requires as many as 30 states.

The active engine suspension system design has been carried out making use of a virtual simulation, analysis, and verification environment. This has been used to perform realistic closed-loop system evaluations covering all control object physical characteristics including non-linearities, and also to generate linearisations of the control object for control synthesis.

Two different kinds of non-linearities are shown to be lacking when the control object is linearised about engine static equilibrium position. Those are non-linear material characteristics of the engine mounts and large angular engine displacements. To obtain desired performance and closed-loop stability, it is demonstrated that both non-linearities have to be taken into account.

To deal with those non-linearities, a time varying state space control object representation has been assumed. Making use of this representation, a Gain Scheduled control scheme has been designed. Generally, Gain Scheduling is suitable when dealing with slow variations of the control object working point relative to its dynamics. For the particular system of interest, the consequence of this is shown to be a limitation in the scope of excitations that could be dealt with. The engine excitation has been parameterised using ramping speed α and nominal torque level L. In terms of these parameters, all engine excitations corresponding to idle and engine driving operating conditions as well as other transient excitations are shown to be possible to handle and effectively suppress, except those corresponding to very high values of α and L, where control object dynamics change rapidly.

For excitations close to the limits described above where the Gain Scheduling approach fails, the designed feedback control scheme generates rather large control forces amplitudes. Therefore, assuming engine mount actuators limited to ±300 N, the effects of input saturation have been investigated using describing function analysis. Two different controller implementations using computed and applied control force for state observation has been considered. Unexpectedly, to avoid closed-loop self-oscillations due to input saturation, the computed control force has to be used for state observation.

To summarise, it is clear that feedback control theory could be used to design an AES system with desired broad band attenuation at the expense of pretty low stability margins. However, it must be emphasised that this conclusion is with respect to this particular problem and could not be generalised. Details such as number, locations, and directions of sensors and actuators will of course influence the AES system design. For example, considering only the force transmitted from the torque rod to the subframe gives a SISO input-output relationship less sensitive to changes of engine equilibrium operating point than the MIMO relationship used throughout this report. As a consequence, desired closed loop performance and stability might be achievable without making use of Gain Scheduling.

To select the most suitable control approach for this problem, the adaptive feedforward approach must also be investigated in details. Feedback control provides the opportunity to deal with broad band attenuation without the feedforward control requirement to track the engine speed. However, considering the issue of sound quality, the feedforward approach is more suitable where the objective is to control individual excitation orders. In some cases, depending on the AES system objectives, a combination of feedforward and feedback is probably to prefer.

No other existing engine signals have been investigated but could lead to more accurate estimations of engine equilibrium operating point. If so, no extra sensor is necessary for Gain Scheduling and low pass filtering of the scheduling parameter would not be necessary.

Finally, the unexpected saturation effect is another interesting issue for further investigation. For more specific studies, it is also recommended to evaluate the above mentioned control approaches in practise.

APPENDIX

A.1 Control Object Model Data

This section presents the geometry of the engine suspension layout, masses and inertial properties of the bodies, and the stiffnesses and damping characteristics of the mounts and bushings.

A.1.1 Rigid Bodies

	Engine	Torque Rod
Mass [kg]	268.7	0.13
Center of gravity [mm]	(1559.6, 41.4, 554.7)	(1872.0, -106.3, 315.0)
I_{XX} [kgmm^2]	23960000	463.6
I_{YY} [kgmm^2]	11330000	463.6
I_{ZZ} [kgmm^2]	24040000	1.60
I_{XY} [kgmm^2]	-800000	0.0
I_{ZX} [kgmm^2]	440000	0.0
I_{YZ} [kgmm^2]	2340000	0.0

Table A.1 *Rigid Bodies Data*

Position	Global co-ordinates [mm]
LHS Mount	(1606.0, -412.5, 725.0)
RHS Mount	(1510.4, 476.9, 778.7)
Torque Rod Front Bushing	(1822.0, -107.5, 315.0)
Torque Rod Rear Bushing	(1510.4, 476.9, 778.7)

Table A.2 *Mounts and bushings locations*

A.1.2 Mounts and Bushings Damping

	Translational [Ns/mm]			Rotational [Nmms/deg]		
Position	x	y	z	x	y	z
LHS Mount	0.1	0.1	0.15	0.0262	0.0279	0.0271
RHS Mount	0.1	0.1	0.15	0.0262	0.0279	0.0271
Torque Rod Rear Bushing	0.1	0.1	0.15	0.0262	0.0279	0.0271
Torque Rod Front Bushing	0.15	0.15	0.15	1.5	1.6	1.55

Table A.3 *Damping with respect to global co-ordinate system*

A.1.3 Mounts and Bushings Stiffnesses

The figures below present the non-linear static stiffness characteristics of the mounts and bushings in all directions.

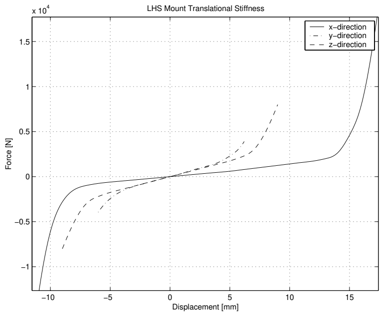

Figure A.1 *LHS mount static translational stiffnesses characteristics in x-(solid), y-(dash-dotted), and z(dashed)-directions with respect to global co-ordinate system*

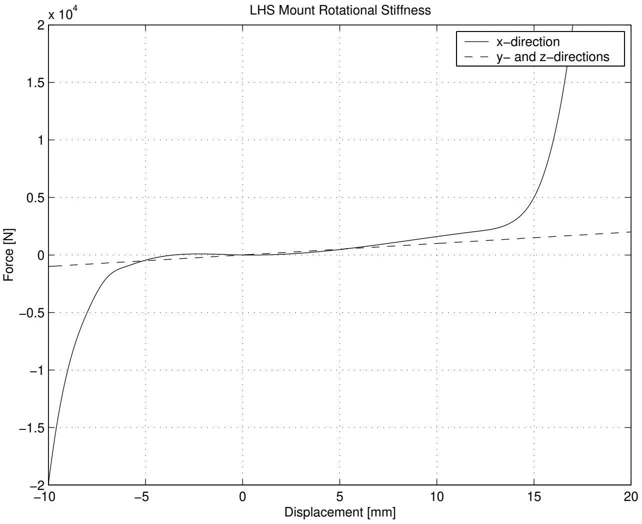

Figure A.2 *LHS mount static rotational stiffnesses characteristics with respect to global co-ordinate system*

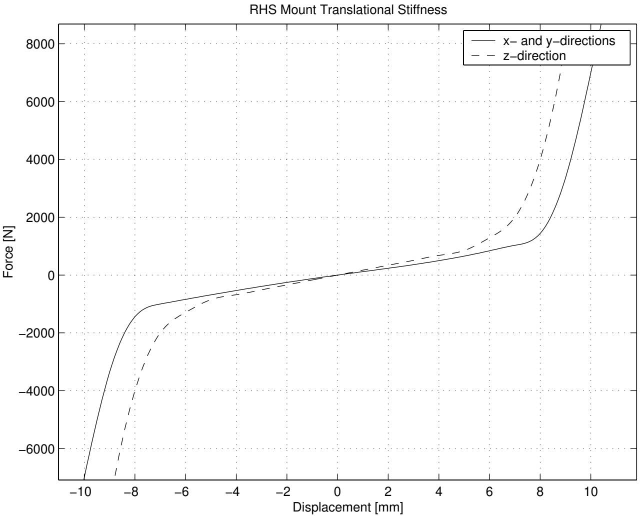

Figure A.3 *RHS mount static translational stiffnesses characteristics with respect to global co-ordinate system*

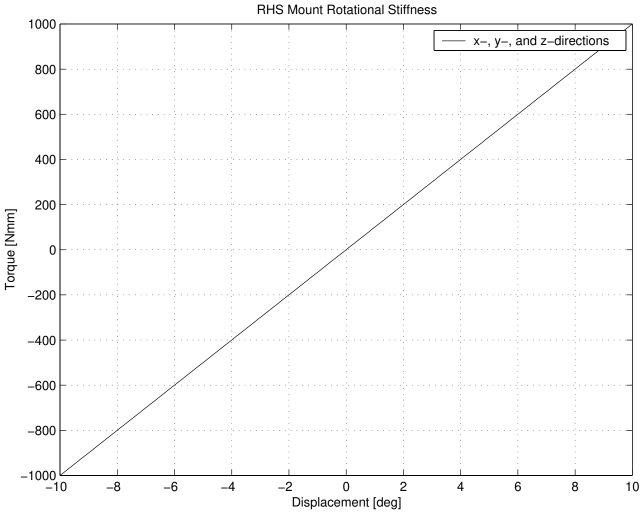

Figure A.4 *RHS mount static rotational stiffnesses characteristics with respect to global co-ordinate system*

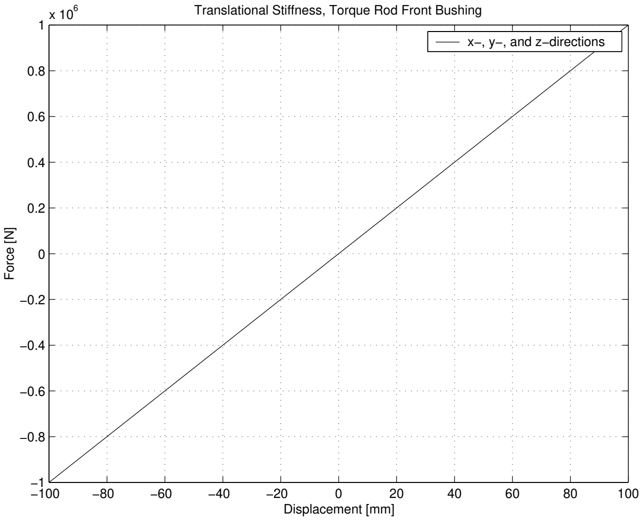

Figure A.5 *Torque rod front bushing static translational stiffnesses characteristics with respect to global co-ordinate system*

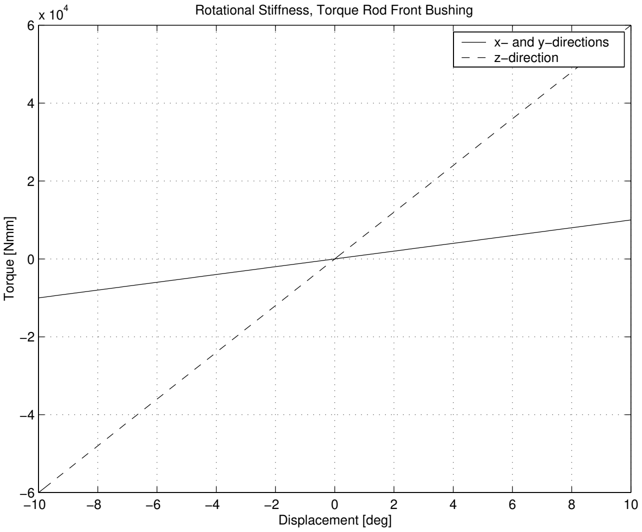

Figure A.6 *Torque rod front bushing static rotational stiffnesses characteristics with respect to global co-ordinate system*

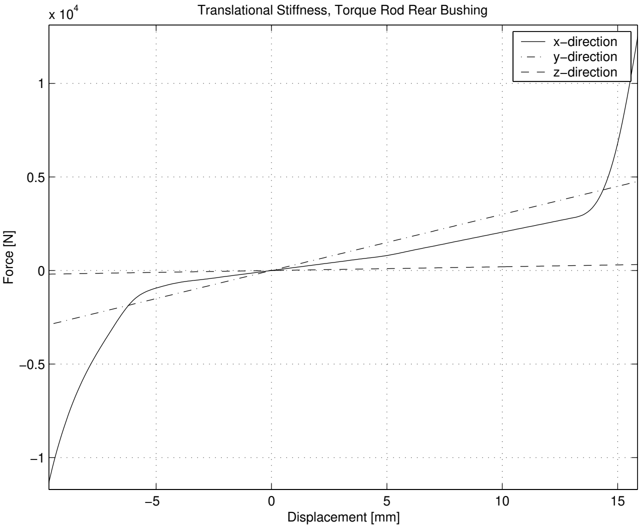

Figure A.7 *Torque rod rear bushing static translational stiffness characteristics with respect to global co-ordinate system*

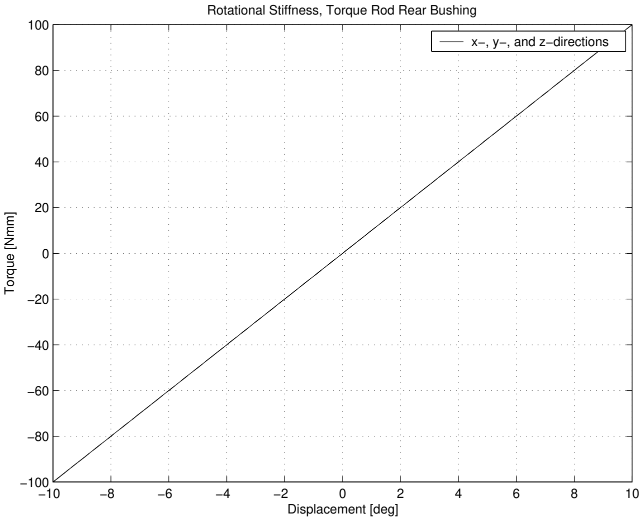

Figure A.8 *Torque rod rear bushing static rotational stiffness characteristics with respect to global co-ordinate system*

A.2 Modified Control Object Model Data

A.2.1 Mounts and Bushings Stiffnesses

Modifications of mounts and bushings static stiffnesses characteristics that have been performed in Section 8.2, are according to the figures below.

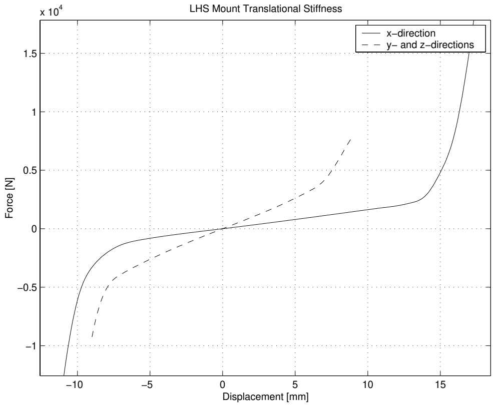

Figure A.9 *LHS mount static translational stiffnesses characteristics with respect to global co-ordinate system*

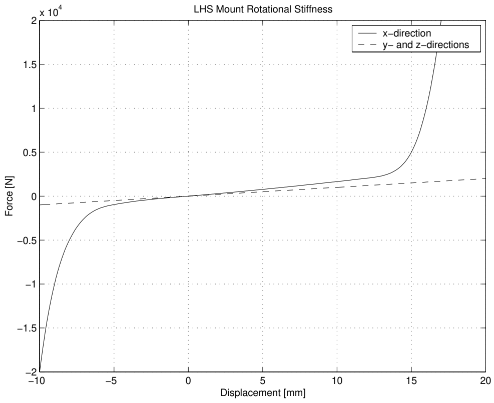

Figure A.10 *LHS mount static rotational stiffnesses characteristics with respect to global co-ordinate system*

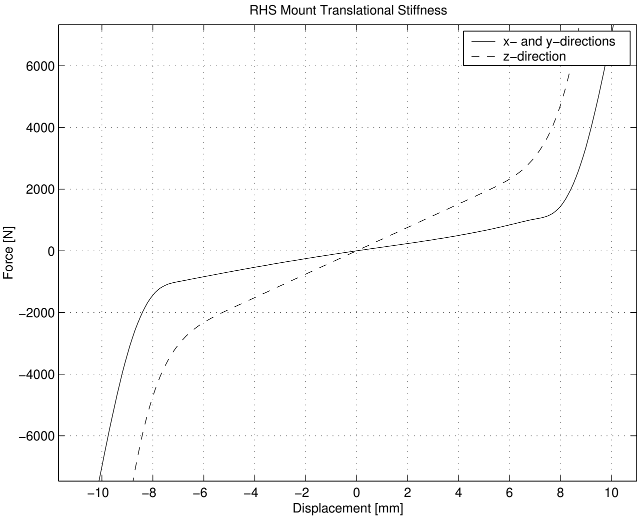

Figure A.11 *RHS mount static translational stiffnesses characteristics with respect to global co-ordinate system*

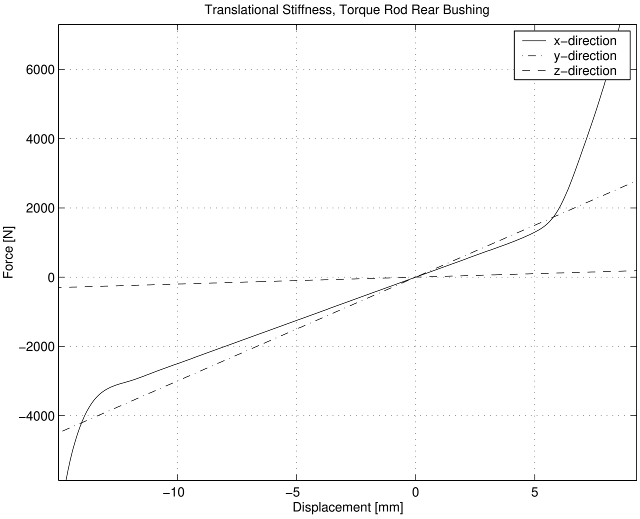

Figure A.12 *Torque rod rear bushing static translational stiffnesses characteristics with respect to global co-ordinate system*

A.3 Linearised Control Object Model Data

The transfer functions of the nine elements of G in (4.10) and the matrix N in (4.9) are

$$G_{11} = \frac{\begin{array}{r} s^{24} + 6.4 \cdot 10^{4} s^{23} + 9.5 \cdot 10^{8} s^{22} + 2.4 \cdot 10^{13} s^{21} + 2.1 \cdot 10^{17} s^{20} \\ +2.9 \cdot 10^{21} s^{19} + 1.6 \cdot 10^{25} s^{18} + 1.2 \cdot 10^{29} s^{17} + 4.0 \cdot 10^{32} s^{16} + 8.4 \cdot 10^{35} s^{15} \\ +1.1 \cdot 10^{39} s^{14} + 6.0 \cdot 10^{41} s^{13} + 9.3 \cdot 10^{43} s^{12} + 9.2 \cdot 10^{45} s^{11} + 1.2 \cdot 10^{48} s^{10} \\ +5.1 \cdot 10^{49} s^{9} + 5.9 \cdot 10^{51} s^{8} + 1.3 \cdot 10^{53} s^{7} + 1.4 \cdot 10^{55} s^{6} + 1.6 \cdot 10^{56} s^{5} \\ +1.6 \cdot 10^{58} s^{4} + 8.1 \cdot 10^{58} s^{3} + 7.4 \cdot 10^{60} s^{2} + 6.0 \cdot 10^{60} s + 5.1 \cdot 10^{62} \end{array}}{\begin{array}{r} s^{24} + 6.4 \cdot 10^{4} s^{23} + 9.5 \cdot 10^{8} s^{22} + 2.4 \cdot 10^{13} s^{21} + 2.1 \cdot 10^{17} s^{20} \\ +2.9 \cdot 10^{21} s^{19} + 1.6 \cdot 10^{25} s^{18} + 1.2 \cdot 10^{29} s^{17} + 4.0 \cdot 10^{32} s^{16} + 8.4 \cdot 10^{35} s^{15} \\ +1.1 \cdot 10^{39} s^{14} + 6.0 \cdot 10^{41} s^{13} + 9.8 \cdot 10^{43} s^{12} + 1.2 \cdot 10^{46} s^{11} + 1.6 \cdot 10^{48} s^{10} \\ +8.9 \cdot 10^{49} s^{9} + 1.1 \cdot 10^{52} s^{8} + 3.3 \cdot 10^{53} s^{7} + 3.6 \cdot 10^{55} s^{6} + 6.3 \cdot 10^{56} s^{5} \\ +6.4 \cdot 10^{58} s^{4} + 6.1 \cdot 10^{59} s^{3} + 5.8 \cdot 10^{61} s^{2} + 2.4 \cdot 10^{62} s + 2.1 \cdot 10^{64} \end{array}}$$

$$G_{12} = \frac{\begin{array}{r} 1619 s^{22} + 1.0 \cdot 10^{8} s^{21} + 1.5 \cdot 10^{12} s^{20} + 3.9 \cdot 10^{16} s^{19} + 4.0 \cdot 10^{20} s^{18} \\ +4.8 \cdot 10^{24} s^{17} + 2.6 \cdot 10^{28} s^{16} + 2.0 \cdot 10^{32} s^{15} + 6.4 \cdot 10^{35} s^{14} + 1.4 \cdot 10^{39} s^{13} \\ +1.8 \cdot 10^{42} s^{12} + 9.5 \cdot 10^{44} s^{11} + 1.3 \cdot 10^{47} s^{10} + 7.0 \cdot 10^{48} s^{9} + 8.7 \cdot 10^{50} s^{8} \\ +1.8 \cdot 10^{52} s^{7} + 2.1 \cdot 10^{54} s^{6} + 1.6 \cdot 10^{55} s^{5} + 2.1 \cdot 10^{57} s^{4} - 6.1 \cdot 10^{56} s^{3} \\ +4.6 \cdot 10^{59} s^{2} - 5.4 \cdot 10^{60} s - 2.4 \cdot 10^{62} \end{array}}{\begin{array}{r} s^{24} + 6.4 \cdot 10^{4} s^{23} + 9.5 \cdot 10^{8} s^{22} + 2.4 \cdot 10^{13} s^{21} + 2.1 \cdot 10^{17} s^{20} \\ +2.9 \cdot 10^{21} s^{19} + 1.6 \cdot 10^{25} s^{18} + 1.2 \cdot 10^{29} s^{17} + 4.0 \cdot 10^{32} s^{16} + 8.4 \cdot 10^{35} s^{15} \\ +1.1 \cdot 10^{39} s^{14} + 6.0 \cdot 10^{41} s^{13} + 9.9 \cdot 10^{43} s^{12} + 1.2 \cdot 10^{46} s^{11} + 1.6 \cdot 10^{48} s^{10} \\ +8.9 \cdot 10^{49} s^{9} + 1.1 \cdot 10^{52} s^{8} + 3.3 \cdot 10^{53} s^{7} + 3.6 \cdot 10^{55} s^{6} + 6.3 \cdot 10^{56} s^{5} \\ +6.4 \cdot 10^{58} s^{4} + 6.1 \cdot 10^{59} s^{3} + 5.8 \cdot 10^{61} s^{2} + 2.4 \cdot 10^{62} s + 2.1 \cdot 10^{64} \end{array}}$$

$$G_{13} = \frac{\begin{array}{r} 146 s^{22} + 1.9 \cdot 10^{7} s^{21} + 7.6 \cdot 10^{11} s^{20} + 1.1 \cdot 10^{16} s^{19} + 2.1 \cdot 10^{20} s^{18} \\ +1.7 \cdot 10^{24} s^{17} + 1.5 \cdot 10^{28} s^{16} + 7.2 \cdot 10^{31} s^{15} + 1.9 \cdot 10^{35} s^{14} + 3.4 \cdot 10^{38} s^{13} \\ +3.6 \cdot 10^{41} s^{12} + 1.7 \cdot 10^{44} s^{11} + 2.4 \cdot 10^{46} s^{10} + 2.0 \cdot 10^{48} s^{9} + 2.5 \cdot 10^{50} s^{8} \\ +8.9 \cdot 10^{51} s^{7} + 1.0 \cdot 10^{54} s^{6} + 1.7 \cdot 10^{55} s^{5} + 1.8 \cdot 10^{57} s^{4} + 1.1 \cdot 10^{58} s^{3} \\ +1.3 \cdot 10^{60} s^{2} - 5.7 \cdot 10^{59} s + 6.1 \cdot 10^{61} \end{array}}{\begin{array}{r} s^{24} + 6.4 \cdot 10^{4} s^{23} + 9.5 \cdot 10^{8} s^{22} + 2.4 \cdot 10^{13} s^{21} + 2.1 \cdot 10^{17} s^{20} \\ +2.9 \cdot 10^{21} s^{19} + 1.6 \cdot 10^{25} s^{18} + 1.2 \cdot 10^{29} s^{17} + 4.0 \cdot 10^{32} s^{16} + 8.4 \cdot 10^{35} s^{15} \\ +1.1 \cdot 10^{39} s^{14} + 6.0 \cdot 10^{41} s^{13} + 9.9 \cdot 10^{43} s^{12} + 1.2 \cdot 10^{46} s^{11} + 1.6 \cdot 10^{48} s^{10} \\ +8.9 \cdot 10^{49} s^{9} + 1.1 \cdot 10^{52} s^{8} + 3.3 \cdot 10^{53} s^{7} + 3.6 \cdot 10^{55} s^{6} + 6.3 \cdot 10^{56} s^{5} \\ +6.4 \cdot 10^{58} s^{4} + 6.1 \cdot 10^{59} s^{3} + 5.8 \cdot 10^{61} s^{2} + 2.4 \cdot 10^{62} s + 2.1 \cdot 10^{64} \end{array}}$$

$$G_{21} = \frac{\begin{array}{r} 2422s^{22} + 1.6 \cdot 10^{8} s^{21} + 2.3 \cdot 10^{12} s^{20} + 5.9 \cdot 10^{16} s^{19} + 5.1 \cdot 10^{20} s^{18} \\ +7.1 \cdot 10^{24} s^{17} + 4.0 \cdot 10^{28} s^{16} + 3.0 \cdot 10^{32} s^{15} + 9.7 \cdot 10^{35} s^{14} + 2.0 \cdot 10^{39} s^{13} \\ +2.7 \cdot 10^{42} s^{12} + 1.4 \cdot 10^{45} s^{11} + 2.0 \cdot 10^{47} s^{10} + 1.1 \cdot 10^{49} s^{9} + 1.3 \cdot 10^{51} s^{8} \\ +2.8 \cdot 10^{52} s^{7} + 3.2 \cdot 10^{54} s^{6} + 2.9 \cdot 10^{55} s^{5} + 3.2 \cdot 10^{57} s^{4} + 4.4 \cdot 10^{57} s^{3} \\ +7.4 \cdot 10^{59} s^{2} - 5.7 \cdot 10^{60} s - 3.5 \cdot 10^{62} \end{array}}{\begin{array}{r} s^{24} + 6.4 \cdot 10^{4} s^{23} + 9.5 \cdot 10^{8} s^{22} + 2.4 \cdot 10^{13} s^{21} + 2.1 \cdot 10^{17} s^{20} \\ +2.9 \cdot 10^{21} s^{19} + 1.6 \cdot 10^{25} s^{18} + 1.2 \cdot 10^{29} s^{17} + 4.0 \cdot 10^{32} s^{16} + 8.4 \cdot 10^{35} s^{15} \\ +1.1 \cdot 10^{39} s^{14} + 6.0 \cdot 10^{41} s^{13} + 9.9 \cdot 10^{43} s^{12} + 1.2 \cdot 10^{46} s^{11} + 1.6 \cdot 10^{48} s^{10} \\ +8.9 \cdot 10^{49} s^{9} + 1.1 \cdot 10^{52} s^{8} + 3.3 \cdot 10^{53} s^{7} + 3.6 \cdot 10^{55} s^{6} + 6.3 \cdot 10^{56} s^{5} \\ +6.4 \cdot 10^{58} s^{4} + 6.1 \cdot 10^{59} s^{3} + 5.8 \cdot 10^{61} s^{2} + 2.4 \cdot 10^{62} s + 2.1 \cdot 10^{64} \end{array}}$$

$$G_{22} = \frac{\begin{array}{r} s^{24} + 6.4 \cdot 10^{4} s^{23} + 9.5 \cdot 10^{8} s^{22} + 2.4 \cdot 10^{13} s^{21} + 2.1 \cdot 10^{17} s^{20} \\ +2.9 \cdot 10^{21} s^{19} + 1.6 \cdot 10^{25} s^{18} + 1.2 \cdot 10^{29} s^{17} + 4.0 \cdot 10^{32} s^{16} + 8.4 \cdot 10^{35} s^{15} \\ +1.1 \cdot 10^{39} s^{14} + 6.0 \cdot 10^{41} s^{13} + 9.1 \cdot 10^{43} s^{12} + 8.2 \cdot 10^{45} s^{11} + 1.0 \cdot 10^{48} s^{10} \\ +4.2 \cdot 10^{49} s^{9} + 4.8 \cdot 10^{51} s^{8} + 1.0 \cdot 10^{53} s^{7} + 1.1 \cdot 10^{55} s^{6} + 1.2 \cdot 10^{56} s^{5} \\ +1.2 \cdot 10^{58} s^{4} + 5.6 \cdot 10^{58} s^{3} + 5.1 \cdot 10^{60} s^{2} + 3.4 \cdot 10^{60} s + 2.9 \cdot 10^{62} \end{array}}{\begin{array}{r} s^{24} + 6.4 \cdot 10^{4} s^{23} + 9.5 \cdot 10^{8} s^{22} + 2.4 \cdot 10^{13} s^{21} + 2.1 \cdot 10^{17} s^{20} \\ +2.9 \cdot 10^{21} s^{19} + 1.6 \cdot 10^{25} s^{18} + 1.2 \cdot 10^{29} s^{17} + 4.0 \cdot 10^{32} s^{16} + 8.4 \cdot 10^{35} s^{15} \\ +1.1 \cdot 10^{39} s^{14} + 6.0 \cdot 10^{41} s^{13} + 9.9 \cdot 10^{43} s^{12} + 1.2 \cdot 10^{46} s^{11} + 1.6 \cdot 10^{48} s^{10} \\ +8.9 \cdot 10^{49} s^{9} + 1.1 \cdot 10^{52} s^{8} + 3.3 \cdot 10^{53} s^{7} + 3.6 \cdot 10^{55} s^{6} + 6.3 \cdot 10^{56} s^{5} \\ +6.4 \cdot 10^{58} s^{4} + 6.1 \cdot 10^{59} s^{3} + 5.8 \cdot 10^{61} s^{2} + 2.4 \cdot 10^{62} s + 2.1 \cdot 10^{64} \end{array}}$$

$$G_{23} = \frac{\begin{array}{r} -88s^{22} - 1.2 \cdot 10^{7} s^{21} - 4.7 \cdot 10^{11} s^{20} - 7.5 \cdot 10^{15} s^{19} - 1.4 \cdot 10^{20} s^{18} \\ -1.2 \cdot 10^{24} s^{17} - 1.1 \cdot 10^{28} s^{16} - 5.6 \cdot 10^{31} s^{15} - 1.6 \cdot 10^{35} s^{14} - 3.0 \cdot 10^{38} s^{13} \\ -3.3 \cdot 10^{41} s^{12} - 1.6 \cdot 10^{44} s^{11} - 2.3 \cdot 10^{46} s^{10} - 1.6 \cdot 10^{48} s^{9} - 1.9 \cdot 10^{50} s^{8} \\ -6.3 \cdot 10^{51} s^{7} - 6.9 \cdot 10^{53} s^{6} - 1.2 \cdot 10^{55} s^{5} - 1.2 \cdot 10^{57} s^{4} - 9.7 \cdot 10^{57} s^{3} \\ -8.3 \cdot 10^{59} s^{2} - 1.5 \cdot 10^{60} s - 8.3 \cdot 10^{61} \end{array}}{\begin{array}{r} s^{24} + 6.4 \cdot 10^{4} s^{23} + 9.5 \cdot 10^{8} s^{22} + 2.4 \cdot 10^{13} s^{21} + 2.1 \cdot 10^{17} s^{20} \\ +2.9 \cdot 10^{21} s^{19} + 1.6 \cdot 10^{25} s^{18} + 1.2 \cdot 10^{29} s^{17} + 4.0 \cdot 10^{32} s^{16} + 8.4 \cdot 10^{35} s^{15} \\ +1.1 \cdot 10^{39} s^{14} + 6.0 \cdot 10^{41} s^{13} + 9.9 \cdot 10^{43} s^{12} + 1.2 \cdot 10^{46} s^{11} + 1.6 \cdot 10^{48} s^{10} \\ +8.9 \cdot 10^{49} s^{9} + 1.1 \cdot 10^{52} s^{8} + 3.3 \cdot 10^{53} s^{7} + 3.6 \cdot 10^{55} s^{6} + 6.3 \cdot 10^{56} s^{5} \\ +6.4 \cdot 10^{58} s^{4} + 6.1 \cdot 10^{59} s^{3} + 5.8 \cdot 10^{61} s^{2} + 2.4 \cdot 10^{62} s + 2.1 \cdot 10^{64} \end{array}}$$

$$G_{31} = \frac{\begin{array}{r} +5.7 \cdot 10^{6} s^{21} + 3.6 \cdot 10^{11} s^{20} + 4.7 \cdot 10^{15} s^{19} + 1.1 \cdot 10^{20} s^{18} + 7.8 \cdot 10^{23} s^{17} \\ +8.2 \cdot 10^{27} s^{16} + 3.6 \cdot 10^{31} s^{15} + 9.3 \cdot 10^{34} s^{14} + 1.6 \cdot 10^{38} s^{13} + 1.6 \cdot 10^{41} s^{12} \\ +6.7 \cdot 10^{43} s^{11} + 9.1 \cdot 10^{45} s^{10} + 7.9 \cdot 10^{47} s^{9} + 9.0 \cdot 10^{49} s^{8} + 3.3 \cdot 10^{51} s^{7} \\ +3.4 \cdot 10^{53} s^{6} + 5.6 \cdot 10^{54} s^{5} + 5.6 \cdot 10^{56} s^{4} + 2.7 \cdot 10^{57} s^{3} + 2.7 \cdot 10^{59} s^{2} \\ -1.4 \cdot 10^{60} s - 9.2 \cdot 10^{61} \end{array}}{\begin{array}{r} s^{24} + 6.4 \cdot 10^{4} s^{23} + 9.5 \cdot 10^{8} s^{22} + 2.4 \cdot 10^{13} s^{21} + 2.1 \cdot 10^{17} s^{20} \\ +2.9 \cdot 10^{21} s^{19} + 1.6 \cdot 10^{25} s^{18} + 1.2 \cdot 10^{29} s^{17} + 4.0 \cdot 10^{32} s^{16} + 8.4 \cdot 10^{35} s^{15} \\ +1.1 \cdot 10^{39} s^{14} + 6.0 \cdot 10^{41} s^{13} + 9.9 \cdot 10^{43} s^{12} + 1.2 \cdot 10^{46} s^{11} + 1.6 \cdot 10^{48} s^{10} \\ +8.9 \cdot 10^{49} s^{9} + 1.1 \cdot 10^{52} s^{8} + 3.3 \cdot 10^{53} s^{7} + 3.6 \cdot 10^{55} s^{6} + 6.3 \cdot 10^{56} s^{5} \\ +6.4 \cdot 10^{58} s^{4} + 6.1 \cdot 10^{59} s^{3} + 5.8 \cdot 10^{61} s^{2} + 2.4 \cdot 10^{62} s + 2.1 \cdot 10^{64} \end{array}}$$

$$G_{32} = \frac{\begin{array}{r} -4.0 \cdot 10^{6} s^{21} - 2.5 \cdot 10^{11} s^{20} - 3.3 \cdot 10^{15} s^{19} - 7.5 \cdot 10^{19} s^{18} - 5.6 \cdot 10^{23} s^{17} \\ -5.8 \cdot 10^{27} s^{16} - 2.6 \cdot 10^{31} s^{15} - 6.8 \cdot 10^{34} s^{14} - 1.1 \cdot 10^{38} s^{13} - 1.1 \cdot 10^{41} s^{12} \\ -4.9 \cdot 10^{43} s^{11} - 6.8 \cdot 10^{45} s^{10} - 5.0 \cdot 10^{47} s^{9} - 6.0 \cdot 10^{49} s^{8} - 2.1 \cdot 10^{51} s^{7} \\ -2.2 \cdot 10^{53} s^{6} - 4.1 \cdot 10^{54} s^{5} - 4.0 \cdot 10^{56} s^{4} - 3.5 \cdot 10^{57} s^{3} - 3.1 \cdot 10^{59} s^{2} \\ -7.1 \cdot 10^{59} s - 5.4 \cdot 10^{61} \end{array}}{\begin{array}{r} s^{24} + 6.4 \cdot 10^{4} s^{23} + 9.5 \cdot 10^{8} s^{22} + 2.4 \cdot 10^{13} s^{21} + 2.1 \cdot 10^{17} s^{20} \\ +2.9 \cdot 10^{21} s^{19} + 1.6 \cdot 10^{25} s^{18} + 1.2 \cdot 10^{29} s^{17} + 4.0 \cdot 10^{32} s^{16} + 8.4 \cdot 10^{35} s^{15} \\ +1.1 \cdot 10^{39} s^{14} + 6.0 \cdot 10^{41} s^{13} + 9.9 \cdot 10^{43} s^{12} + 1.2 \cdot 10^{46} s^{11} + 1.6 \cdot 10^{48} s^{10} \\ +8.9 \cdot 10^{49} s^{9} + 1.1 \cdot 10^{52} s^{8} + 3.3 \cdot 10^{53} s^{7} + 3.6 \cdot 10^{55} s^{6} + 6.3 \cdot 10^{56} s^{5} \\ +6.4 \cdot 10^{58} s^{4} + 6.1 \cdot 10^{59} s^{3} + 5.8 \cdot 10^{61} s^{2} + 2.4 \cdot 10^{62} s + 2.1 \cdot 10^{64} \end{array}}$$

$$G_{33} = \frac{\begin{array}{r} s^{24} + 6.4 \cdot 10^{4} s^{23} + 9.0 \cdot 10^{8} s^{22} + 2.4 \cdot 10^{13} s^{21} + 2.0 \cdot 10^{17} s^{20} \\ +2.8 \cdot 10^{21} s^{19} + 1.5 \cdot 10^{25} s^{18} + 1.2 \cdot 10^{29} s^{17} + 3.9 \cdot 10^{32} s^{16} + 8.2 \cdot 10^{35} s^{15} \\ +1.1 \cdot 10^{39} s^{14} + 5.9 \cdot 10^{41} s^{13} + 9.5 \cdot 10^{43} s^{12} + 1.1 \cdot 10^{46} s^{11} + 1.4 \cdot 10^{48} s^{10} \\ +7.0 \cdot 10^{49} s^{9} + 8.3 \cdot 10^{51} s^{8} + 2.1 \cdot 10^{53} s^{7} + 2.3 \cdot 10^{55} s^{6} + 3.0 \cdot 10^{56} s^{5} \\ +3.0 \cdot 10^{58} s^{4} + 1.7 \cdot 10^{59} s^{3} + 1.5 \cdot 10^{61} s^{2} + 6.0 \cdot 10^{60} s + 4.3 \cdot 10^{62} \end{array}}{\begin{array}{r} s^{24} + 6.4 \cdot 10^{4} s^{23} + 9.5 \cdot 10^{8} s^{22} + 2.4 \cdot 10^{13} s^{21} + 2.1 \cdot 10^{17} s^{20} \\ +2.9 \cdot 10^{21} s^{19} + 1.6 \cdot 10^{25} s^{18} + 1.2 \cdot 10^{29} s^{17} + 4.0 \cdot 10^{32} s^{16} + 8.4 \cdot 10^{35} s^{15} \\ +1.1 \cdot 10^{39} s^{14} + 6.0 \cdot 10^{41} s^{13} + 9.8 \cdot 10^{43} s^{12} + 1.2 \cdot 10^{46} s^{11} + 1.6 \cdot 10^{48} s^{10} \\ +8.9 \cdot 10^{49} s^{9} + 1.1 \cdot 10^{52} s^{8} + 3.3 \cdot 10^{53} s^{7} + 3.5 \cdot 10^{55} s^{6} + 6.3 \cdot 10^{56} s^{5} \\ +6.4 \cdot 10^{58} s^{4} + 6.1 \cdot 10^{59} s^{3} + 5.8 \cdot 10^{61} s^{2} + 2.4 \cdot 10^{62} s + 2.1 \cdot 10^{64} \end{array}}$$

Clearly, these high order polynomials are awkward to handle. The calculations are therefore conducted using state-space representation.

$$N = \begin{bmatrix} 0 & 0 & 0 \\ 0 & 0 & 0 \\ 0 & 0 & 0 \\ 0 & 0 & 0 \\ 0 & 0 & 0 \\ 0 & 0 & 0 \\ 4.1286e-005 & -5.4741e-005 & 4.6652e-005 \\ 0 & 0 & 0 \\ -4.0449e-005 & 6.6907e-005 & -5.2046e-006 \\ 0 & 0 & 0 \\ -8.7174e-005 & -1.4968e-005 & -8.3185e-006 \\ 0 & 0 & 0 \\ 0 & 0 & 0 \\ 0 & 0 & 0 \\ 0 & 0 & 0 \\ 0 & 0 & 0 \\ 0 & 0 & 0 \\ 0 & 0 & 0 \\ 0 & 0 & 0 \\ 0 & 0 & 0 \\ 0 & 0 & 0 \\ 0 & 0 & 0 \\ 0 & 0 & 0 \\ 0 & 0 & 0 \end{bmatrix}$$

A.4 LQG Design Parameters

The filters and parameters below are used in the LQG design in Chapter 5.

A.4.1 Initial Design

The design parameters for the initial LQG design corresponding to Figure 5.3 are

$$\begin{aligned} R_1 &= I \\ R_2 &= I \\ G_u &= I \\ G_z &= I \cdot \sqrt{10^{15}} \\ G_n &= I \end{aligned}$$

$$G_d = \frac{10^{-3}(1+s/(2\pi \cdot 2))^5}{(1+s/(2\pi \cdot 50))^5(1+s/(2\pi \cdot 450)^5} \cdot I$$

A.4.2 Final Design

The design parameters for the final LQG design corresponding to Figures 5.7 and 5.8 are

$$\begin{aligned} R_1 &= I \\ R_2 &= 100I \\ G_u &= I \\ G_n &= I \end{aligned}$$

$$G_z = \frac{10^{-5}(1 + s/(2\pi \cdot 0.1))^3}{(1 + s/(2\pi \cdot 10))^3} \cdot I$$

$$G_d = \frac{10^{-3}(1 + s/(2\pi))^5}{(1 + s/(2\pi \cdot 50))^5(1 + s/(2\pi \cdot 450)^5} \cdot I$$

A.5 Broad Band H_2 Design Parameters

The weighting functions used in the H_2 design of the broad band controller described in Section 6.3, are here presented.

A.5.1 Initial Design

The weighting function used in the initial H_2 design corresponding to Figures 6.5 and 6.6 is as follows

$$W_S = w_{s1} \cdot w_{s2} \cdot I$$

where

$$\begin{aligned} w_{s1} &= \frac{10.924(s^2 + 87s + (2\pi \cdot 11)^2)^3}{(s^2 + 110s + (2\pi \cdot 16.5)^2)^3} \\ w_{s2} &= \frac{(s^2 + 5000s + (2\pi \cdot 500)^2)^3}{11 \cdot (s^2 + 3000s + (2\pi \cdot 333)^2)^3} \end{aligned}$$

A.5.2 Final “Trade-Off” Design

A.5.3 Initial Design

The weighting functions used in the H_2 trade-off design corresponding to Figures 6.8, 6.9 and 6.10, are as follows

$$W_S = w_{s1} \cdot w_{s2} \cdot I$$

where

$$w_{s1} = \frac{10.924(s^2 + 87s + (2\pi \cdot 11)^2)^3}{(s^2 + 110s + (2\pi \cdot 16.5)^2)^3}$$

$$w_{s2} = \frac{(s^2 + 5000s + (2\pi \cdot 500)^2)^3}{11 \cdot (s^2 + 3000s + (2\pi \cdot 333)^2)^3}$$

$$W_u = \frac{1000(1 + s/(2\pi))^2}{(1 + s/(2\pi \cdot 0.01))^2} \cdot I$$

A.6 Narrow Band H_2 Design Parameters

The weighting functions used in the H_2 design of the narrow band controller described in Section 6.4, are here presented.

A.6.1 Initial Design

The weighting function used in the initial H_2 design corresponding to Figures 6.18 and 6.19 is as follows

$$W_S = w_{s1} \cdot w_{s2} \cdot w_{s3} \cdot w_{s4} \cdot I$$

where

$$w_{s1} = \frac{s^2 + 100s + (2\pi E)^2}{s^2 + 0.001s + (2\pi E)^2}$$

$$w_{s2} = \frac{s^2 + 100s + (2\pi 2E)^2}{s^2 + 0.001s + (2\pi 2E)^2}$$

$$w_{s3} = \frac{s^2 + 100s + (2\pi 2.5E)^2}{s^2 + 0.001s + (2\pi 2.5E)^2}$$

$$w_{s4} = \frac{s^2 + 100s + (2\pi 5E)^2}{s^2 + 0.001s + (2\pi 5E)^2}$$

A.6.2 Final Design

The weighting functions used in the final H_2 design corresponding to Figures 6.20, 6.21, and 6.22, are as follows

$$W_S = w_{s1} \cdot w_{s2} \cdot w_{s3} \cdot w_{s4} \cdot I$$

where

$$\begin{aligned} w_{s1} &= \frac{s^2 + 100s + (2\pi E)^2}{s^2 + 0.001s + (2\pi E)^2} \\ w_{s2} &= \frac{s^2 + 100s + (2\pi 2E)^2}{s^2 + 0.001s + (2\pi 2E)^2} \\ w_{s3} &= \frac{s^2 + 100s + (2\pi 2.5E)^2}{s^2 + 0.001s + (2\pi 2.5E)^2} \\ w_{s4} &= \frac{s^2 + 100s + (2\pi 5E)^2}{s^2 + 0.001s + (2\pi 5E)^2} \end{aligned}$$

$$W_u = \frac{10^5(1 + s/(2\pi 30))^7}{(1 + s/(2\pi 2.5))^5(1 + s/(2\pi 50000))^2} \cdot I$$

Bibliography

[1] ADAMS, a registered trademark of Mechanical Dynamics Inc., 2301 Commonwealth Bouleward, Ann Arbour, Michigan 48105, USA.

[2] D. P. Atherton. *Nonlinear Control Engineering*. 1982. ISBN 0-442-30486-2.

[3] E. F. Berkman and E. K. Bender. Perspectives on active noise and vibration control. *JOURNAL OF SOUND AND VIBRATION*, January 1997.

[4] G. H. Blackwood and A. H. von Flotow. Active control for vibration isloation despite resonant base dynamics. *DSC-Vol. 38, Active Control of Noise and Vibration, ASME 1992*.

[5] J. C. Doyle. Guaranteed margins for LQG regulators. IEEE TRANSACTIONS ON AUTOMATIC CONTROL, 23(4), August 1978.

[6] S. J. Elliot, C. C. Boucher, and P. A. Nelson. The behaviour of a multiple channel active control system. IEEE TRANSACTIONS ON SIGNAL PROCESSING, 40(5), May 1992.

[7] S. J. Elliot and P. A. Nelson. Algorithm for multichannel LMS adaptive filtering. *ELECTRONIC LETTERS*, 21(21), October 1985.

[8] S. J. Elliot, I. M. Stothers, and P. A. Nelson. A multiple error LMS algorithm and its application to the active control of sound and vibration. IEEE

TRANSACTIONS ON ACOUSTICS, SPEECH, AND SIGNAL PROCESSING, 35(10), October 1987.

[9] S.J. Elliot and P. A. Nelson. An adaptive algorithm for multichannel active control. In *Proceedings of The Institute of Acoustics*, 1986.

[10] S.J. Elliot and I. M. Stothers. A multichannel adaptive algorithm for the active control of start-up transients. In *Proceedings of the 213rd Euromech Colloquium, Marseille, 8-11 September*, 1986.

[11] S.J. Elliot, I.M. Stothers, P. A. Nelson, A. M. McDonald, D. C. Quinn, and T. J. Saunders. The active control of engine noise inside cars. In *Proceedings of INTER-NOISE 88*, 1988.

[12] C. R. Fuller, S. J. Elliot, and P. A. Nelson. *Active Control of Vibration.* ACADEMIC PRESS, 1997. ISBN 0-12-269441-4.

[13] T. Glad and L. Ljung. *Reglerteori, flervariabla och olinjära metoder.* Studentlitteratur, 1997. ISBN 91-44-00472-9.

[14] S. Hasegawa, T. Tabata, A. Kinoshita, and H. Hyodo. The development of an active noise control system for automobiles. *Society of Automotive Engineers Paper 922086*, 1992.

[15] R. A. Hyde and K. Glover. The application of schduled H_∞ controllers to a VSTOL aircraft. IEEE TRANSACTIONS ON AUTOMATIC CONTROL, 38(7), July 1993.

[16] C. E. Kaplow. Active local vibration isolation applied to a flexible space telescope. *JOURNAL OF GUIDANCE AND CONTROL*, 3(3), 1980.

[17] G. Kim and R. Singh. Engine vibration control using passive, active, and adaptive hydraulic mount systems. *Society of Automotive Engineers Paper 932897*, 1993.

[18] L. Ljung. *System Identification, Theory for the User.* Prentice Hall, 1999. ISBN 0-13-656695-2.

[19] J. M. Maciejowski. *Multivariable Feedback Design.* Addison-Wesley, 1989. ISBN 0-201-18243-2.

[20] A. M. McDonald, S. J. Elliot, and M. A. Stokes. Active noise and vibration control within the automobile. In *Proceedings of the International Symposium on Active Control of Sound and Vibration, Acoustical Society of Japan, Tokyo*, 1991.

[21] L. Meirovitch. *Dynamics and control of structures.* Wiley-Interscience, 1989. ISBN 0-471-62858-1.

[22] M. Müller, H. G. Eckel, M. Leibach, and W. Bors. Reduction of noise and vibration in vehicles by an appropriate engine mounting system and active absorbers. *Society of Automotive Engineers Paper 960185*, 1996.

[23] M. Müller, T. Siebler, and H. Gärtner. Simulation of vibrating vehicle structures as part of the design process of engine mount systems and vibration absorbers. *Society of Automotive Engineers Paper 952211*, 1995.

[24] M. Müller and T. W. Siebler. Methods for the reduction of noise and vibration in vehicles using an appropriate engine mount system. *Society of Automotive Engineers Paper 942414*, 1994.

[25] M. Müller, U. Weltin, D. Law, M. Roberts, and T. W. Siebler. The effect of engine mounts on the noise and vibration behaviour of vehicles. *Society of Automotive Engineers Paper 940607*, 1994.

[26] Y. Nakaji, S. Satoh, T. Kimura, T. Hamabe, Y. Akatsu, and H. Kawazoe. Development of an active control engine mount system. *Vehicle System Dynamics*, 32:185–198, 1999.

[27] E. I. Rivin. A primer on engine mounts. *Automotive Engineering*, 1986.

[28] H. Sano, T. Takahashi, D. Isihara, T. Yamashita, K. Terai, and Y. Nakamura. Development of active control systems for low-frequency road noise combined with audio system. *Society of Automotive Engineers of Japan*, 32(4):105–112, 2001.

[29] U. Schönhoff, P. Eisenträger, and R. Nordmann. Reduction of finite element models of flexible structures for controller design and integrated modelling. In *the International Conference on Noise and Vibration Engineering, ISMA25, Leuven, Belgium*, 2000.

[30] U. Schönhoff, P. Eisenträger, K. Wandner, H. Kärcher, and R. Nordmann. End-to-end simulation of the image stability for the airborne telescope SOFIA. In *Astronomical Telescopes and Instrumentaitons, München, Germany*, 2000.

[31] R. Shoureshi, J. Vance, and R. Gasser. Automotive applications of active noise and vibration control. In *Proceedings of the American Control Conference, Albuquerque, New Mexico*, pages 2910–14, 1997.

[32] V. N. Sohoni and J. Whitesell. Automatic linearisation of constrained dynamical models. *Transactoins of the ASME, Vol. 108*, September 1986.

[33] J. Spanos, Z. Rahman, and A. von Flotow. Active vibration isolation on an experimental flexible structure. In *Proceedings of the SPIE North American Conference on Smart Structures and Intelligent Systems, Albuquerque, New Mexico, SPIE*, volume 1917, pages 1917–60, 1993.

[34] K. J. Åström and T. B. Wittenmark. *Adaptive Control*. Addison-Wesley, 1989.

[35] T. J. Sutton, S.J. Elliot, A. M. McDonald, and T. J. Saunders. Active control of road noise inside vehicles. *Noise Control Eng. J.*, 42(4), Jul-Aug 1994.

[36] N. Tanaka and Y. Kikushima. Rigid support active vibration isolation. *Journal of Sound and Vibration*, 125(3), 1998.

[37] T. Ushijima and S. Kumakawa. Active engine mount with piezo-actuator for vibration control. *Society of Automotive Engineers Paper 930201*, 1993.

[38] B. G. Watters, R. B. Coleman, G. L. Duckworth, and E. F.Bukman. A perspective on an active machinery isolation. In *Proceedings of the* 27^{t}h *Conference on Decision and Control, Austin, Texas*, pages 2033–2038, 1988.

[39] B. Widrow, J. M. McCool, M. G. Larimore, and C. R. Johnson. Stationary and nonstationary learning characteristics of the LMS adaptive filter. In Proceedings of the IEEE, vol. 64, No. 8, August 1976.

[40] B. Widrow and S. D. Stearns. *Adaptive Signal Processing.* Prentice Hall, 1985.

[41] B. Widrow and E. Walach. On the statistical efficiency of the LMS algorithm with nonstationary inputs. IEEE transaction on information theory, Vol. IT-30, no. 2, March 1984.

[42] Y. Yu, N. G. Naganathan, and R. V. Dukkipati. Review of automobile vehicle engine mounting systems. *Int. J. Vehicle Design*, 24(4), 2000.

[43] M. W. Zehn and M. Enzmann. Active vibration control based on finite element models: How to gaing a valid model. In *the International Conference on Noise and Vibration Engineering, ISMA25, Leuven, Belgium*, 2000.

[44] K. Zhou, J. C. Doyle, and K. Glover. *Robust and Optimal Control.* Prentice Hall, 1996. ISBN 0-13-456567-3.